Identifying Target Genes related to Respiratory Network Dysfunction in a Mouse Model for the Rett Syndrome

Dissertation

for the award of the degree

„Doctor rerum naturalium" (Dr. rer. nat.)

Division of Mathematics and Natural Sciences

of the Georg-August-Universität Göttingen

submitted by

Steffen Vogelgesang

from Merseburg

Göttingen 2012

Dr. Dr. Till Manzke

(**1st Reviewer**, advisor and member of the thesis committee)

Dept. of Neuro- and Sensory Physiology, University Medical Center,

Georg August University of Göttingen

Prof. Dr. Swen Hülsmann

(**2nd Reviewer**)

Dept. of Neurophysiology and Cellular Biophysics, University Medical Center,

Georg August University of Göttingen

Prof. Dr. Gabriele Flügge

(Member of the thesis committee)

Clinical Neurobiology Laboratory,

German Primate Center, Göttingen

Prof. Dr. Andreas Wodarz

(Member of the thesis committee)

Stem Cell Biology, Dept. of Anatomy and Cell Biology, University Medical Center,

Georg August University of Göttingen

Date of oral examination: 19.11.2012

Dedicated to my grandmother Ms. Elisabeth Ernst

Contents

CONTENTS

CONTENTS

Abstract

Rett Syndrome is a severe neurological disorder caused by mutations in the X-chromosome-linked *MECP2* gene, which encodes the transcription factor methyl-CpG binding protein 2 (MeCP2). Symptoms become obvious during early childhood and include life-threatening breathing abnormalities accompanied by severe periods of apnea causing intermitted hypoxia and frequently sudden death. Gene expression analysis in MeCP2 deficient mice revealed a pathologically strong expression in the gene encoding for the serotonin receptor 5B (5-HTR_{5B}) in the ventral respiratory group (VRG), which includes the region important for respiratory rhythm generation.

Extensive protein analysis showed that 5-HTR_{5B} is naturally truncated and displayed an unusual intracellular localization on tubular and vesicular membranes. Despite truncation, the protein is able to bind inhibitory G-proteins, which consequently decreases intracellular cAMP concentration. In MeCP2 knockout mice the persistent cAMP reduction in the VRG caused disturbed breathing. Mice, which additionally lack the *Htr5b* gene, revealed normal respiratory network output activity. Moreover, these double-knockout mice appeared healthier concerning bodyweight and size and showed extended lifespan.

Administration of forskolin, an adenylyl cyclase activator that elevates intracellular cAMP concentration, normalized breathing in MeCP2 deficient mice. Therefore, the application of cAMP elevating drugs might be an effective pharmacological strategy to treat breathing disturbances in Rett patients.

Abbreviations

1-9

3'	3'-phosphate-end
5'	5'-phosphate-end
5-HT	5-hydroxytryptamine (serotonin)
5-HTR$_X$	serotonin receptor (protein)
8-OH-DPAT	8-hydroxy-2-dipropylaminotetralin hydrobromide

A

A	adenine
ab	antibody
AC	adenylyl cyclase
AMPA	α-amino-3-hydroxy-5-methyl-4-isoxazolepropionic acid
amp	ampicillin
AP	alkaline phosphatase
ATP	adenosine-5'-triphosphate

B

Bp	base pair
BötC	Bötzinger complex
BSA	bovine serum albumin

C

C	cytosine
°C	degree centigrade (Celsius)
cAMP	cyclic adenosine monophosphate
cDNA	complementary desoxyribonucleic acid
CpG	cytosine-phosphate-guanine dinucleotide
CLSM	confocal laser scanning microscopy
C-terminus	carboxy terminus
CV	coefficient of variation

D

d	day
Da	dalton
DAG	diacylglycerol
ddH$_2$O	double distilled water
DEPC	diethylene pyrocarbonate
dH$_2$O	distilled water
DMEM	Dulbecco's modified eagle medium
DNA	desoxyribonucleic acid
DRG	dorsal respiratory group
dsDNA	double-stranded DNA
dNTP	deoxynucleotide triphosphate

E-F

ECL	enhanced chemiluminescence
e.g.	exempli gratia
eGFP	enhanced green fluorescent protein
ELISA	enzyme-linked immunosorbent assay
ER	endoplasmic reticulum
FCS	fetal calf serum
fig.	figure

G

G	guanine
g	gram
GAPDH	glyceraldehyde-3-phosphate-dehydrogenase
GFAP	glial fibrillary acidic protein
GFP	green fluorescent protein

H-K

h	hour
HtrX	serotonin receptor (gene)
Ig	immunoglobulin
IHC	immunohistochemistry
IO	inferior olive
IO_{Pr}	inferior olive, principal nucleus
IR	immunoreactivity
HRP	horse radish peroxidase
k	kilo

L

λ	lambda (wavelength)
l	litre
LB	Luria Bertani medium / lysogenic broth

M

µ	Mikro
m	milli
M	moles per litre
mAb	monoclonal antibody
Mecp2	Methyl-CpG-binding protein 2
min	minute
mRNA	messenger ribonucleic acid
MWM	molecular weight marker

N

n	nano
n =	number of experiments
NA	ambigual nucleus
NCBI	national center for biotechnology information

NMDA	n-methyl-d-aspartate
N-terminus	amino terminus
NTS	nucleus solitary tract

O-P

OD	optical density (absorbance)
P	postnatal stage
PBS	phosphate buffered saline
PCR	polymerase chain reaction
PKA	protein kinase A
PKC	protein kinase C
PLC	phospholipase C
pre-BötC	pre-Bötzinger complex

Q-S

q-PCR	quantitative real time PCR
RT	room temperature
RTT	Rett syndrome
s	second
SEM	standard error oft the mean

T

T	thymine
tab.	table
Taq	Thermus aquaticus
TBS	Tris buffered saline
TM	transmembrane domaine

U-Z

u	units
v	volume
v/v	volume per volume
VRG	ventral respiratory group
WT	wild type
w/v	weight per volume

1. Introduction

'What do you want, boy or girl?' An expectant mother asks her husband. 'I don't mind, the main thing is our child will be healthy'. That is the answer of almost all expectant parents. But for 1 in 10,000 newborn girls these wishes don't come true when the girls are diagnosed with Rett syndrome.

1.1. Rett syndrome

Rett syndrome (RTT) first described by the Vienna physician Andreas Rett (Rett, 1966) has been classified as a progressive neurodevelopmental disorder (International Statistical Classification of Diseases and Related Health Problems (ICD-10): F84.10) caused by different mutations in the X-chromosome-linked *MECP2* gene (Amir et al., 1999). It attracted attention by the medical community as Hagberg and colleagues reported 38 cases from girls (Hagberg et al., 1983). With an estimated evidence of 1 in 10,000 - 15,000 at an age of 32, RTT is the second most common cause for mental retardation after Down syndrome in female (Hagberg, 1985; Percy & Lane, 2004; Fehr et al., 2011).

Affected children apparently develop normal. After six to 18 months of age, stagnation occurs (Stage I) followed by a period of rapid developmental regression (Stage II) where the children lose some of already learned skills, such as walking and purposeful hand use. This phase is accompanied with the onset of deceleration of head growth, which leads to microcephaly by the second year of life (Hagberg et al., 1983). The accelerated loss of communication skills and mobility leads to apathetic behavior and social unresponsiveness (Nomura, 2005). Other autistic features such as expressionless face, lack of eye-to-eye contact and social smiling as well as hypersensitivity to sound become obvious between the regression period, but is less noticeable after school age at a pseudo stationary period (Stage III) (Zappella, 1997; Gillberg, 1986). Characteristic features are also stereotypic hand movements, teeth grinding, night crying, anxiety, and physical complaints, such as gait apraxia, ataxia, dystonia, seizures, severe constipation, oropharyngeal dysfunctions, cardiac abnormalities, osteopenia, and disturbed breathing (Mount et al., 2001; Steffenburg et al., 2001; Hagberg et al., 1983). Despite having a normal appetite, patients lose muscle mass and weight (Chahrour & Zoghbi, 2007).

The last stage is accompanied by accelerated motor deterioration (stage IV). Patients who reached higher age are often wheelchair bound, which in many cases results in scoliosis. Some patients develop motor symptoms characteristic for Parkinson's disease (Hagberg, 2005; Roze et al., 2007). Although the mortality rate increases 1.2% per annum, some RTT patients survive into the sixth or seventh decade (Kerr et al., 1997; Zoghbi et al., 2007).

1.1.1. Disturbed breathing in Rett syndrome

One of the most prominent and striking features is disturbed breathing rhythm. More than half of the RTT patients show breathing irregularities such as forced and deep breathing, air swallowing, Valsalva's maneuvers, breath holding, hyperventilation and apneustic breathing during wakefulness (Lugaresi et al., 1985; Elian et al., 1991; Glaze et al., 1987) as well as during sleep (Rohdin et al., 2007).

About 25% of them show clinically relevant phases of apnea lasting longer than 45 seconds that often occur after hypocapnia caused by hyperventilation (Kerr & Julu, 1999; Schlüter et al., 1995; Kerr et al., 1990).

During apnea, oxygen saturation can drop to life-threatening 50% of normal (Southall et al., 1988; Marcus et al., 1994), which may contribute to sudden death in 25% of RTT patients (Weese-Mayer et al., 2008; Smeets et al., 2012; Kerr & Engerström, 2001).

Early on, respiratory dysfunction was associated with an impaired serotonergic modulation depending on the immaturity of brainstem neurons (Kerr & Julu, 1999; Julu et al., 1997; Rhodin et al., 2007; Smeets et al., 2006).

1.1.2. Genetic background

95% of patients with classical RTT carry mutations in the *MECP2* gene. The gene resides on the X-chromosome (Xq28) and codes for the methyl-CpG binding protein 2 (MeCP2), which was discovered by selective binding to symmetrical 5'-methylated cytosines within a single CpG dinucleotide (Lewis et al., 1992; Meehan et al., 1992; D'Esposito et al., 1996).

Most of these *MECP2* mutations emerge sporadically in the male germ line and hence are inherited from the father (Trappe et al., 2001). Over the past few years more than 2,000 different *MECP2* mutations varying from missense, nonsense, and frame shift mutations as well as larger deletions and insertions have been reported

(Amano et al., 2000; Hampson et al., 2000; Xiang et al., 2000; Archer et al., 2006; Bienvenu et al., 2000; Laccone et al., 2004; Philippe et al., 2006). However, eight mutations, which are mostly caused by C→T transversions, occur more frequently (Bienvenu & Chelly, 2007; Wan et al., 1999).

The gonosomal localization of *MECP2* is causal for the gynecotropism of the disease. As the majority of X-chromosomal genes, *MECP2* is subject to X-chromosome inactivation (XCI). XCI due to gene dosage compensation leads to a mosaic expression pattern of *MECP2* in hemizygotic females. The partial compensation of the mutated *MECP2* allele in turn leads to survival of affected females.

Since the discovery of the genetic cause, there are increasing reports of males diagnosed with RTT that exhibit either a mild form of *MECP2* mutation or an unusual XXY-karyotype known as Klinefelter syndrome (Jan et al., 1999; Meloni, 2000; Schwartzman et al., 2001; Budden et al., 2005; Mittal et al., 2011; Dayer et al., 2007). Males with dire mutations of *MECP2* rarely live beyond 2 years. In one such case, the patient, 16 months of age, succumbed to respiratory failure (Schüle et al., 2008).

In females there are ongoing attempts to correlate the degree of *MECP2* mutation with the severity of the RTT phenotype.

Missense mutations or mutations affecting the C-terminal end of the MeCP2 protein lead to a less severe RTT phenotype than nonsense mutations in its N-terminal region or frame shift mutations (Zapella et al., 2001; Charman et al., 2005; Cheadle et al., 2000). The nonsense mutation Arg270X (codon that codes for arginine at place 270 of the protein) has been associated with increased mortality (Jian et al., 2005).

Another major source for phenotype variability is the XCI pattern, which has been shown by monozygotic twins who carry identical *MECP2* mutations, but exhibit different phenotypes (Coleman et al., 1987; Migeon et al., 1995).

The choice of either the maternal or the paternal X chromosome that will be inactivated normally happens in a random fashion during female embryogenesis and is maintained in descendent cells throughout the lifetime. However, in female patients as well as in mouse models for RTT, a skewed XCI has been observed (Wan et al., 1999; Migeon et al., 1995; Braunschweig et al., 2004; Chahrour & Zoghbi, 2007; Ishii et al., 2001). The investigators showed that the X-chromosome, which carries the mutated *MECP2* gene, is inactivated more frequently than the chromosome that

carries the healthy *MECP2* copy. According to the authors, this effect might be caused by a positive selection and may explain milder forms of RTT.

1.1.3. The methyl-CpG binding protein 2 - MeCP2

The human *MECP2* gene and the mouse ortholog *Mecp2* reside on the X-chromosome and consist of 4 exons (Quaderi et al., 1994; D'Esposito et al., 1996). Alternative polyadenylation within the 3'-untranslated region (UTR) of the fourth exon leads to 4 differentially expressed mRNAs varying in their size, but not in their open reading frame (D'Esposito et al., 1996; Reichwald et al., 2000). The shortest 1.8 kb and especially the longest 10.2 kb transcripts are more abundantly expressed in the brain than the 5.4 kb and the 7.2 kb-transcript, which are the predominant forms in the lung and the spleen (Pelka et al., 2005; Shahbazian et al., 2002a). In 2004, a second MeCP2 isoform was discovered encoded by the *Mecp2e1* mRNA, which is generated by alternative splicing of the exon 2. The lack of exon 2 of the *Mecp2e1* mRNA results in a protein with 498 aa. Hence, it is 21 amino acids larger and possesses a changed N-terminus in comparison with the protein, which is encoded by the *Mecp2e2* transcript (Mnatzakanian et al., 2004; Kriaucionis & Bird, 2004).

With 90%, the *Mecp2e1* transcript represents the dominant form in the brain, where it is basically strongly expressed in comparison to other organs and tissues. Smaller amounts of the *Mecp2* mRNA have also been proven in the lung, thymus as well as in the spleen (Kriaucionis & Bird, 2004).

The well characterized human MeCP2 protein (fig. 1.1) consists of an N-terminal methyl-CpG binding domain and a C-terminal repression domain (TRD) (Nan et al. 1993; Nan et al., 1997). By means of an internal nuclear localization sequence (NLS), which resides within the TRD (Nan et al., 1996), it is transported into the cell nucleus. There it binds preferably to symmetrically methylated cytosines within a single CpG dinucleotide (Lewis et al., 1992; Meehan et al., 1992). By means of the co-repressor Sin3a (Nan et al., 1998), MeCP2 can recruit histone deacetylases (HDACs) that is commonly known as a starting point for chromatin remodeling and for densely packed DNA formation, called heterochromatin. Heterochromatin formation is closely linked to silencing of genes, chromosomal segments, and even whole chromosomes, hence, it regulates epigenetical processes, such as imprinting, position effect, histone code, X-chromosomal inactivation, maternal effects, etc. (Boyes and Bird, 1991; Kass et al., 1997; Henikoff, 2000).

The role of MeCP2 in epigenetical gene silencing has been strengthened by studies showing that MeCP2 is primarily located in heterochromatic DNA foci, such as satellite DNA, centromeres and telomeres and that it can directly repress the transcription of selected genes, e.g. UBE3A, GABRB3, Crh, Fkbo5 and Bdnf (Nan et al., 1997b; Samaco et al., 2009; Nuber et al., 2005; Chen et al., 2003; Martinowich et al., 2003). Furthermore MeCP2 can inhibit the expression and transposition of retrotransposons in a methyl-CpG dependent manner (Muotri et al., 2010).

It has also been shown that MeCP2 can bind to non-methylated DNA as well as to whole nucleosomes directly. Because in a single cell the number of MeCP2 protein copies is as abundantly expressed as nucleosomes exist and MeCP2 can even replace the histone 1 within a histone octamer, it would seem that MeCP2 is more a global regulator than a simple transcriptional repressor. The theory is underscored by microarray analyses from different brain regions comparing mRNA expression between *Mecp2* ko and wt mice. Many genes have been shown to be de-regulated (Jordan et al., 2007; Urdinguio et al., 2008; Ben-Shachar et al., 2009; Chahrour et al., 2008). Surprisingly, most of them were down-regulated in the absence of MeCP2. Several genes, such as Sst, Oprk1, and Gprin1 are directly activated by MeCP2 through a direct interaction with the transcriptional activator cAMP responsive element binding protein 1 (CREB1) (Chahrour et al., 2008).

Although MeCP2 is considered to be important during brain development, it is most abundantly accumulated in postmitotic adult neurons, where it is thought to be indispensible for maturation, synaptogenesis, and the maintenance of neuronal function (Kishi & Macklis, 2004; Guy et al., 2011). Smaller amounts of MeCP2 are also found in glial cells supporting neurons to their axonal outgrowth (Ballas et al., 2009).
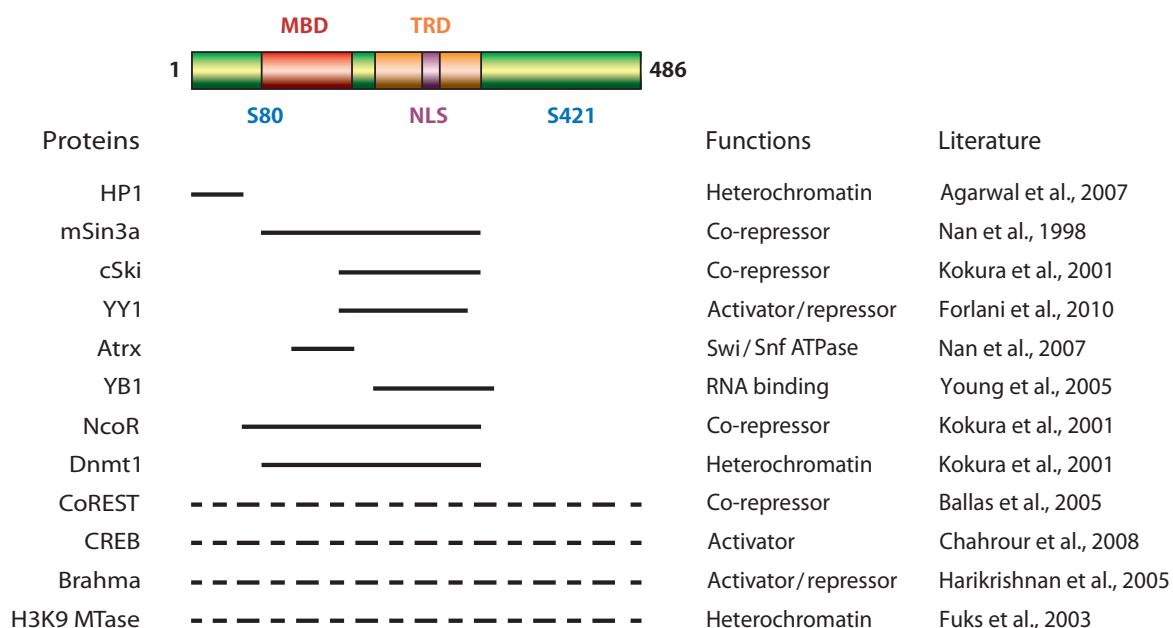
Figure 1.1. **Schematic representation of the human methyl-CpG protein 2 (MeCP2) protein with potential binding partners and their function.**

The protein consists of 486 amino acids and possesses a N-terminal CpG-binding domain, a C-terminal transcription repression domain (TRD), and a nuclear localization sequence (NLS). Horizontal lines show the binding region of identified interaction protein partners and their function on the right. Dashed lines indicate that interaction region is not defined yet. S80 and S421 indicate serine residues susceptible for phosphorylation (modified according to Guy et al., 2011).

1.1.4. The mouse model of Rett syndrome

The transcription factor MeCP2 is of particular interest, not only as a single gene responsible for the complex RTT disorder with its broad spectrum of symptoms, but also in its role of modulating epigentical processes.

Pathological effects on the murine brain due to *Mecp2* mutations could help to identify genes involved in fundamental neurophysiological and molecular processes that are currently poorly understood. Therefore, various mouse models have been developed (Shahbazian et al., 2002b; Dani et al., 2005; Chahrour et al., 2008; Chen et al., 2001; Guy et al., 2001; Guy et al., 2007; Goffin et al., 2012).

In this study, male *Mecp2$^{-/y}$* mice with a knockout of *Mecp2* (Rett mice), which are maintained on a C57BL/6 background and generated by Guy and colleagues in 2001 using Cre-*loxP* technology, was used as animal model for RTT pathology.

This mouse model displays many RTT-related motor disturbances within a relative developmental time frame that corresponds to the human disorder. Similar to RTT patients, *Mecp2$^{-/y}$* mice show no initial disturbed phenotype. Between postnatal day (P) 14 and P21 they start to develop a stiff and uncoordinated gait produced mainly in the hind limbs.

Almost all *Mecp2$^{-/y}$* mice show reduced body and brain weight relative to wt mice. These mice are less mobile and unresponsive to external stimuli, frequently exhibit hind limb clasping and tremor, and are in poor general condition before dying at approximately 54 days of age (Chen et al., 2001; Guy et al., 2007). At autopsy, brains are smaller and lighter. Neuronal cell bodies and nuclei are reduced in the hippocampus, cerebral cortex, and the cerebellum (Chen et al., 2001). Hemizygous *Mecp2$^{-/+}$* female mice show no initially significant phenotype. Unlike MeCP2 deficient male mice, they show a later onset of symptoms. Between 3 to 9 months of age, one-half of the *Mecp2$^{-/+}$* mice develop obvious symptoms, including hind limb clasping, breathing abnormalities and inertia, but to a milder degree (Guy et al., 2001).

1.1.5. Breathing phenotype in *Mecp2$^{-/y}$* mice

In vivo investigations by whole body plethysmography demonstrate that at birth almost all MeCP2-deficient mice show normal breathing until 28 days of age. Henceforward, more and more individuals develop an arrhythmic breathing pattern with increased variability in the duration of the respiratory cycle. Between one and two months of age, almost all *Mecp2$^{-/y}$* mice as well as elder hemizygous *Mecp2$^{-/+}$* female mice (> 3 months of age) display an unambiguous disturbed erratic breathing phenotype with characteristically frequent apneas lasting one to two seconds (Guy et al., 2001; Viemari et al., 2005; Abdala et al., 2010). *In situ* studies of phrenic and vagal motor nerve activity patterns revealed that this is caused by a prolonged post-inspiratory phase (Stettner et al., 2007). Similar to human RTT patients, apnea is often accompanied by preceding hyperventilation cycles, but is not a result of impaired sensing of peripheral oxygen chemoreceptors (Bissonnette and Knopp, 2008). After onset, these breathing disturbances worsen, and it is assumed that the mice eventually die from respiratory arrest, usually around P56. Before attempting to analyze the progression of breathing dysrhythmias in RTT, it is essential to consider how respiratory rhythm and ventilation seem to be controlled in the healthy mammalian respiratory network.

1.2. The ponto-medullary respiratory network

Airflow into and out of the lungs is a fundamental process that provides the organism with oxygen and removes carbon dioxide from the blood. Effective ventilation in mammals is normally supported through a respiratory rhythm consisting of three sequential temporal phases: inspiration (I), post-inspiration (post-I), and expiration (E) (Richter, 1982; Ramirez & Richter, 1996).

The constitutive 3-phase rhythm originates from the functional interactions between six different classes of bulbar respiratory neurons, each distinguished according to rhythm and pattern of membrane potential and action potential discharge (fig. 1.2).
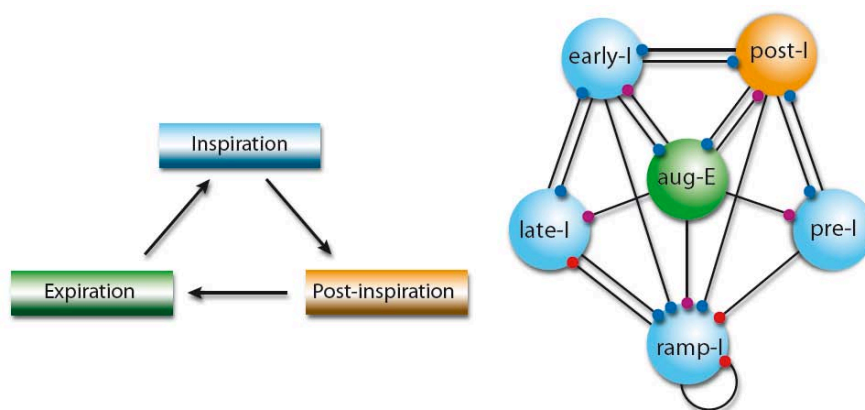
Figure 1.2. Schema of a simplified oscillator model of the respiratory network.
The neuronal respiratory rhythm is divided into inspiration (I), post-inspiration (post-I), and expiration (E). According to this oscillator model, the three-phase rhythm is generated by six distinct classes of respiratory neurons. Pre-inspiratory (pre-I), early-inspiratory (early-I), ramp-inspiratory (ramp-I) and late inspiratory (late-I) neurons regulate the I-phase. Ramp-I neurons trigger discharges in phrenic and inspiratory intercostal motoneurons. Post-I and late-I neurons are involved in inspiratory phase termination. Early-I neurons delay the onset of post-I and late-I neuron discharges. E-neurons fire during active expiration, and pre-I neurons are thought to contribute to phase transition from inspiration to expiration. In this network model, reciprocal GABAergic and glycinergic inhibition between the respiratory neurons plays a pivotal role in cycling between the three phases. The six types of neurons receive tonic excitatory synaptic drive from glutaminergic neurons of the reticular activating system (RAS) and brainstem chemoreceptor network.

The network depicted here is mainly located within the ventral respiratory group (VRG), a bilaterally distributed column in the ventral region of the medulla (fig. 1.3). In addition to the VRG neurons depicted here, others with similar rhythmic respiratory properties are found in the nucleus of the solitary tract (NTS) on the dorsal region of the medulla, and in the nucleus Kolliker-Fuse (K-F) and medial parabrachial region (MPBR) of the pons. The NTS is a primary receiving area for pulmonary sensory afferents, and along with K-F and MPBR neurons, plays a role in lung inflation-dependent depression of inspiration and in other aspects of ventilatory control (Rybek et al., 2004). Within the VRG resides the pre-Bötzinger complex (pre-BötC), which appears to be of particular importance for modulation of the respiratory rhythm. It contains five of the six major classes of respiratory neurons that are thought to be crucial for rhythm generation (Smith et al., 1991; Connelly et al., 1992). Bilateral lessoning of the pre-BötC abolishes the respiratory rhythm (Ramirez et al., 1998). In addition, other regions of the VRG also contain neurons with identical discharge properties along with synaptic connections that establish them as being important for

respiratory rhythm control (Ezure, 1990). In line to their synaptic projections, membrane potential oscillations and firing patterns, 4 classes of VRG neurons have been identified as being active during inspiration. Ramp-I neurons exhibit a slow rising, ramp-like discharge pattern. Many of them are bulbospinal and have excitatory synaptic connections with phrenic and intercostal inspiratory motoneurons, while others project to vagal pulmonary motoneurons. They give rise to the discharge patterns and timing that regulate contractions of the chest wall, diaphragm, and control the patency of the tracheobronchial airways. Late-I and post-I neurons have inhibitory synaptic inputs to ramp-I neurons that lead to termination of the inspiratory phase. Early-I neurons have reciprocal inhibitory connections with post-I and late-I neurons. When early-I discharge is terminated by intrinsic membrane conductances, post-I and late-I neurons are released from inhibition and fire to terminate inspiration. Late-E (E_2) neurons of the caudal VRG discharge to promote active contraction of the expiratory intercostal muscles and abdomen. They are not essential for constitutive breathing since expiration for the most part is passive. Pre-I neurons discharge in parallel with cessation of E_2 neurons, hence they are thought to contribute to phase transition from expiration to inspiration.

1.3. Neurochemical control of respiratory rhythm in the VRG

The six classes of VRG neurons receive tonic excitatory glutamatergic input from neurons of the brainstem reticular activating system (RAS) and brainstem chemoreceptor network, resulting in activation of postsynaptic AMPA and NMDA receptors. In addition, VRG neurons interact antagonistically through glycinergic and GABAergic inhibitory synaptic connections (Ezure et al., 1990; Merril et al., 1983; Bianchi et al., 1995; Schmid et al., 1996). Simultaneous blockade of glycine and GABA receptors within the pre-BötC with strychnine and bicuculline leads to loss of rhythmic breathing in *in vivo* and *in vitro* (Pierrefiche et al., 1998; Paton et al., 1994; Paton & Richter, 1995) and disrupts respiratory rhythmic neuron discharges in *in vitro* experiments (Ramirez et al., 1996).

Respiratory network rhythm and pattern is also modulated by an assortment of synaptically released neurochemicals such as ATP, neurokinins, histamine, acetylcholine, dopamine, noradrenalin, opioids, and serotonin.
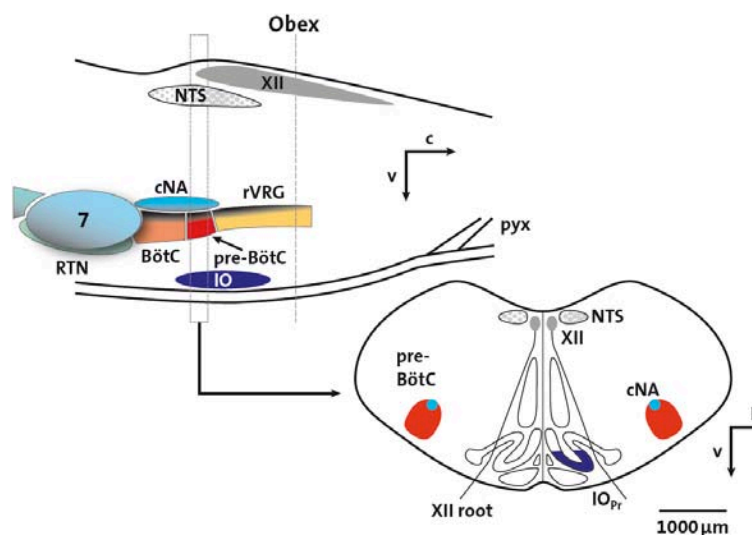
Figure 1.3. Schema of the localization of regions important for respiratory rhythm generation. The schematic representation shows a sagittal (left) and a transversal section (right) from a mouse brainstem. The breathing center, which hosts the respiratory network (colored) is column-like bilaterally arranged. The pre-Bötzinger complex (pre-BötC, red) is of special importance for the respiratory rhythm generation. The principal nucleus of the inferior olive (IO_{Pr}) is shown as an anatomical landmark for the pre-BötC. Abbreviations: thalamic reticular nucleus (RTN), compact part of the nucleus ambiguus (cNA), Bötzinger complex (BötC), nucleus tractus solitarii (NTS), ventral respiratory group (VRG), hypoglossal nucleus (XII), pyramidal decussation (pyx), rostral (r), caudal (c), lateral (l).

1.4. Serotonin

The biogenic monoamine serotonin (5-hydroxytryptamine; 5-HT) was originally isolated from the blood serum and found to increase constrictor tone in a variety of blood vessels (Rapport et al., 1948). It is synthesized in a two-step mechanism from the precursor amino acid L-tryptophan (5-HTP), catalyzed by the rate-limiting enzyme tryptophan hydroxylase (TPH) and by amino acid decarboxylase (DDC). After release and binding to its receptors, serotonin is removed from the synaptic cleft by re-uptake through the serotonin transporter SERT. Intracellular serotonin can either be restored in vesicles by vesicular monoamine transporter (VMAT2) or be degraded to 5-hydroxyindolacetic acid (5-HIAA) by monoamine oxidase A (MAO-A) (Hilaire et al., 2010).

Although roughly 95% of serotonin is built and located in enterochromaffin cells in the gastrointestinal tract regulating intestinal mobility, which is important for the energy balance (Tecot, 2007), 5-HT and its receptors are present in all organs and tissues,

including the brain (Berger et al., 2009). Serotonin is involved in almost al basic physiological functions and behaviors, such as eating, cognition, sleep, stress, aggression, circadian rhythmicity, neuroendocrine functions, and breathing (Ciarleglio et al., 2011; Dinan, 1996; Geldenhuys et al., 2011; España & Scammell, 2011; Bailer & Kaye, 2011; Magalhães et al., 2010). Moreover, due to its influence on cell division, neuronal maturation, and axonal outgrowth, serotonin is also involved in developmental processes (Sodhi & Sanders-Bush, 2004).

1.4.1. Serotonin in the brain

The presence of serotonin in the mammalian brain was first described in the 1950s (Twarog & Page, 1953). It is mainly located and produced by cell bodies, which are located in the previous defined raphé nuclei. The raphé nuclei represents nine discrete cell clusters (B1 - B9) within the pons and the upper medulla lying to either side of the midline (Dahlström & Fuxe, 1964; Steinbusch, 1981). Each nucleus projects to different regions within the CNS (fig. 1.4). Nuclei, which are more rostrally and dorsally located (B6 - B9), innervate via the median forebrain bundle many parts of the cortex, hippocampus, limbic system, and hypothalamus, whereas fibers from nuclei that are located caudally (B1 - B4) mainly project to the gray matter of the spinal cord and the brainstem (Hornung, 2003; Törk, 1990; Jacobs & Azmita, 1992). Due to the strong innervation and the ubiquitous expression of serotonin receptors in almost all cytoarchitectonic regions of the brain it is not surprising that an impaired serotonergic system is associated with several neurological aliments, such as obsessive-compulsive disorder, anxiety, disorders of energy balance, autism, schizophrenia, and depression (Woolley & Shaw, 1954; Kinney et al., 2011).
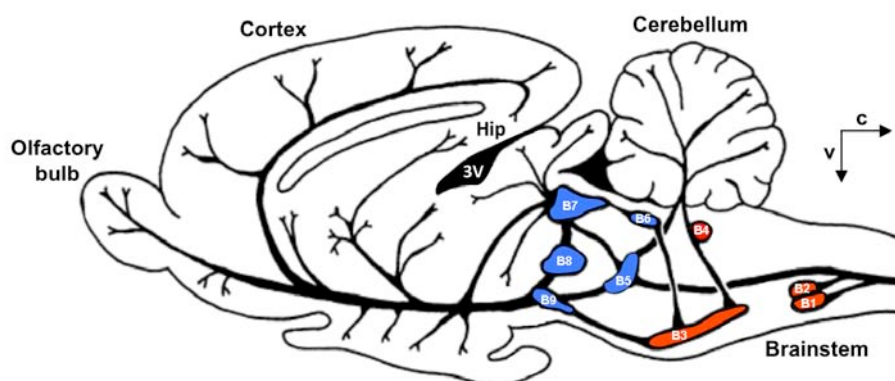
Figure 1.4. Schema of the anatomical localization of the rodent serotonergic system.

The cell bodies of serotonergic neurons are located in distinct nuclei (B1 - B9) innervating almost all regions of the brain. The more dorsal and medullary located nuclei (B1 - B4, red) project to various regions in the brainstem including the respiratory system. Abbreviations: hippocampus (Hip), third ventricle (3V), caudal (c), ventral (c).

1.4.2. Expression and function of serotonin receptors in the respiratory network

The pivotal role of the serotonergic system for stable breathing has been shown in many studies over the past three decades (Fallert et al., 1979; Monteau & Hillaire, 1991; Hilaire et al., 1993; Lindsay & Feldman, 1993; Morin et al., 1991; Lalley, 1986; Lalley et al., 1995; Bou-Flores et al., 2000; Pena & Ramirez, 2002; Richter et al., 2003; Ladewig et al., 2004; Ptak et al., 2009).

Hence, it is not surprising that the disturbed breathing pattern of diverse neurological disorders including Prader Willi syndrome (PWS), Joubert syndrome (JS), sleep apnea syndrome (SAS), congenital central hypoventilation syndrome (CCHS), and sudden infant death syndrome (SIDS) have attributed to impaired serotonergic transmission (Ren et al., 2003; Pagliardini et al., 2005; Gaultier & Gallego, 2008; Saito et al., 1999; Waters, 2010; Weese-Mayer et al., 2008; Paterson et al., 2009).

The brainstem respiratory network is densely innervated by predominantly descending fibers from serotonergic neurons of the caudal raphé nuclei (Connelly et al., 1989; Holtman, 1988). These neurons are tonically active and exhibit ongoing discharges to release continuously serotonin, which presumably influences breathing and respiratory responses to hypoxia (Richter et al., 1999; Depuy et al., 2011).

The importance of the serotonergic system to the rhythmic activity is further supported by abundant 5-HT receptor expression in the respiratory network (Richter et al., 2003; Hilaire et al., 2010).

According to the International Union of Basic and Clinical Pharmacology (IUPHAR) serotonin receptors are divided into seven sub-families (Hoyer et al., 1994).

With the exception of 5-HT$_{3A-C}$ receptors, which are ligand-gated ion channels, 5-HT receptors belong to a large group of G-protein-coupled receptors (GPCRs) (fig. 1.5). It is known that thirteen of the approximately 1,000 identified genes that the mammalian genome codes for GPCRs (O'Callaghan et al., 2012; Fredriksson et al., 2003) are selectively activated by serotonin (Hoyer et al., 2002) (fig. 1.5). Alternative splicing of the C-terminus of 5-HT$_4$ and 5-HT$_7$ receptors as well as alternative RNA editing of 5-HT$_{2C}$ receptors additionally increase the number of serotonin receptor isoforms (Burns et al., 1997; Blondel et al., 1998; Heidmann et al., 1997; Azim et al., 2012).
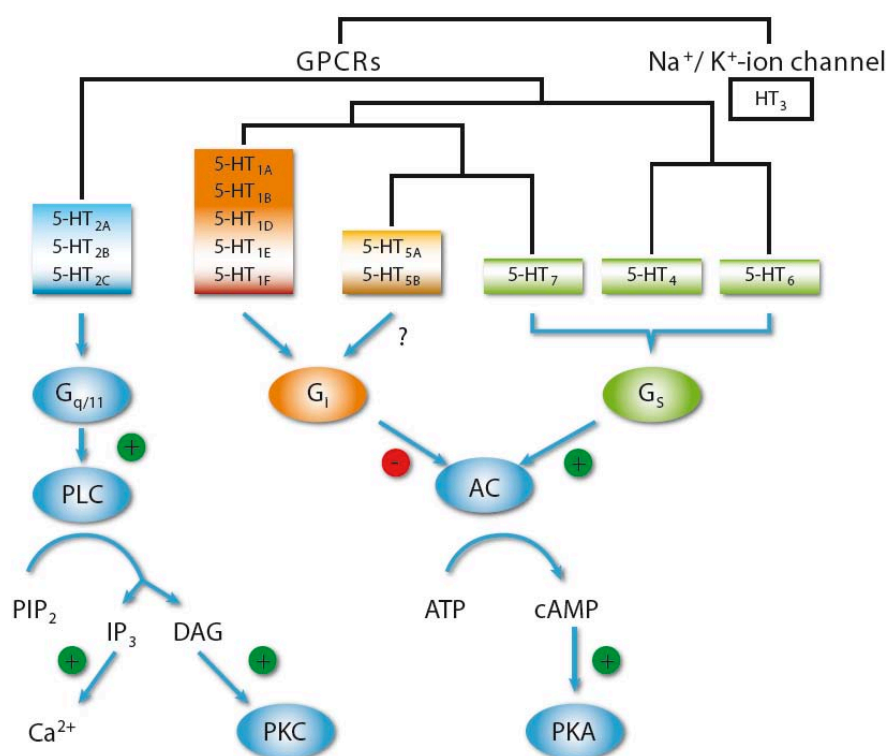
Figure 1.5. Phylogenetic tree of the serotonin receptor (5-HTR) family and their signaling properties.

Except for the 5-HT$_3$ subclass, which represents a ligand-gated Na$^+$/K$^+$ ion channel, all 5-HT receptors belong to the superfamiliy of Rhodopsin-like G-protein coupled receptors (class A). 5-HTR$_2$ subclass activates phospholipase C (PLC) by the G-protein G$_{q/11}$, which cleaves phosphatidylinositol 4,5-bisphosphate (PIP$_2$) in inositol 1,4,5-trisphosphate (IP$_3$) and diacylglycerol (DAG), which in turn results in an increase of intracellular Ca^{2+} and activation of protein kinase C (PKC). The remaining 5-HTRs either increase or decrease the intracellular cAMP level by activation or inhibition of the adenylyl cyclase C (AC) mediated by the inhibitory (G$_i$) or stimulatory G-protein (G$_s$) pathway. Increased cAMP

concentrations activate the protein kinase A (PKA). The putative G-protein of 5-HTR_5 are currently unknown, but are expected to bind to G_i due to sequence homology to 5-HTR_{1A}.

As is typical for metabotropic GPCRs, serotonin receptors are integral membrane proteins comprising seven hydrophobic transmembrane domains connected by three intracellular loops (termed I1 - I3) and three extracellular loops (termed E1 - E3). Furthermore, serotonin receptors possess an extracellular N-terminus and an intracellular C-terminus, where they couple to their corresponding heterotrimeric G-protein.

Depending on the class of the alpha subunit of the heterotrimeric G-protein associated with the serotonin receptor, they switch on different signaling pathways.

Activation of the 5-HT_2 receptor class turns on the $G\alpha_{q/11}$ mediated signaling pathway, which results in the activation of phospholipase C (PLC), leading to elevation of second messengers diacyl glycerol (DAG) and inositol 1,4,5-trisphosphate (IP_3) and, subsequently, to an increase of the cytoplasmic Ca^{2+} concentration. 5-HT_4, 5-HT_6, and 5-HT_7 receptors couple preferably to stimulatory G-proteins ($G\alpha_s$) leading to activation of the AC and consequently to intracellular cAMP elevation.

The 5-HTR_1 class comprises 5 subtypes (A - F; currently there is no 5-HTR_{1C} defined), which couple preferably to inhibitory G-proteins ($G\alpha_i/G\alpha_o$) to inhibit adenylyl cyclase avoiding cAMP formation (Bockaert et al., 2006).

The two members of the 5-HT_5 subclass are distinguishable from other serotonin receptor classes, but less characterized in their physiological response (Hoyer et al., 2008). In rodents they share an unusual high homology (> 75%), but they exhibit only a low amino acid sequence homology (< 50%) to other serotonin receptors especially in their transmembrane regions (Noda et al., 2004; Hoyer et al., 2002). 5-HTR_{5A} has been shown to couple also to $G\alpha_i/G\alpha_o$, whereas the corresponding G-protein for the 5-HTR_{5B} is still unknown (Francken et al., 1998; Hannon & Hoyer 2008).

The expression of several 5-HT receptors within the respiratory network and their relevance for stable breathing has been described over the past two decades (Richter et al., 2003). For example, activation of the 5-HTR_{1A} is known to overcome apneustic breathing caused by pharmacological treatment or disturbances within the brainstem respiratory network (Garner et al., 1989; Lalley et al., 1994; Wilken et al., 1997; El-Khatib & Jamaleddine, 2003). The augmentation of 5-HTR_{1A}-mediated inhibitory glycinergic inward Cl^- currents in predominantly early-I neurons results in disinhibition of antagonistically connected post-I-neurons, which leads to termination

of the inspiratory phase (Manzke et al., 2009; Manzke et al., 2010). Moreover, pharmacological activation of $5\text{-}HT_4$ receptors reverses opioid induced breathing depression without loss of analgesia (Manzke et al., 2003), and pre-synaptically located $5\text{-}HT_{1B}$ receptors modulate the central excitatory synaptic drive to phrenic motoneurons (Di Pasquale et al., 1997). The $5\text{-}HTR_{2A}$, which is abundantly expressed in neurons of the pre-BötC, stimulates breathing and helps to maintain gasping during hypoxia or ischemia (Lalley et al., 1995; Pena & Ramirez, 2002; Niebert et al., 2011; Tryba et al., 2006; Toppin et al., 2007). The $5\text{-}HTR_{2A}$ seems to be constantly activated by serotonin, since receptor blockade decreases the frequency of the phrenic nerve discharges in *in situ* (Niebert et al., 2011). An activating effect on phrenic nerve discharge pattern has also been reported for $5\text{-}HTR_{2B}$ (Niebert et al., 2011) and $5\text{-}HTR_{2C}$.

The modulation effects through serotonin receptors targets predominantly glycinergic inhibitory interneurons affecting inhibition of antagonistically connected respiratory neurons, but is also important for synchronization of synergistic neurons (Lalley et al., 1994; Lalley et al., 1995; Manzke et al., 2009; Manzke et al., 2010)

Systemic administration of selective $5\text{-}HTR_7$ agonists reduces respiratory frequency in rats studied in *in situ* experiments (Manzke et al., 2009). As the receptor is important for developmental brain plasticity, it may play a role in the maturation and correct integration of the respiratory network (Shevtsova et al., 2011).

1.4.3. Serotonergic system in RTT

Serotonergic effects on breathing disturbances were originally attributed to direct modulation of the respiratory rhythm (Nomura et al., 1987; Segawa, 2001; Kerr & Julu, 1999) or to effects on neurodevelopmental processes such as cell division, neuronal migration, cell differentiation, and synaptogenesis (Lauder, 1993; Azmitia 2001; Vitalis & Parnavelas, 2003).

Although in *Mecp2* null mice the serotonergic transmission is deregulated no alterations in the raphé nuclei and its ascendant serotonergic fibers are observed at P21 and P56 (Santos et al., 2010). Some groups reported reduced levels of serotonin in different brain regions and in the cerebrospinal fluid in both human patients as well as in MeCP2 deficient mice (Zoghbi et al., 1989; Paterson et al., 2005; Viemari et al., 2005). Additionally, some patients show abnormalities in the serotonin transporter (SERT).

However, until now there is no information about specific genes involved in the serotonergic transmission, which may be altered in regions of the respiratory network of *Mecp2*$^{-/y}$ mice.

2. Aim of this work

As the foundation for this dissertation study, the hypothesis was established that impaired serotonergic transmission and/or failure of glycinergic inhibition contributes to breathing disturbances in RTT patients. Accordingly, a major goal of this thesis is to investigate gene expression of specific serotonin receptors and transporters as well as glycine receptor subunits and transporters within the VRG in a mouse model for RTT that has a knockout in the *Mecp2* gene encoding for the transcription factor MeCP2. Positive findings will hopefully lead to a detailed examination of potential candidates in terms of their gene regulation, signaling pathway, and their pathological effects on breathing.

As serotonin receptors are forceful targets for pharmacological treatment, this study may contribute to find new strategies to treat life-threatening breathing disturbances in RTT patients.

3. Materials and Methods

3.1. Materials

Materials used in this thesis are listed in the following tables. Unless otherwise stated, materials were purchased from companies located in Germany.

3.1.1. Instruments

Autoclave	
Systec 5075 ELV	Systec GmbH (Wettenberg)
Blotting-Apparatus	
iBlot	Invitrogen (Karlsruhe)
Cell-counting chamber	
Neubauer cell chamber	Labor Optic (Friedrichsdorf)
Countess®	Invitrogen
Centrifuges	
5415R	Eppendorf (Hamburg)
Centrifuge 5415D	Eppendorf
Mikro 200R	Hettich (Tuttlingen)
Documentation	
AlphaImager EC (western blot)	Alpha Innotec Corporation (San Leandro, USA)
*BioVision Video documentation (*agarose gel)	Peqlab (Erlangen)
Electrophoresis chambers	
Horizontal, self-made (agarose gel)	by workshop UMG (Göttingen)
Vertical, *XCell SureLock*	Invitrogen
Freezers	
Comfort (-20°C)	Liebherr (Biberach)
U535 Innova (-80°C)	New Brunswick Scientific (Edison, USA)
Heat blocks	
Thermofixer comfort	Eppendorf
Thermostat 5320	Eppendorf
Incubators	
Incucell	IUL Instruments (Königswinter)

Sanyo CO2-Inkubator MCO 18AIC	MS Laborgeräte (Wiesloch)
Unimax2010	Heidolph (Schwabach)

Luminometer

Infinite M200 PRO	Tecan (Crailsheim)

Microtoms

CM1510S	Leica Microsystems (Bensheim)
Frigomobil	Reichert-Jung (Seefeld)
Hm 400	Microm (Walldorf)
Ultramikrotom	Leica

Microscopes

EM 900	Zeis (Göttingen)
Meta-LSM 510	Zeiss

Peristaltic pump

Pump 101U	Watson and Marlow (Rommerskirchen)

pH meter

inoLab pH 720	WTW (Weilheim)

Pipettes

2.5-, 10-, 20-, 100-, 200, 1000-µl	Eppendorf
10-, 20-, 100-, 200, 1000-µl	Gilson (Limburg-Offheim)
300-µl multichannel	Eppendorf
accu-jet	BRAND GmbH & CoKG (Wertheim)
Macro pipette controller	BRAND GmbH & CoKG,
Multipipette plus	Eppendorf

Photometer

NanoDrop 1000 Spectrophotometer	Thermo Fisher Scientific (Dreieich)

Power supplies

EV-231	Biotec-Fischer (Reiskirchen)
Power-Pac 3000	BIO-RAD (München)

Shakers / wheeled walker

Duomax 1030	Heidolph Instruments
Roller Shaker "Assistent" RM5	Glaswarenfabrik Hecht (Sondheim)
Rotamax 120	Heidolph Instruments
Titramax 1000	Heidolph Instruments
Genius 3	IKA (Staufen)

Sterile bench

HeraSafe HSP	Heraeus (Berlin)

Scales

572	Kern & Sohn (Balingen-Frommern)
Alt 100-5AM	Kern & Sohn

Thermocyclers

Labcylers	SensoQues (Göttingen)
C100 Thermal Cycler / CFX96 Real-Time System	Bio-Rad

Ultrasonic homogenizer

HD2070 MS72	BANDELIN electronic (Berlin

Water bath

Ultrasonic cleaner	VWR International (Darmstadt)

3.1.2. Consumables

Aluminum foil	Roth (Karlsruhe)
Cell culture plates (4-, 6-, 24-well; 60 cm^2 dishes)	Nunc (Langenselbold)
Centrifuge tubes (15-, 50-ml)	Greiner (Frickenhausen)
Combitips (1-, 5-, 10-ml)	Eppendorf (Hamburg)
Coverslips (24 x 50 mm)	Roth (Karlsruhe)
Glasware	Duran Group (Mainz)
Microtiter plates (96-well)	Nunc
Microscope slides (Superfrost® Plus)	Thermo Fisher Scientific (Dreieich)
Nitrile gloves	Top glove (Duisburg)
Parafilm	Pechiney (Chicago, USA)
PCR plates (96-well)	BIO-RAD (Müchen)
Pipette tips (10-, 100-, 200-, 1000-µl)	nerbe plus (Winsen/Luhe)
Reaction tubes (0.2-, 0.5-, 1.5-, 2-ml)	nerbe plus
Surgery	B. Braun (Melsungen)

(cannula, scalpels, syringes)

Serological pipettes (5-, 10-, 25-, 50-ml)	Techno Plastic Products (Trasadingen, Suisse)

3.1.3. Chemicals, biochemical and miscellaneous reagents

Name	Abbreviation /Chemical formula	Company
1,4-Dithiothreitol	DDT	AppliChem (Darmstadt)
Acetic acid (100%)		Roth (Karlsruhe)
Acetone		Roth
Agarose (for electrophoresis)		Peqlab (Erlangen)
ß-Mercaptoethanol	β-ME	Merck (Darmstadt)
BSA fraction V		Roth
Calcium chloride	$CaCl_2$	Roth
Chloroform		Roth
Dapi Fluoromount-G		Southern Biotech (Birmingham, USA)
Desoxynucleosid-5'-triphosphate (dNTPs, 100mM)		Invitrogen (Karlsruhe)
Dimethyl sulfoxide	DMSO	Sigma-Aldrich (Taufkirchen)
ECL Western Blot kit		Amersham, GE Healthcare (München)
Ethanol, absolute ultra pure	EtOH	Roth
Ethanol, denatured (99%)		CVH (Hannover)
Ethidium bromide		Merck
Ethylenediaminetetraacetic acid	EDTA	Roth
Ficoll 70		Sigma-Aldrich
GeneRuler® 1 kb-DNA-Ladder		Fermentas (St. Leon-Rot)
GeneRuler® 100 bp-DNA-Ladder		Fermentas
Glucose		Roth
Glycerol		Sigma-Aldrich
Glycine		Roth
GlycoBlue		Ambion

Hydrochloric acid (32%)	HCl	Roth
IGEPAL CA-630		Sigma-Aldrich
Immersion oil		Zeiss (Göttingen)
Isopropanol (ultra pure)		Roth
LB Agar		Roth
LB Broth		Roth
Lipofectamine2000		Invitrogen
Lithium chloride	LiCl	Roth
Magnesium chloride	$MgCl_2$	Roth
Magnesium sulfate	$MgSO_4$	Roth
Methanol	MeOH	Roth
Nuclease-Free Water		Ambion
Paraformaldehyde	PFA	Roth
Ponceau S		Sigma
Potassium chloride	KCl	Roth
Potassium dihydrogen phosphate	KH_2PO_4	Roth
Precision Plus Protein™ Kaleidoscope™ protein standard		BIO-RAD
Protease inhibitor cocktail		Fermentas
Roti phenol		Roth
Saccharose		Roth
Salmon Sperm DNA/Protein A Agarose		Millipore (Eschborn)
Sodium acetate	NaAc	Roth
Sodium azide	NaN_3	Roth
Sodium chloride	NaCl	Roth
Sodium deoxycholate		Roth
Sodium dodecyl sulfate	SDS	Roth
Sodium hydrogen carbonate	$NaHCO_3$	Roth
Sodium hydrogen phosphate	Na_2HPO_4	Roth
Sodium hydroxide	NaOH	Roth
Tris		Roth
Triton X-100		Sigma-Aldrich
Trizol		Invitrogen

Tween® 20	Sigma-Aldrich

3.1.4. Kits and ready-to-use material

Name	Company	Application
D_C Protein Assay	BIO-RAD (München)	Protein determination
DirectX Direct Cyclic AMP	ARBOR ASSAYS (Michigan, USA)	cAMP measurements
Dual-Luciferase® Reporter Assay	Promega (Mannheim)	Promoter assay
HISpeed Plasmid Maxi	Qiagen (Hilden)	Plasmid preparation
iBlot Gel Transfer Stacks Nitrocellulose, Regular	Invitrogen (Karlsruhe)	Protein transfer
iScript cDNA Synthesis	BIO-RAD	cDNA synthesis
Novex 4 - 20% Tris Glycine Gel	Invitrogen	SDS page
OIAprep Spin	Qiagen	Plasmid preparation
QIAquick Gel Extraction	Qiagen	DNA purification
QIAquick PCR Purification	Qiagen	DNA purification

3.1.5. Enzymes

Name (conc.)	Company	Application (final conc.)
Alkaline phosphatase (1 u/µl)	Fermentas (St. Leon-Rot)	Cloning (1: 30)
Benzonase (250 u/µl)	Sigma-Aldrich (Taufkirchen)	Protein extraction (1: 1,000)
*Bmt*l (10 u/µl)	NEB	DNA restriction (1 : 30)
DNase (10 u/ml)	Fermentas	RNA extraction (1 : 50)
*EcoR*l (10 u/µl)	NEB	DNA restriction (1 : 30)
Fast SYBR® Green (2x)	Applied Biosystems	q-PCR (1x)
Proteinase K (16.4 mg/ml)	Fermentas	ChIP (1 : 100)
RNase (10 mg/ml)	Fermentas	ChIP (1 : 1,000)
T4 DNA Ligase (1 u/µl)	Fermentas	Cloning (1: 20)

*Xho*I (10 u/µl)	NEB	DNA restriction (1 : 30)

3.1.6. Plasmids

Name	**Insert**	**Application**
pcDNA3.1(-)	-	Eukaryotic overexpression
pEGFP-Endo	Fusion construct of eGFP and Rab7 (Choudhury et al., 2002)	Eukaryotic overexpression (marker for endosomes)
pEYFP-ER	Fusion construct of eYFP and targeting sequence of calreticulin (Fliegel et al.,1989)	Eukaryotic overexpression (marker for endoplasmic reticulum)
pEYFP-Lyso	Fusion construct of eYFP and Lamp1 (Sherer et al., 2003)	Eukaryotic overexpression (marker for lysosome)
pEYFP-Mem	Fusion construct of EYFP and N-terminal 20 amino acids of neuromodulin (Skene & Viràg, 1989)	Eukaryotic overexpression (marker for cell membrane)
pEYFP-Mito	Fusion construct of eYFP and the mitochondrial targeting sequence from of human cytochrome c oxidase (Rizzuto et al., 1989)	Eukaryotic overexpression (marker for mitochondria)
pGL4	*Htr5* promoter	Promoter assay
pTarget	*Mecp2*	Eukaryotic overexpression
pTarget	Fusion construct of GFP and $G_{\alpha i3}$	
pTarget	Fusion construct of GFP and $G_{\alpha s}$	

3.1.7. Primers for q-PCR

Gene	**Accession number**	**Sequence (5'→ 3')**
		Forward **Reverse**
Glra1	NM_020492.3	CATTGTATTCTTCAGCCTTGC ACAAGTCAGGCTTCCAGATG
Glra2	NM_183427.4	CAAACCACTTCAGGGAAGC CAAATCCAGGGAATCATCTG
Glra3	NM_080438.2	GGATCCCGGGCCTCCTTACC

		TCCCTCACCTCATCATCCGTGTC
Glra4	NM_010297.2	TGTTCTCTACAGCATCAGATTG CAGGATGACGATGAGTAGGC
Glrb	NM_010298.5	GTACTTGTGCCCATCTCAGC GTCAGTGCATCTGAGCCTCT
Gphn	NM_145965.2	CCAAGATCCTTCTTTGTTGGGTGGG AGAGAGCATGCCCAGAGGTGTG
Slc6a9	NM_145965.2	AGTCAAGTCTTCAGGGAAAGTG TTGGTGATACTGATAATGACGC
Slc6a5	NM_148931.3	CACCACTACCATACCGGAG TCCACACAGACACAGGACC
Atf7	NM_146065.1	TGCCCAGCCACAGGTCTCTC AGGCTGCAGCTCTGTTTCGC
Mapk14	NM_011951.3	GGAGGAATTCAATGACGTGTACCTGG CATCAGTGTGCCGAGCCAGC
Gapdh	NM_008084.1	CAAGCTCATTTCCTGGTATGAC AGGCCCCTCCTGTTATTATG
Hprt	NM_013556.2	ATTAGCGATGATGAACCAGG GTCAGCAAAGAACTTATAGCCC
Htr1a	NM_008308.4	AACTATCTCATCGGCTCCTT GATTGCCCAGTACCTGTCTA
Htr1b	NM_010482.1	CTCCATCTCTATTTCGTTGC GTCTTGTTGGGTGTCTGTTT
Htr1d	NM_008309.4	CCATCCATCTTGCTCATTAT CACCTGGTTGAAAAGAGAG
Htr1f	NM_008310.3	TTTCTACATCCCGCTTGTAT TCGGACAAGGATTTTTCTAA
Htr2a	NM_172812.2	TGTGATGCTTTTAACATTGC CCAACTTACTCCCATGCTAC
Htr2b	NM_008311.2	GAACATCCTTGTGATTCTGG AGGCAGTTGAAAAGAGAACA
Htr2c	NM_008312.4	CTATTTTCAACTGCGTCCAT ATTCACGAACACTTTGCTTT
Htr3a	NM_013561.2	TGGTCCTAGACAGAATAGCC GGTCTTCTCCAAGTCCTGA
Htr4	NM_008313.4	CCTCACAGCAACTTCTCCTT TCCCCTGACTTCCTCAAATA
Htr5a	NM_008314.2	TGCTCTTTGTGTACTGGAAA

		ACGTATCCCCTTCTGTCTG
Htr5b	NM_010483.3	GGAGTCTGAGATGGTGTTCA AATATCCAAGCCACAGGAAT
Htr6	NM_021358.2	CTGAGCATGTTCTTTGTCAC CATGAAGAGGGGATAGATGA
Htr7	NM_008315.2	GTTAGTGTCACGGACCTCAT ATCATTTTGGCCATACATTT
Slc6a4	NM_010484.2	AAGCCAAGCTGATGATGTAA TCCTCACATATCCCAGTCAG
Tph2	NM_173391.3	CAGGGTCGAGTACACAGAAG CTTTCAGAAACATGGAGACG
Ddc	NM_001190448.1	GCAGTGCCTTTATCTGTCCT GAATCCTGAGTCCTGGTGAC
Mecp2	NM_010788.3	TCCTTGGACCCTAATGATTT TTTCACCTGAACACCTTCTG

3.1.8. Primers for sequence verification

Application	Sequence (5' --> 3') **Forward** **Reverse**
Htr5b WT (Genotyping)	CTCTGCAGTCGGTTTGATG GTAGAGTCACCACAAGCAC
Htr5b KO (Genotyping)	GCAGCGCATCGCCTTCTATC GTGCTGGGATTAGAAGTCC
Mecp2 WT (Genotyping)	GACCCCTTGGGACTGAAGTT CCACCCTCCAGTTTGGTTTA
Mecp2 KO (Genotyping)	CCATGCGATAAGCTTGATGA CCACCCTCCAGTTTGGTTTA
T7 (pcDNA3.1(-); Insert sequencing)	TAATACGACTCACTATAGGG
Bgh (pcDNA3.1(-); Insert sequencing)	CTAGAAGGCACAGTCGAGG

3.1.9. Primers for cloning

Gene (CDS)	Sequence (5' → 3')	Restriction side
eGFP, eCFP, eYFP	fw: A**GAATTC**GCCGCCGCCATTGTGAGCAAGGGCGAGGAGCTG	*Eco*RI
	rev: AAA**AAGCTT**TCATTACTTGTACAGCTCGTCCATGC	*Hind*III
mCherry	fw: AAA**GAATTC**GCCGCCGCCATTGTGAGCAA	*Eco*RI
	rev: TTT**AAGCTT**ACTTGTACAGCTCGTCCATG	*Hind*III
Htr1a	fw: AAA**GCTAGC**ATGGATCTGCCTGTAAACTTG	*Bmt*I
	rev: A**GAATTC**TTGTTGCTTGGAGAAGAAGACCTTG	*Eco*RI
Htr5a	fw: AAA**GCTAGC**ATGGATATGTTCAGTCTTGGCCAG	*Bmt*I
	rev: A**GAATTC**GCGGCAGAACTTGCACTTGATGATC	*Eco*RI
Htr$_{5b}$FL (full-length)	fw: AAA**GCTAGC**ATGGAAGTTTCTAACCTCTC	*Bmt*I
	rev: TTT**GAATTC**TCTCTGCTTAGTAAAGAGGC	*Eco*RI
Htr$_{5b}$TR (trunc)	fw: AAA**GCTAGC**ATGGAAGTTTCTAACCTCTC	*Bmt*I
	rev: TTT**GAATTC**TCTCTGCTTAGTAAAGAGGC	*Eco*RI
Htr7	fw: AAA**GCTAGC**ACCATGATGGACGTTAACAGCAG	*Bmt*I
	rev: TTT**GAATTC**TGTATCATGACCTTTTTTCCCAC	*Eco*RI

3.1.10. Primary antibodies

Antibody (species)	Company	Application (final conc.)
Anti-5-HTR$_{5B}$ (rabbit)	Abcam (ab101907)	IHC (1 µg/ml)
Anti-5-HTR$_{5B}$ (rabbit)	Homemade	IHC (1 µg/ml) WB (2 µg/ml)
Anti-GAPDH (mouse)	Biotrend (6C5)	WB 0.2 µg/ml)
Anti-MeCP2 (rabbit)	Cell Signaling (D4F3)	ChIP (0.5 µg/ml) WB (1 µg/ml)

3.1.11. Secondary antibodies

Antibody	Conjugate	Company	Application
goat anti-rabbit IgG	Atto 488	Sigma-Aldrich (Taufkirchen)	IHC
goat anti-rabbit IgG	Chromeo 546	Active Motif (Carlsbad, USA)	IHC
goat anti-rabbit IgG	Atto 647	Sigma-Aldrich	IHC
goat anti-mouse IgG	Chromeo 546	Active Motif	IHC
goat anti-mouse IgG	Atto 488	Sigma-Aldrich	IHC
goat anit-mouse IgG	HRP	DAKO (Hamburg)	WB
goat anti-rabbit IgG	HRP	DAKO (Hamburg)	WB
rabbit mAb IgG	-	Cell Signaling (DA1E)	Isotyp control; ChiP

3.1.12. Pharmacological substances

Name	Company	Application (final conc.)
8-OH-DPAT	Tocris	WHBP (0.2 - 0.4 µM)
Ampicillin	Sigma	Bacterial culture (50 µg/ml)
Ethidium bromide	Merck	Nucleic acid visualization (0.25 µg/ml)
Forene (isofluran)	Company	Animal preparation
Forskolin	Tocris	cAMP (1 µM) WHBP (1 µM)
Norcuronium bromide	Tocris	WHBP (2.5 ng/ml)
Rp-cAmps	Tocris	WHBP (0.2 - 0.4 µM)
Serotonin	Sigma-Aldrich (Taufkirchen)	Receptor stimulation (10 µM)

3.1.13. Media and supplements for cell culture

Reagent	Company	Application (Dilution)
Dulbecco's Modified Eagle's Medium (DMEM, high glucose)	Gibco BRL (Eggenstein)	Maintenance
Dulbecco's PBS	Gibco	Washing
Fetal calf serum (FCS, heat inactivated)	Gibco	cell culture (1 : 10)
Optimem	Gibco	Transfection, approach
Penicillin (10,000 U/ml) / streptomycin (10 mg/ml) mix	Gibco	cell culture (1 : 100)

3.1.14. Cell line

Name	Origin	Source
N1E-115 (mouse)	Neuroblastoma tumor	Amano et al., 1972

3.1.15. Mouse lines

Name	Genotype	Background	Source
C57BL/6J	wt		Jackson Laboratory
129P2(C)-Mecp2tm1-1Bird	$Mecp2^{-/y}$	C57BL/6J	Guy et al., 2001
129SvEvBrd	$Htr5b^{-/-}$	C57BL/6J	Taconic (Denmark)
TgN-(hGFAP-EGFP)		C57BL/6J	

3.1.16. Computer software

Program / Internet side	Company / address	Application
ClustalW2	http://www.ebi.ac.uk/Tools/msa/clustalw2/	Sequence analysis
FinchTV	Geospiza (USA)	Sequence analysis
LabChart	ADInstruments (Spechbach)	Data analysis
LSM Image Browser	Zeiss (Göttingen)	Image processing
Magellan	Tecan (Männedorf)	Data analysis

NCBI	http://www.ncbi.nlm.nih.gov/	Basical information
Office Excel	Microsoft (Unterschleißheim)	Data analysis
Office Word	Microsoft	Writing
Photoshop	Adobe Systems (München)	Image processing
Primer-Blast	http://www.ncbi.nlm.nih.gov/tools/primer-blast/	Primer generation
Prism	GraphPad (La Jolla, USA)	Data analysis
SerialCloner	SerialBasics (Internet, free)	Sequence comparison
TMHMM Server v. 2.0	http://www.cbs.dtu.dk/services/TMHMM/	Protein analysis

3.1.17. Universal washing buffers

Buffers were prepared with double distilled water (ddH2O) of a deionization facility (Millipore) and afterwards autoclaved for 20 min at 121°C and 1.1 bar. X-fold stock solutions were diluted to 1-fold before using. Specific buffers are indicated in the method section.

10x PBS	
1.5 M	NaCl
38 mM	NaH_2PO_4
162 mM	Na_2HPO_4
pH	7.4

10x TBS	
100 mM	Tris
1.5 M	NaCl
pH	7.6

1x TE	
10 mM	Tris
1 mM	EDTA
pH	8.0

TBS-T	
10 %	10x TBS
0.05 %	Tween20
pH	7.6

3.2. Methods

The experimental procedures were performed in accordance with European Community and National Institutes of Health guidelines for the Care and Use of Laboratory Animals. The Ethics Committee of the Georg-August-University, Göttingen, Germany approved the study.

3.2.1. Animal work

This section describes origin, generation, and handling of all mouse models used in this study at all conducted approaches.

3.2.1.1. Animal models

The *Mecp2* knockout mouse (*Mecp2$^{-/y}$*), which is a model for Rett syndrome, strain B6.129P2(C)-Mecp2tm1-1Bird (Guy et al., 2001) maintained on a C57BL/6J background was obtained from The Jackson Laboratory (Bar Harbor, ME, USA). *Mecp2* knockout males (*Mecp2$^{-/y}$*) were generated by crossing hemizygous *Mecp2$^{+/-}$* females with C57BL/6J wild type males. The knockout mouse model for serotonin receptor 5B, strain (129SvEvBrd), maintained on a C57BL/6J background was obtained from Taconic (Denmark). The *Mecp2$^{-/y}$,Htr5b$^{-/-}$*-double-knockout mice were obtained by crossbreeding female filial 1 (F1) generation (*Mecp2$^{+/-}$,Htr5b$^{+/-}$*) mice with male *Mecp2$^{+/y}$,Htr5b$^{+/-}$* mice. TgN-(hGFAP-EGFP) transgenic mice, which express enhanced green fluorescent protein (EGFP) under the control of the human glial fibrillary acidic protein (hGFAP) promoter (Nolte et al., 2001), were kindly provided by Prof. Hülsmann, Dept. of Neurophysiology and Cellular Biophysics, University of Göttingen.

3.2.1.2. Housing

Animals were kept in a temperature- und humidity-controlled 12 h light-dark rhythm and had free access to water and standardized pellet food.

3.2.1.3. Genotyping

The genotype of newborn mice were determined using PCR on DNA isolated from mice tail biopsies. For PCR condition and primer sequences for genotype identification refer to 3.1.8.

3.2.1.4. Preparation of fresh brain tissue for quantitative PCR, western blot, and cAMP measurement

Before decapitation, mice were deeply anesthetized with isofluran until they were unresponsive to painful stimulus. After opening the skull the brain was isolated and immediately frozen on dry ice. For long-term storage brains were transferred to -80°C.

3.2.1.5. Fixation of brain tissue for immunohistochemistry

Mice were deeply anesthetized with isoflurane until they were unresponsive to painful stimulus. Mice were transcardially perfused with 50 ml 0.9% NaCl (10 ml/min) to remove the blood followed by 4% PFA/PBS to start brain fixation. After removal from the skull, brains were post-fixed for 4 h with 2% PFA/PBS at 4°C. For cryoprotection tissue was transferred first to 10% Sucrose/PBS for 2 h and afterwards to 30% Sucrose/PBS at 4°C overnight and eventually frozen at -28°C.

3.2.1.6. Human brain tissue for immunohistochemistry

Paraformaldehyde-fixed (4%) human brainstem tissue of healthy young casualties (1 - 2 years of age) was obtained from the tissue bank of the Department of Legal Medicine, University of Göttingen, and kindly provided by Prof. Michael Klintschar.

3.2.2. Determination of breathing rhythm

3.2.2.1. Working heart brainstem preparation (WHBP)

ACSF	
1.25 mM	$MgSO_4$
1.25 mM	KH_2PO_4
5 mM	KCl
125 mM	NaCl
2.5 mM	$CaCl_2$
25 mM	$NaHCO_3$
10 mM	glucose
0.1785 mM	Ficoll 70

In collaboration with Anna-Maria Bischoff (Department of Neuro- and Sensory Physiology, Georg-August University of Göttingen), who did the technical work, the output of the neuronal breathing rhythm was measured by recording of the phrenic nerve activity (PNA) during the *in situ* working heart brainstem preparation (WHBP). This method was developed by Paton (Paton et al., 1996) and enables pharmacological manipulation of the breathing rhythm by application of drugs. Furthermore, in contrast to other approaches such as *en bloc* brainstem preparations or acute slice culture the WHBP is suitable for studying of the 3-phase rhythm in adult mammals (Richter & Spyer, 2001).

Mice were deeply anesthetized with isoflurane until they were unresponsive to painful pinch into their forepaw. Animals were then decerebrated at the pre-collicular level and cerebellectomized, bisected below the diaphragm, and the skin was removed. The upper body was placed in a recording chamber and perfused retrogradely at 10 - 20 ml/min via the thoracic aorta with artificial cerebrospinal fluid (ACSF) aerated with carbogen (5% CO_2 / 95% O_2; pH 7.35). The perfusate was warmed to 30°C as measured in the scull base, filtered twice and re-circulated. Norcuronium-bromide 2.5 ng/ml was added for muscle relaxation. The perfusion pressure was adjusted to 50 to 65 mmHg. Using a glass suction electrode, phrenic nerve discharges were recorded as an index of central respiratory rhythm. Drugs were added to the perfusate for specific pharmacological manipulation.

3.2.2.2. Plethysmography

In collaboration with Prof. Swen Hülsmann (Department of Molecular Neurohysiology and Cellular Biophysics, Georg-August University of Göttingen) ventilation was measured by whole-body-plethysmography that allows measuring pressure changes, resulting from the warming of the inspired air and cooling during expiration (Drorbaugh and Fenn, 1955).

Mice were placed in a custom made Plexiglas chamber (300 ml volume) that was connected to a differential low-pressure transducer (*DP1 03*, Validyne Engineering, Northridge, CA). The other channel of the differential pressure transducer was connected to a 300 ml reference chamber to make measurement mostly independent from other pressure changes (Bartlett & Tenney, 1970). The pressure transducer was connected to a sine wave carrier demodulator (*CD-15).* Pressure fluctuations were Band-Pass filtered (1.5 - 500 Hz), amplified (four times) before storing. For digitization an *ITC-16* interface (InstruTECH/HEKA, Lambrecht) was used controlled

by *Axograph 4.8* software (Axon Instruments, Foster City, CA) and sampling rated of 1 kHz. Animals were allowed to freely explore the chamber. To prevent accumulation of CO_2 in the chamber, we introduced a bias flow using the 150 ml/min suction of a *Normocap®* CO_2-sensor (Datex, Instrumentarium Oy, Helsinki, Finland), thus the CO_2 concentration could be kept below 3%. Pressure measurements were semi-automatically analyzed by the threshold search event detection method of "clampfit" (Molecular Devices, Sunnyvale, CA). Breathing frequencies were calculated as the reciprocal of the averaged inspiratory interval. The Coefficient of variation was calculated for the interval (CV = STD/mean). Furthermore the irregularity score (IS) was calculated (IS = $100*ABS(Int_n - Int_{n-1})/Int_{n-1}$ for each respiratory cycle.

3.2.3. Cell culture

Adherent mouse N1E-115 neuroblastoma cells obtained from the American Type Culture Collection (ATCC) were maintained in Dulbecco's modified Eagle's medium (DMEM) supplemented with 10% fetal calf serum (FCS, heat inactivated for 30 min at 56°C) and 1% penicillin/streptomycin at 37°C under 5% CO_2 in 10 cm dishes. Cells were splitted every 2 to 3 days depend on the confluence. Therefore, the medium was removed and the cells were washed with 37°C pre-warmed PBS and then cells were rinsed off mechanically and thoroughly resuspended 1 : 3 to 1 : 5 in fresh DMEM.

3.2.3.1. Cell seeding

Cultured cells were harvested and thoroughly separated before counting by means of Neubauer counting chamber using light microscopy. Cell concentration was adjusted to 500,000 cells/ml in pre-warmed culture media. Total volume of seeding was depending on the approach and the well size and is indicated in the table. Cells were incubated at 37°C under 5% CO_2 overnight to allow attachment on the bottom or coverslip.

Well / size (cm^2)	Seeded cells	Incubation volume (ml)	Approach
4-well / 2	100,000	0.5	Imaging
6-well / 9.6	500,000	2	Protein, cAMP, luciferase promotor, and [^{35}S]GTP$_\gamma$S assay
IBIDI / 9.6	500,000	2	Imaging

3.2.3.2. Transient transfection of N1E-115 cells

4 - 7 µl *Lipofectamine2000* reagent and 1 to 2 µg of expression plamids were separately mixed with 25 or 200 µl Optimem media. After incubation for 5 min at RT both batches were mixed and incubated for further 10 to 20 min at RT. Culture medium from overnight seeded cells was replaced by 200 or 500 µl Optimem. 50 or 400 µl mixture was added to the cells drop-wise and incubated for 4 h to 6 h at 37°C under 5% CO_2. Afterwards Optimem was replaced by DMEM and the cells were incubated overnight at 37°C under 5% CO_2.

3.2.3.3. Pharmacological treatment of cells - measurement of cAMP

The second messenger cyclic 3',5'-adenosine monophosphate (cAMP) has great relevance in many intracellular signal transduction cascades. It is ubiquitously present in animal, as well as in bacteria, and plants (Gerhring, 2010). Cyclic AMP is biologically synthesized from ATP by the adenylyl cyclase and is inactivated through enzymatic cleavage by the phosphodiesterase.

In order to measure the influence of inhibitory G-protein coupled serotonin receptors on the intracellular cAMP concentration, first the cell system has to be activated.

Therefore, transfected cells from 6-well plates were harvested and washed twice with pre-warmed DBPS. Afterwards cells were incubated in 1 ml Optimem in the presence of 10 µM forskolin to elevate cAMP concentrations for 10 min at 37°C while shaking. Next, cells were again incubated for 10 min at the same conditions in presence or absence of 10 µM serotonin. After pelleting the cells for 5 min at 800 xg, cells were diluted in cAMP lysis buffer -provided by Kit- and incubated on ice for 30 min or stored at -80°C.

To measure cAMP in cells as well as in mouse tissue accurately the ELISA-based *DetectX Direct Cyclic AMP* was used according to the regular format of manufacture's protocol. 200,000 cells were employed. Finally, optical density was

measured at 450 nm using *Infinite M200 PRO* luminometer. Cyclic AMP concentrations were calculated by plotting against of known cAMP concentration of a standard curve ranging from 0.616 to 150 pmol/ml. Afterwards concentrations were related to the total protein amount of each sample, which was measured using *DC Protein Assay* (refer to 3.2.5.2.).

3.2.4. Molecular biology

3.2.4.1. Isolation of nucleic acid

3.2.4.1.1. Isolation of whole RNA

In order to quantify gene expression or for cloning an open reading frame of a gene of interest first RNA was isolated from fresh mouse brain tissue using *Trizol*® reagents. Therefore, various brain regions were dissected under visual control using a cryostat and transferred to 900 µl *Trizol*®. Next, tissue was homogenized using hand mortar and incubated for 5 min at RT. After adding of 200 µl chloroform samples were vortexed and incubated for 5 min more at RT. Next, samples were centrifuged at 17,900 xg and 4°C for 10 min and the upper transparent phase (≈ 600 µl) was mixed with equal volume of isopropanol and 1 µl *GlycoBlue™* (Ambion) in order to precipitate and visualize the RNA. Samples were incubated at -28°C for 20 min and thereafter centrifuged at 17,900 xg and 4°C for 20 min. Resulting RNA pellets were washed twice using 75% EtOH. After drying the RNA pellets were resuspended in 43.5 µl nuclease-free water (Ambion). In order to avoid DNA contamination a DNA digestion mix (5 µl 10x DNase I buffer, 1 µl DNase and 0.5 µl *RNaseOut™*) was added to the samples, which were then incubated at 37°C for 15 min. The RNA was again extracted using phenol/chloroform method. Therefore, 150 µl RNase-free water and 200 µl Roti® phenol (containing phenol / chloroform / isoamylalcohol; 25 : 24 : 1) were added to the samples and briefly vortexed. After centrifugation at 10,000 xg for 5 min the upper phase (≈200 µl) was mixed with equal volume of isopropanol and 1 µl *GlycoBlue™* and incubated at -28°C for 20 min. After centrifugation at 4°C and 17,900 xg for 20 min resulting RNA pellets were washed twice with 75% EtOH. After drying the pellet RNA was eluted in appropriate volume of RNase-free ddH_2O and the RNA concentration was determined by spectrophotometric analysis. To determine the integrity RNA was loaded and

separated in an agarose gel. RNA of good quality shows two distinguish bands of which the upper band (28S rRNA) has an as twice as much intensity the lower band represented by the 18S rRNA. RNA was subsequently transcribed into complementary DNA (cDNA) and afterwards stored at -80°C.

3.2.4.1.2. Isolation of DNA from mice tails

In order to determine the genotype of newborn mice DNA was isolated from biopsies of mice tails, incubated in 25 mM NaOH / 0.2 mM EDTA for 3 h at 99°C while shaking at 1,000 rpm. After neutralization with equal volume of 40 mM Tris/HCl pH 5.5 and centrifugation for 10 min at 10,000 xg, 1 µl was taken as template in a subsequent PCR.

3.2.4.1.3. Plasmid multiplication and preparation from *Escherichia coli*

LB-medium	
10 g/l	Tryptone
5 g/l	Yeast extract
5 g/l	NaCl

SOC-medium	
20 g/l	Tryptone
5 g/l	Yeast extract
10 mM	NaCl
10 mM	$MgCl_2$
10 mM	$MgSO_4$
20 mM	Glucose

LB-plate	
10 g/l	LB-medium
2% w/v	Agar

Plasmids were multiplied in *Escherichia coli* strain DH-5α library efficiency (Invitrogen GmbH, Karlsruhe).

3.2.4.1.3.1. Heat shock transformation of bacteria

DH-5α library efficiency bacteria suspensions (Invitrogen) were stored in 50 µl stocks at -80°C. For plasmid transformation stocks were shortly thawed on ice, gently mixed with 10 ng of plasmid or 1 µl of 1 : 3 diluted ligation reaction and incubated on ice for 25 minutes. After heat shocking at 42°C for 45 s bacteria were replaced on ice for further 2 min. Next, bacteria were suspended in 450 µl SOC medium and incubated at 37°C for 60 min while shaking at 600 rpm. Afterwards bacteria were centrifuged at

10,000 rpm for 1 min and 400 µl supernatant was removed. Bacteria were resuspended in the remaining volume (≈ 100 µl) and spread on ampicillin-containing LB-agar plates. After incubation at 37°C for 12 to 16 h, resulting colonies were analyzed for insert-specific plasmids using colony PCR.

3.2.4.1.3.2. Isolation of plasmid DNA

In order to obtain larger amounts of plasmid DNA, bacteria colonies were transferred to 5 ml LB medium (containing 1 µg amp for selection; for even higher amounts of plasmid DNA 50 ml of LB medium in presence of 10 µg amp was inoculated 1 : 1,000 from an overnight pre-culture). After 14 to 16 h at 37°C while shaking at 130 rpm bacteria cultures were centrifuged at 4,000 xg for 10 min at RT. To isolate the plasmid DNA from the bacterial pellets *QIAquick*® for the 5 ml or *HiSpeed*® *Maxi* Kit for the 50 ml batch were used according to manufacturer's instructions.

Both kit procedures are based on the alkaline lysis of bacterial cells and subsequent isolation of plasmid DNA by adsorption onto silica membrane in presence of high salt (Birnboim & Doly, 1979; Vogelstein & Gillespie, 1979). The elution was made in 50 µl for 5 ml batch or 1 ml ddH$_2$O for 50 ml batch.

3.2.4.2. Spectroscopic determination of nucleic acid concentration

The concentration of RNA and DNA was determined by spectrophotometric measurement of the wavelength absorbance at 260 nm using *Nanodrop1000* spectrophotometer. An optical density of 1.0 corresponds with 40 µg/ml single-stranded RNA or 50 µg/ml double-stranded DNA, respectively. As aromatic amino acids have an absorbance maximum at 280 nm the ratio of 260 to 280 was taken as a purity grade. Protein-free nucleic acid samples have a ratio between 1.7 and 2.0.

3.2.4.3. Electrophoretic separation of nucleic acid

50x TAE	
2 M	Tris
5.7 % (v/v)	Acetic acid
50 mM	EDTA
pH	8.0

10 x DNA Loading buffer	
250 mg	Xylencyanol
250 mg	Orange 6
ad 33 ml 150 mM	Tris pH 7.6
60 ml (v/v)	Glycerine
ad 100 ml	H_2O

Agarose gel electrophoresis was used to determine the integrity of RNA and to estimate the size of double-stranded DNA molecules by means of a size standard. Therefore, a 1.5% w/v (in 1x TAE buffer) agarose gel containing 0.4 µg/ml ethidium bromide was overlaid with 1x TAE buffer. DNA samples (at least 100 ng of DNA) were mixed with 6x DNA loading buffer, loaded onto the gel and then separated applying a voltage of 5 V/cm electrodes distance. DNA bands were visualized in UV-light using a BIO-VISION™ fluorescence documentation system.

3.2.4.4. Transcription of RNA into cDNA by reverse transcriptase

The transcription of RNA into complementary DNA (cDNA) is a precondition to amplify RNA. The reverse transcriptase originally isolated from the Moloney Murine Leukemia Virus (MMLV) has an intrinsic RNA as well as a DNA depending polymerase activity. 0.5 or 1 µg RNA per reaction were transcribed using *iScript™ cDNA synthesis* kit according to manufacture's instruction. The reaction was made in a 20 µl batch containing:

20 µl Transcriptase reaction	
4 µl	5x iScript reaction mix
1 µl	Reverse transcriptase
x µl	RNA (0.5 or 1 µg)
ad 20 µl	Nuclease-free water

Transcriptase reaction protocol	
4 min	25°C
30 min	42°C
5 min	85°C
∞	4°C

The cDNA was afterwards diluted 1 : 3 in ddH_2O (Ambion) and stored at -20°C.

3.2.4.5. Polymerase chain reaction (PCR)

The polymerase chain reaction (PCR), which was invented by Mullis et al. (1986), is an effective method to amplify double-stranded DNA using a thermo-stable DNA polymerase. Here, PCR was used for gene cloning and detection of specific DNA sequences by using corresponding primers. Depending on the approach two different polymerases were used. The *Phusion*® polymerase (NEB), which has a 50-fold lower error rate than the *Taq* polymerase (isolated from *Thermus aquaticus*), was taken for gene cloning, whereas *Taq* polymerase (PANScript red, PAN) was used for genotyping, colony PCR, and q-PCR fragment analyzing. Standard reaction mixes typically contained:

PCR reaction mix (PANScript red)	
1x	NH$_4$ reaction buffer
2 mM	MgCl$_2$
0.2 µM	Forward primer
0.2 µM	Reverse primer
1 mM	dNTPs
0.02 U/µl	Taq red
10 - 50 ng	DNA template

PCR reaction mix (Phusion®)	
1x	GC reaction buffer
0.25 µM	Forward primer
0.25 µM	Reverse primer
1.25 mM	dNTPs
0.02 U/µl	Phusion
10 - 50 ng	cDNA template

The PCR was performed using Labcycler (SensoQuest) under the following cycling conditions:

Step	Cycles	Duration	Temperature [°C]
Initial denaturation	1	3 min	95
Denaturation (optional)		30 s	95
Annealing (optional)	3	30 s	60 - 63
Elongation (optional)		45 s - 1 min 15 s	72
Denaturation		30 s	95
Annealing	35 - 40	30 s	64 - 68
Elongation		45 s - 1 min 15 s	72
Final elongation	1	5 min	72
Hold	1	Infinite	10

<u>Colony PCR</u>

To identify plasmid-insert positive bacteria colonies, they were separately picked and resolved in 10 µl ddH$_2$O. 5 µl were taken for inoculation of 500 µl pre-culture. The remaining 5 µl served as template in a subsequent PCR with sequence specific primers.

3.2.4.6. Quantitative real time PCR (q-PCR)

The quantification of mRNA of various genes was measured by q-PCR using *CFX96™ Real-time System* and after (BioRad) and the *Fast SYBR® Green Master Mix* (AppliedBiosystem). 0.75 µl of corresponding cDNA was used as template in a 10 µl-reaction mixture, which contained:

q-PCR reaction mix	
5 µl	2x Fast SYBR® Green Master Mix
0.2 µl	Forward primer (200 nM; final concentration)
0.2 µl	Reverse primer (200 nM; final concentration)
0.75 µl	cDNA template (derived from RNA)
ad 10 µl	ddH$_2$O

The fluorescence dye SYBR® Green intercalates with double-stranded DNA, which occurs after every elongation cycle. The fluorescence is proportional to the amount of double-stranded PCR products and increases exponentially depend on the property of the PCR. When the fluorescence signal is exceeding the background level the cycle number is called the threshold cycle (C_T), which is a measure for the amount of a specific cDNA initially present in the sample. Calculations of gene expression were performed using the $2^{-\Delta\Delta Ct}$ method according to Pfaffl et al. (2001). Hypoxanthine guanine phosphoribosyl transferase (*Hprt*) and glyceraldehyde-3-phosphate dehydrogenase (*Gapdh*) served as reference genes ("housekeeping genes") in the q-PCR, which were performed using the following cycle conditions.

Step	Cycles	Duration	Temperature [°C]
Enzyme activation	1	3 min	95
Denaturation		5 s	95
Annealing / elongation	40	30 s	60
Detection			
Melting curve	1	10 s	95
		in 0.5°C steps	65 - 90

Reference genes were run in duplicates, genes of interest in triplicates.

3.2.4.6.1. Q-PCR Primer design

Specific primer sequences are indispensible for an accurate q-PCR. Sense and antisense primer were derived by means of *Primer-Blast* (http://www.ncbi.nlm.nih.gov/tools/primer-blast/), which is based on the *Primer3* program. The following primer conditions were set:

q-PCR primer conditions	
G/C content	≥ 40% ≤ 60%
Primer length	≥ 18 ≤ 21 nucleotides
Melting temperature	≈ 60°C
Amplicon length	≥ 75 ≤ 250 nucleotides
	exon-spanning (at least one of the primers)
	C or G at the 3' end

Resulting PCR amplicons were analyzed by agarose gelelectrophoresis, isolated, purified, and subsequently sequenced and blasted to confirm the correct identity. The primer efficiency was determined using 4-fold serial dilutions generated from cDNA of each sample. The amplicon of used primer pairs showed a single peak in the melting curve analysis.

3.2.4.7. Molecular cloning of open reading frames from different serotonin receptors

In order to analyze the molecular behavior of serotonin receptors *in vitro* the open reading frame of *Htr1a*, *Htr7*, *Htr5a*, and *Htr5b* as well as their truncated forms were cloned and fused to different fluorescent proteins. These constructs were ligated into

the mammalian expression plasmid pcDNA3.1(-) and expressed in N1E-115 cells. Figure 3.1 shows a schematic representation of the established cloning strategy, which allows a quick change of the C-terminal fluorophore or tag, respectively.
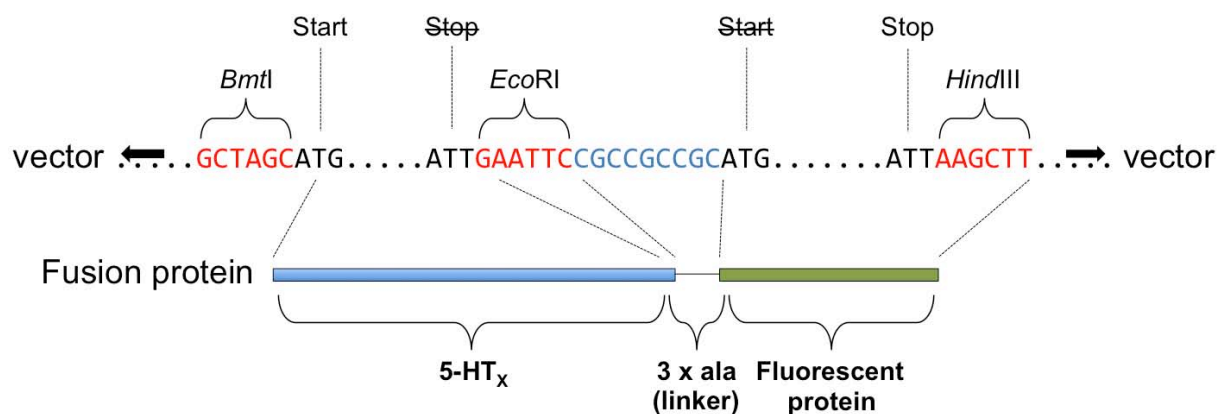

Figure 3.1. Schematic representation of the used cloning strategy.
The coding sequence (CDS) for different serotonin receptors 5-HT$_X$ was ligated between the endonuclease restriction site *Bmt*I and *Eco*RI. The Stop codon was deleted to achieve a continuous open reading frame (ORF) with the CDS from fluorescent proteins, which was cloned between the endonuclease restriction site *Eco*RI and *Hind*III. The start-ATG from the CDS of the fluorescent protein was deleted to avoid alternative protein translation. A linker between the two CDS was introduced consisting of three alanine residues (ala). The fusion construct was ligated into the mammalian expression vector pcDNA3.1(-).

3.2.4.7.1. Gelextraction of DNA fragments

First, the ORF of specific genes or fluorophores were amplified with appropriate primer pairs (refer to 3.1.9) by PCR and separated on an agarose gel. Specific bands were precisely excised and extracted using *QIAquick*® *Gel Extraction* kit following the manufacture's protocol. Isolated DNA was eluted in 30 µl of nuclease-free ddH$_2$O (Ambion).

3.2.4.7.2. Restriction digest of DNA molecules

The insertion of specific endonuclease restriction sites at both ends of an ORF by specific cloning primers enables site-directed insertion into a plasmid. Therefore, 3 µg of pcDNA3.1(-) plasmid or 1 µg of gene or fluorophore ORF were double digested with restriction endonucleases as followed:

DNA origin [µg]	Retriction enzyme (final con.)	Buffer (NEB)	Final volume [µl]
pcDNA3.1(-) plasmid (3 µg)	*Bmt*I (0.8 u/µl)	2	50
	*Hind*III (0.8 u/µl)		
HtrX insert (1 µg)	*Bmt*I (1 u/µl)	2	30
	*Eco*RI (1 u/µl)		
Fluorophore insert (1 µg)	*Eco*RI (1 u/µl)	2	30
	*Hind*III (1 u/µl)		

To avoid self-ligation 1 µl of *FastAP™* alkaline phosphatase (Fermentas) was added to the plasmid reaction digest. Then, reactions were incubated at 37°C for 3 h and afterwards heat inactivated at 75°C for 20 min. Subsequently the restricted DNA was purified.

3.2.4.7.3. Purification of DNA fragments

Purification of DNA from restriction endonucleases and following PCR reactions were performed using *QIAquick PCR Purification* (Qiagen) according to manufacture's instructions. DNA was eluted in 30 µl of nuclease-free ddH$_2$O (Ambion) and afterwards the concentration was measured using *Nanodrop1000*.

3.2.4.7.4. Ligation of DNA molecules

A triple ligation was performed to generate a *HtrX*-fluorophore fusion ORF inserted into the plasmid pcDNA3.1(-). 20-µl-reaction mixtures were performed as followed:

Ligation reaction mix	
100 ng	pcDNA3.1(-) plasmid
3 : 1 (molar ratio over plasmid)	ORF *HtrX*
3 : 1 (molar ratio over plasmid)	ORF fluorophore
2 µl	10x T4 DNA ligase buffer
1 µl	T4 DNA ligase (Fermentas)
ad 20 µl	Nuclease-free ddH$_2$O (Ambion)

Reactions were incubated at RT for 1 h and then heat inactivated at 75°C for 5 min. Afterwards reactions were diluted 1 : 3 with TE buffer. 1 µl was taken for transformation into DH5α competent bacteria.

3.2.4.8. Identification of recombinant DNA by PCR based cycle sequencing

To ensure the correct integrity of recombinant DNA, isolated plasmids were sequenced by cycle sequencing, which was conducted by SeqLab (Göttingen). Therefore, 700 ng of plasmid was diluted with 20 pmol forward or reverse primer and filled up to 7 µl with ddH$_2$O (Ambion). Obtained sequences were blasted by means of *SerialCloner* sequence software.

3.2.4.9. Chromatin immunoprecipitation (ChIP)

FA lysis buffer	
50 mM	HEPES
140 mM	NaCl
1 mM	EDTA
1% (v/v)	Triton X-100
0.1%	Sodium desoxycholate
0.1%	SDS
1% (v/v)	Protease inhibitor cocktail (fresh; Fermentas)
pH	7.5

RIPA buffer	
50 mM	Tris
150 mM	NaCl
2 mM	EDTA
1% (v/v)	IGEPAL CA-630
0.5%	Sodium desoxycholate
0.1%	SDS
1% (v/v)	Protease inhibitor cocktail (fresh; Fermentas)
pH	8.0

Wash buffer (high salt)	
20 mM	Tris
500 mM	NaCl
2 mM	EDTA
1% (v/v)	Triton X-100
0.1%	SDS
pH	8.1

Wash buffer (low salt)	
20 mM	Tris
150 mM	NaCl
2 mM	EDTA
1% (v/v)	Triton X-100
0.1%	SDS
pH	8.1

Wash buffer (LiCl)	
10 mM	Tris
250 mM	LiCl
1 mM	EDTA
1%	Sodium desoxycholate
1% (v/v)	IGEPAL CA-630
pH	8.1

In order to test protein-DNA interactions *in situ* the pre-BötC was dissected from both sides of corresponding 300-µm-cryosections and immediately cross-linked in 1.5% formaldehyde/PBS for 15' at RT. After quenching the reaction with 0.2 M Glycine, and washing 3 x with ice cold PBS, chromatin was solubilized and extracted in FA-buffer for 20 min on ice and subsequently shared into 800 - 1,500 bp fragments by sonication for 15 x 25 s at 0.7 duty and 55 W. 1 : 10 dilutions in RIPA-buffer were pre-cleared by adding 1.5% (v/v) protein A slurry (Millipore) for 30 min at 4°C with rotation. Afterwards samples were incubated at 4°C with rotation overnight in presence of either 3 µg anti-MeCP2 antibodies (Abcam), 3 µg guinea pig anti-rabbit IgG (ZYMED, California, USA) or without antibody as negative control. To isolate immunocomplexes 4% (v/v) protein A slurry (Matrix) was added and incubated for further 1.5 h at 4°C. Matrix was washed 3 times with low salt, high salt, and LiCl wash buffer followed by additional 2 times TE buffer. After elution in freshly prepared 1% SDS / 0.1 M NaHCO3, chromatin was reversely cross-linked by adding 0.2 M NaCl and incubated at 65°C and 1,000 rpm overnight. Subsequently, DNA was recovered by phenol/chloroform extraction, which was already described in 3.2.4.1.1. Amounts of precipitated DNA were subsequently analyzed using real-time PCR.

3.2.4.10. Assay for [^{35}S]GTP$_\gamma$S binding and immunoprecipitation of G-protein α subunits

Reaction buffer	
50 mM	Tris
100 mM	NaCl
2 mM	EDTA
3 mM	MgCl$_2$
1 µM	GDP
pH	7.4

The radioactive [^{35}S]GTP$_\gamma$S assay was performed in cooperation with Dr. Ute Renner, a former employer of the department of Neuro- and Sensory Physiology. Membrane preparations of transiently transfected N1E-115 cells expressing the 5-HT$_{5B}$R linked to mCherry fluorophore and G-protein α subunits (G$_{i3}$ and G$_s$ fused to variants of eGFP) were performed according to the protocol described by Kvachnina et al., 2009. Agonist-promoted binding of [γ^{35}S]guanosine 5-thiotriphosphate to different G proteins induced by stimulation of 5-HTR$_{5B}$ was performed as follows: Membrane preparations were diluted in reaction buffer to a concentration of 1 µg/µl. Each reaction contained 50 µg membrane preparations in a total volume of 100 µl. Reactions were performed in triplicate. After adding [^{35}S]GTPγS (Hartmann Analytic) to a final concentration of 3 nM, samples were incubated for 5 min at 30°C in the presence or absence of 1 µM 5-HT. The reaction was terminated by adding 900 µl of RIPA-buffer (see 3.2.4.9.) for 30 min on ice. Samples were centrifuged at 13,000 xg for 10 min. The supernatants were then transferred into a new tube and samples were agitated for 2 h after addition of 100 µl protein A-Sepharose (Sigma, 20 mg/ml RIPA) and 0.5 µl of anti-GFP antibodies. Immunoprecipitates were washed three times, boiled in 0.5 ml of 0.5% SDS, and radioactivity was measured by scintillation counting.

3.2.4.11. Luciferase reporter assay

The *Htr5b* promoter-luciferase reporter, in which a 4.8 kb mouse *Htr5b* promoter DNA fragment was linked to the firefly luciferase gene (kindly provided by Prof. Maekawa from RIKEN Tsukuba Institute, Japan). One µg of promoter construct together with various amounts (0, 1, or 2 µg) of *Mecp2* expression plasmid and 100 ng of the renilla luciferase expression construct, which served as transfection control and reference protein activity, were co-transfected into N1E-115 cells from 6-well plates. Promoter activity was measured after 16 - 24 h using *Dual-Luciferase®* Reporter Assay System (Promega) according to manufacture's instructions. Luminescence of firefly and renillla activity was measured using *Infinite 200 PRO* luminometer (TECAN).

3.2.4.12. Sandwich-enzyme-linked immunosorbent assay (Sandwich-ELISA)

Triton X-100 lysis buffer	
50 mM	Tris
2 M	NaCl
3.6 %	Triton X-100
pH	8.0

Coating buffer	
16 mM	$NaHCO_3$
34 mM	Na_2CO_3
pH	9.6

Brainstem tissues were homogenized before diluted with 500 µl PBS and supplemented with protease inhibitor cocktail (Fermentas). An equal volume of Triton X-100 lysis buffer was added to the homogenate. The lysis was performed on ice for 30 min with occasional vortexing. After a high-speed centrifugation (100,000 xg) for 1 h at 4°C, removal of the detergent using trichloro-acetic-acid (TCA)-precipitation, and subsequent two-times washing with acetone, the protein content was quantified using *D_C Protein Assay* (BIO-RAD). Sandwich-ELISA procedures were established for the quantification of methyl-CpG binding protein 2 (MeCP2). Both used mouse monoclonal anti-MeCP2-antibodies (clone Men-8, Cat. No. M7443, Sigma-Aldrich) for capturing and rabbit polyclonal anti-MeCP2-antibodies (Institute of Human Genetics, University of Göttingen, Germany) in combination with a horseradish peroxidase (HRP)-conjugated secondary antibody (Code No. 711-035-152, Dianova) for detecting the antigen. Monoclonal anti-MeCP2-antibodies were diluted in coating buffer at a dilution of 10 µg/ml. The microtiter plate was coated with 100 µl antibody solution/well at 4°C overnight. The plate was washed five times with 300 µl washing buffer/well. 250 µl blocking solution (2% BSA dissolved in PBS) was added and applied for 30 min at RT to inhibit non-specific binding sites. The MeCP2-ELISA was standardized using purified MeCP2-protein (PharmedArtis, Aachen). ABTS was used as the chromogenic reagent. ABTS functions as electron donor whereby the substrate H_2O_2 of the enzyme peroxidase becomes reduced. Since the peroxidase-catalyzed conversion follows a short linear kinetic, the color development was measured at different times (5, 10, 15, 20, 30, and 40 min) after the beginning of the enzyme reaction. The specific absorbance was measured at 405 nm (reference wavelength 492 nm).

3.2.5. Protein biochemistry

3.2.5.1. Extraction of total protein from brain tissue

SDS Lysis puffer	
50 mM	Tris
150 mM	NaCl
2 mM	EDTA
2% (w/v)	SDS
1% (v/v)	IGEPAL CA-630
5 u	Benzonase®
1% (v/v)	Protease inhibitor cocktail (freshly added; Fermentas)
pH	6.8

Brain regions of interest were dissected from freshly frozen brains under visual control and immediately grinded up in adequate amounts of SDS lysis buffer using a hand pestle. 5 µl *Benzonase*® (Sigma-Aldrich) was added to remove nucleic acid contamination. Extractions were kept on ice for 30 min with periodical vortexing. Lysates were centrifuged for 20 min at 10,000 xg and 4°C. The supernatants were collected and quantified for protein concentration using a BSA standard curve.

3.2.5.2. Determination of protein concentration

Protein concentration was determined using the D_C *Protein Assay* (BIO-RAD), which tolerates high SDS concentrations. The test is based on protein determination according to Lowry (Lowry et al., 1951). The reaction between copper and proteins in an alkaline environment leads to a reduction of the Folin's reagent, mainly caused by aromatic amino acid residues, such as tyrosine and tryptophan, which are present in the protein. This method, which is ten to twenty times as sensitive as measurement of the ultraviolet light absorbance at 280 nm and about 100 times as sensitive as the biuret reaction, leads finally to an intensive blue staining, which can be measured by light absorbance at 690 nm.

Kits provided Buffer

Buffer A, reagent S, working reagent S' (Mixture of A and S 20 : 1), Buffer B

First, a BSA standard curve with samples of known protein concentrations, ranging from 200 - 1,500 µg/ml was prepared in lysis buffer. 5 µl of standard or 1 : 4 diluted protein lysate were added to 25 µl S' and briefly mixed. After addition of 200 µl buffer B reactions were briefly agitated and incubated for at least 15 min at RT. The resulting color change was measured by absorbance at 690 nm using *Nanodrop1000* photometer. The protein concentrations were calculated by blotting extinctions against known BSA standards by means of the *Nanodrop1000*-internal software. All standards as well as protein samples were run in triplicates. After protein determination samples were adjusted to protein concentration of 2 µg/µl.

3.2.5.3. Discontinuous sodium dodecyl sulfate polyacrylamide gel electro-phoresis (SDS-PAGE)

5x Laemmli sample buffer	
250 mM	Tris
7% (w/v)	SDS
10 mM	EDTA
50%	Glycerine
50 mM	EDTA
7% (v/v)	β-MercaptoEtOH (fresh)
pH	6.8

10 x Running buffer	
250 mM	Tris
2 M	Glycine
10% (w/v)	SDS
pH	8.3

The constant intercalation of the negative charged dodecyl sulfate into native proteins (1.4 g SDS per 1 g protein) leads to a masking of their own net charge and to linearization. This enables the separation of proteins according to their molecular size in an electric field during poly acrylamide electrophoresis (Laemmli, 1970; Laemmli & Favre, 1973). The relative mobility of a given protein is linearly depending on the logarithm of its relative molecular mass (Weber & Osborne, 1969). Protein lysates were mixed with 5x Laemmli sample buffer plus 10% of the reducing agent β-mercaptoethanol and incubated for 10 min at 90°C. Subsequently 50 - 100 µg of protein and 10 µl of *Precision Plus Protein™ Kaleidoscope™* protein standard (BIO-RAD) were loaded on precast polyacrylamide gel Novex® (4 - 20%) and separated at 24 mA in presence of running buffer.

3.2.5.4. Immunoblot and detection of specific proteins

In order to prove particular proteins by a specific antibody, separated proteins of the SDS-PAG were transferred onto nitrocellulose membranes using the *iBlot*® *-7-Minute Blotting System*. In contrast to dry and semi-dry methods, buffer conditions and ions, required for the protein transfer, are provided by specific *iBlot*® *Gel Transfer Stacks* (Invitrogen). First, PAG was briefly washed in ddH_2O and placed on the bottom anode stack, which contains an integrated 0.2 µm nitrocellulose membrane. Afterwards a ddH_2O-soaked filter paper was placed on the PAG, the top cathode stack was placed, and air bubbles were removed. After assembling the *iBlot*® *Disposable Sponge* the proteins were plotted at 23 V for 7 minutes. To check the efficiency of the protein transfer the membrane was incubated in Ponceau solution for 1 min. After removing the Ponceau staining by washing the membrane in TBS-T three times (5 min each), the membrane was blocked in 5% BSA/TBS-T for 1 h at RT to inhibit non-specific binding sites. After washing 3 x 5 min with TBS-T the primary antibody was applied in appropriate concentrations (0.5 - 2 µg/ml) diluted in 2% BSA/PBS for 3 h at RT or alternatively at 4°C overnight.

3.2.6. Fluorescence detection - confocal laser-scanning microscopy (CLSM)

The confocal laser-scanning microscopy (CLSM) technique enables the detection of proteins in tissue sections using protein-specific antibodies, which are direct or indirect (by a secondary antibody) labeled with a fluorophore. The combination of fluorophores together with lasers of different wavelengths permits the simultaneous detection of different proteins or structures, respectively. Furthermore, this technique was used to localize recombinant fluorescent fusion proteins. For that, adherent transfected cells were fixed after 16 - 24 h with 2% PFA/PBS for 15 min at RT and afterwards washed three times with PBS. Finally, cells were covered in mounting medium.

3.2.6.1. Immunohistochemistry

Forty-µm-thick transversal sections ranging from the lumbar spinal cord to the pons were cut from fixed brains using a *Frigomobil*-cryostat (Reichert-Jung). Sections were washed three times in PBS 5 min at RT and then permeabilized with 0.2% Triton X-100/PBS for 30 min at RT. After washing 3 times with PBS non-specific binding sites were blocked with 5% BSA/PBS for 1 h at RT. After washing with PBS three

times of 10 min each, sections were incubated for 4 hours at RT or, alternatively, 16 hours at 4°C in primary antibody solution (2% BSA/PBS, antibody concentration of 2 - 5 µg/ml) followed by three washing steps for 15 min each. Sections were incubated for 3 hours at RT in the dark with species-specific secondary antibodies conjugated to various fluorophores, diluted 1 : 1,000 in 2% BSA/PBS. After extensive washing (three times, 15 min each) sections were mounted onto microscope-slides and coverslipped with fluorescent mounting medium. Neuronal immunofluorescence was analyzed with a confocal laser-scanning microscope META-LSM 510 (Zeiss, Germany) using laser lines at 405 nm (Diode laser), 488 nm (Ar/Kr laser), 543 nm (He/Ne laser), or 633 nm (He/Ne laser) alone or in combination. Wavelengths were separated by using the META module of the LSM. For data acquisition and analysis of confocal images the LSM 510 software (Zeiss, Germany) was applied. Images were taken at 2,048 x 2,048 dpi and were imported into Adobe Photoshop CS5, were digitally adjusted if necessary for brightness and contrast, and were assembled into plates.

3.2.7. Electron microscopy

In collaboration with Dr. Wiebke Möbius (Department of Neurogenetics, Max Planck Institute for Experimental Medicine, Göttingen) immunoelectron microscopy of ultrathin cryosections was performed as described previously (Feldmann et al., 2011). In brief, wild type and MeCP2-deficient mice were anesthetized with isofluorane (1-Chloro-2,2,2-trifluoroethyl-difluoromethylether, Abott, Wiesbaden, Germany) and perfused transcardially with 4% formaldehyde (Serva) in 0.1 M phosphate buffer. Vibratome sections of the brainstem were infiltrated with 2.3 M sucrose in 0.1 M phosphate buffer over night. Small blocks from the region of the inferior olive and the VRG were mounted onto aluminum pins for ultramicrotomy and frozen in liquid nitrogen. Ultrathin cryosections were immunolabeled with rabbit antibodies specific for 5-HTR$_{5B}$ and protein A-gold (10 nm) obtained from the Cell Microscopy Center, Department of Cell Biology, University Medical Center Utrecht, The Netherlands. Sections were analyzed with a LEO EM912AB (Zeiss, Oberkochen) and digital micrographs were obtained with an on-axis 2,048 x 2,048-CCD camera (TRS, Moorenweis).

3.2.8. Statistics

Physiological experiments using the working heart brainstem preparation (WHBP) were statistically analyzed using repeated ANOVA with Bonferroni´s *post-hoc test* and were performed using *GraphPad Prism*. Differences were considered statistically significant at the $p < 0.05$ level. Data are presented as mean ± standard error of the mean (SEM) or standard deviation (SD) (n = number of experiments). To quantify the phrenic nerve activity (PNA) from electrophysiological recordings a representative measurement of one-minute duration before and after each drug application (15 min interval) was integrated with *LabChart* software. The coefficient of variation (CV in %) was used as an index for the relative variability (SD divided by the mean) of time durations analyzed for bursts per minute derived from integrated recordings of phrenic nerve activity (∫PNA) (n = number of animals).

4. Results

This chapter summarizes the contribution of the glycinergic and especially of the serotonergic system to the disturbed breathing in a mouse model for the Rett syndrome. This phenotype is fully developed at postnatal day 40 (P40). Furthermore, this section provides new insights into the regulation, characteristics, and function of the serotonin receptor 5B.

4.1. Developmental expression of *Mecp2* in the VRG

To confirm a direct influence of MeCP2 on breathing disturbances in the Rett mouse we analyzed the expression of both *Mecp2* mRNA in the VRG and the translated protein MeCP2 in the brainstem of wt mice at different developmental stages (P7, P15, P21, or P40). The bilateral-arranged VRG includes the pre-BötC, which is considered to be important for respiratory rhythm generation.

4.1.1. *Mecp2* mRNA expression in the VRG at different developmental stages

To investigate the gene expression of *Mecp2* in wt mice, first mRNA was isolated from the VRG at different developmental stages (P7, P15, P21, or P40) and transcribed into cDNA, which served as a template in a subsequent quantitative PCR (q-PCR). The relative amount of *Mecp2* mRNA was high at the early stage P7 (1.876 ± 0.3505; fig. 4.1A) but significantly reduced at P15 (1.078 ± 0.2462; $p < 0.05$) and even lower at P21 (0.8437 ± 0.1841). At P40 the level of *Mecp2* mRNA increased slightly again to 1.053 ± 0.1006.

4.1.2. MeCP2 protein expression in the brainstem at different developmental stages

In order to determine the developmental expression of MeCP2 protein quantitatively an enzyme-linked immunosorbent assay (ELISA) was developed and performed with protein lysate from brainstem of wt mice that includes the VRG. MeCP2 protein values were related to total protein content and indicated as (MeCP2/total protein) x 10^{-7} in figure 4.1B. A high level of MeCP2 protein was detected at P7 as well as at P40, whereas in the intermediate stages P15 and P21 the protein expression was significantly lower. In comparison with the early stage P7 (12.00 ± 1.30), the relative amount of MeCP2 at P15 was significantly reduced to 9.80 ± 0.26 ($p < 0.01$) and

further decreased to 7.34 ± 0.13 (p < 0.001) at P21. At P40 the level of MeCP2 protein increased to a level similar to P7 (11.00 ± 0.06, p <0.0001).
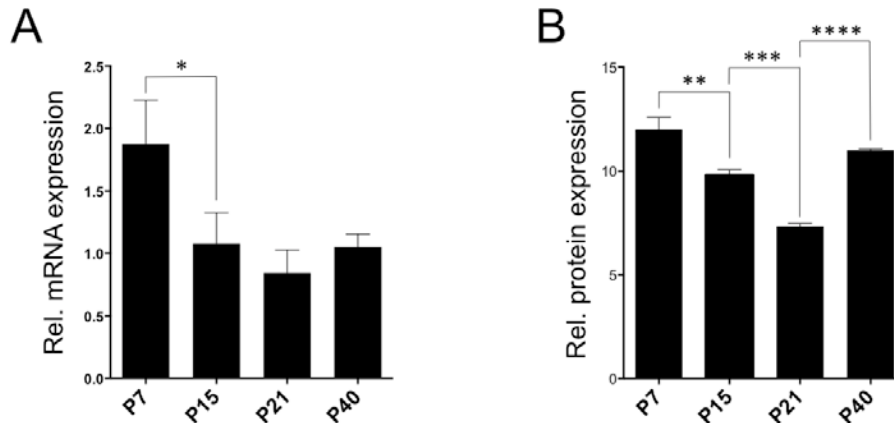

Figure 4.1. Developmental gene expression of *Mecp2*/MeCP2 in wt mice.
Mecp2 was measured quantitatively (**A**) at the RNA level in the VRG using q-PCR (n = 3) and (**B**) at the protein level in lysates from whole brainstem using ELISA procedure (n = 3) at 4 different developmental stages (P7, P15, P21, P40). The bar diagrams represent mean values and standard deviations (* = p ≤ 0.05; ** = p ≤ 0.01; *** = p ≤ 0.001; **** = p ≤ 0.0001; one-way ANOVA).

4.2. Identification of deregulated genes in the VRG

As MeCP2 expression in wt mice is high at P40 it was concluded that MeCP2 has an influence on gene expression in the VRG at this particular developmental period when the disturbed breathing phenotype in MeCP2 deficient mice is fully developed. Therefore, mRNA expression from genes associated with the glycinergic and the serotonergic system, which are important for respiratory network activity (Richter et al., 2003), was investigated using q-PCR from total RNA of the VRG.

4.2.1. Q-PCR analysis of components of the glycinergic system

Glycine is the most abundant inhibitory neurotransmitter in the brainstem (Lynch, 2004). Reciprocal inhibition of antagonistically connected glycinergic neurons is the indispensable drive for the respiratory rhythm (Richter & Spyer, 2001). Simultaneous blockade of glycinergic and GABA-ergic inhibition suppresses breathing (Paton & Richter, 1995). To test whether disturbed breathing in the Rett mouse originate from alterations in glycinergic transmission, important components of the glycinergic system were analyzed for their mRNA expression in the VRG of *Mecp2*$^{-/y}$ mice in comparison with wt mice. The ionotropic glycine receptor has a pentameric structure,

composed of five integral membrane subunits (Kuhse et al., 1995), which are encoded by different genes.

However, there was no significant change in the mRNA expression between wt and *Mecp2$^{-/y}$* mice in the VRG at P40 (fig. 4.2), neither for the glycine receptor subunits α1 (*Glra1*), α2 (*Glra2*), α3 (*Glra3*), α4 (*Glra4*), nor for the β subunit (*Glrb*). The strongest expression was observed for the glycine receptor β subunit, whereas the α2 and the α4 subunit were hardly detectable. No alterations in the mRNA expression were also found for the vesicular glycine transporter 1 (*Slc6a9*) and the synaptic glycine transporter 2 (*Slc6a5*). The mRNA level of gephyrin (*Gphn*), which plays a role in the assembling of glycine receptors (Fritschy et al., 2008) revealed also no alteration. Taken together, none of the investigated glycinergic genes were changed in the Rett mouse compared to wt.
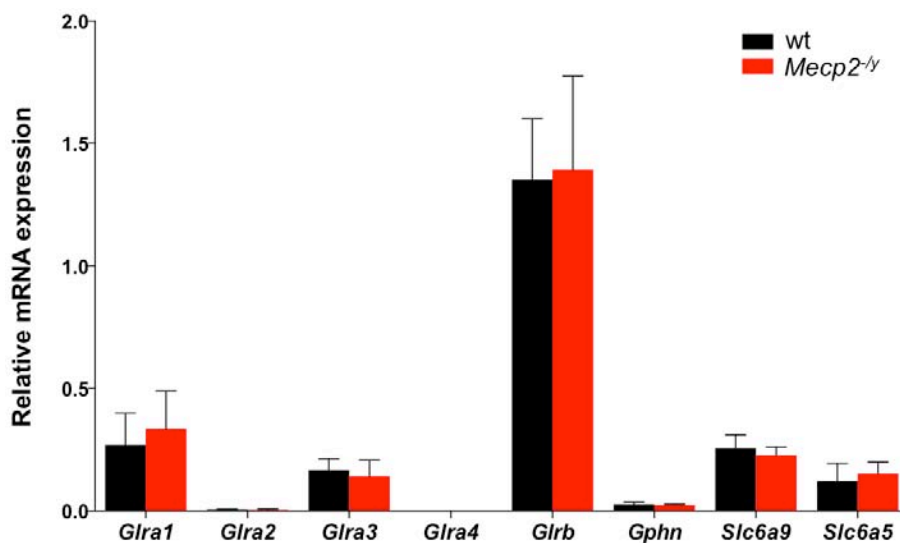

Figure 4.2. Comparison of mRNA expression of the glycinergic system in wt vs. *Mecp2$^{-/y}$* mice in the VRG at P40.

Messenger RNA level was measured by q-PCR. The bar diagram represents mean values and standard deviation from n = 5 biological replicates of the glycine receptor subunits α1 (*Glra1*), α2 (*Glra2*), α3 (*Glra3*), α4 (*Glra4*) and β (*Glrb*), the glycine transporter 1 (*Slc6a9*) and 2 (*Slc6a3*) and gephyrin (*Gphn*). None of the gene showed significant change in their mRNA expression (one-way ANOVA).

4.2.2. Quantification of mRNA expression of serotonergic components in the VRG

Serotonin (5-HT) is an important neuromodulator for breathing and its receptors (5-HTR) are widely expressed in the respiratory network (Richter et al., 2003; Manzke et al., 2009). To investigate the putative influence of the serotonergic system on breathing disturbances in the Rett mouse, 5-HT receptors as well as serotonin transporters and enzymes involved in the biosynthesis of serotonin were investigated for their mRNA expression in the VRG at P40 and compared with wt, which was set to 1. Q-PCR analysis revealed that 4 of altogether 12 investigated serotonergic genes were deregulated in the VRG of Rett mice. The mRNA level of *Htr2c* was reduced to roughly a half compared with wt (wt vs. *Mecp2*$^{-/y}$; 1.000 ± 0.073 vs. 0.481 ± 0.045; p ≤ 0.001), whereas the mRNA level for *Htr1d* (wt vs. *Mecp2*$^{-/y}$; 1.000 ± 0.197 vs. 2.230 ± 0.326, p ≤ 0.05) and dopamine decarboxylase (*Ddc*) (wt vs. *Mecp2*$^{-/y}$; 1.000 ± 0.157 vs. 3.590 ± 0.956, p ≤ 0.05) were increased by 2 or 3.5-fold, respectively. However, the strongest deregulation was observed for the *Htr5b* gene, which showed a 76-fold higher mRNA expression rate in the VRG of Rett mice in comparison with wt at P40. Because of deregulation of serotonergic genes in the VRG, especially the enormous alteration of the *Htr5b* gene, it was concluded that this might have effect on breathing disturbances in the Rett mouse. Hence, *Htr5b* was subject to deeper investigations.
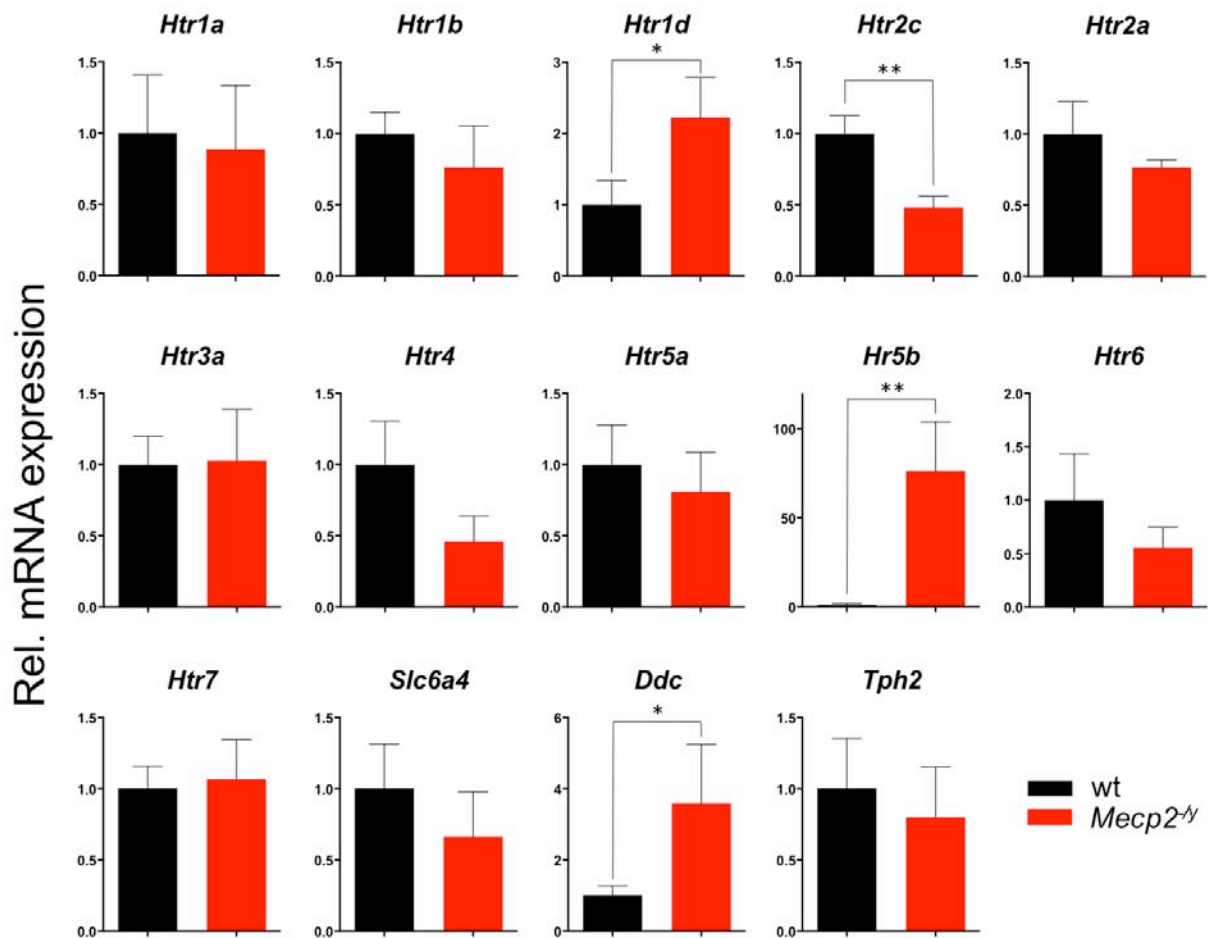
Figure 4.3. Comparison of mRNA expression of the serotonergic system in wt vs. *Mecp2$^{-/y}$* mice in the VRG at P40.

Messenger RNA level in the VRG was measured by q-PCR. The bar diagrams represent the results of separate q-PCR analysis with mean values and standard error of the mean from n = 3 biological replicates of genes for the serotonin receptors *Htr1a*, *Htr1b*, *Htr1d*, *Htr2c*, *Htr2a*, *Htr3a*, *Htr4*, *Htr5a*, *Htr5b*, *Htr6*, *Htr7*, the serotonin transporter (*Slc6a4*), and the enzymes dopamine decarboxylase (*Ddc*) and tryptophan hydroxylase 2 (*Tph2*). Asterisks indicate significance (* = p ≤ 0.05; ** = p ≤ 0.01; t-test).

4.2.2.1. Analysis of region specific *Htr5b* mRNA expression

To clarify whether the *Htr5b* mRNA is ubiquitously up-regulated in the Rett mouse throughout the brain, q-PCR analysis was performed from various brain regions at P40 (fig. 4.4). Besides the VRG, a significant increase of *Htr5b* mRNA in the cortex of Rett mice was observed. In contrast to the strong up-regulation seen in the VRG (fig. 4.3), this increase was only moderate by 2.5-fold compared to wt, which was set to 1 (wt vs. *Mecp2$^{-/y}$*; 1.00 ± 0.054 vs. 2.63 ± 0.105; p ≤ 0.001). Other regions investigated (cerebellum, hippocampus, and inferior olive) did not show any significant *Htr5b* mRNA alteration between wt and Rett mice.
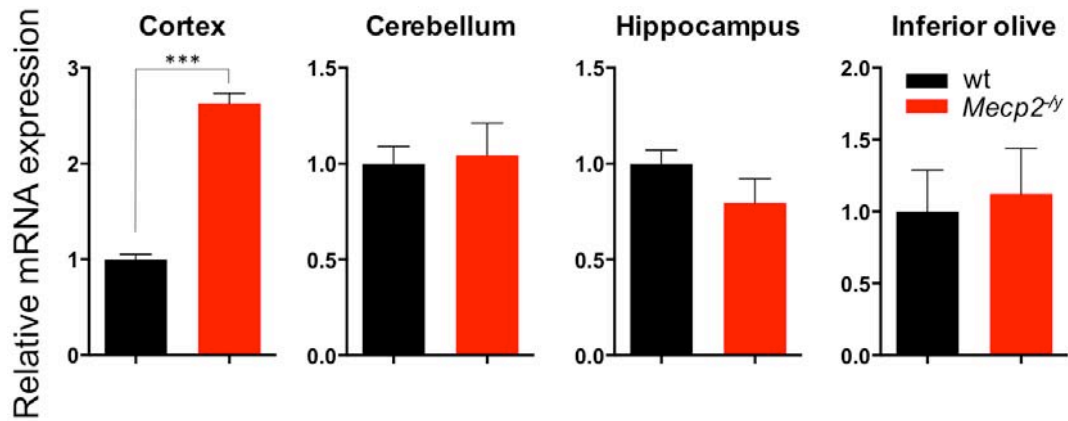
Figure 4.4. Comparison of *Htr5b* mRNA expression in wt vs. *Mecp2^{-/y}* mice from different brain regions at P40.

Htr5b mRNA expression level from cortex, cerebellum, hippocampus, and inferior olive were measured by q-PCR. The bar diagrams represent mean values and SEM of n = 3 biological replicates. Wild type was set to 1. Asterisks indicate significance (*** = p ≤ 0.001; student´s t-test).

Overall, a systemic alteration of *Htr5b* mRNA expression in the brain of Rett mice in comparison with wt mice was not observed at development stage P40. The strong dysregulation was mainly restricted to the VRG region in the brainstem.

4.2.2.2. Developmental expression of *Htr5b* in wt and Rett mice

Q-PCR studies of *Htr5b* in the VRG were performed from 4 different postnatal development stages (P7 - P40). No differences in the *Htr5b* mRNA expression were detected between wt and Rett mice at P7, P15, and P21. As already shown in fig 4.3, an *Htr5b* dysregulation was observed only at P40, which correlates with the onset of breathing disturbances in the Rett mouse.
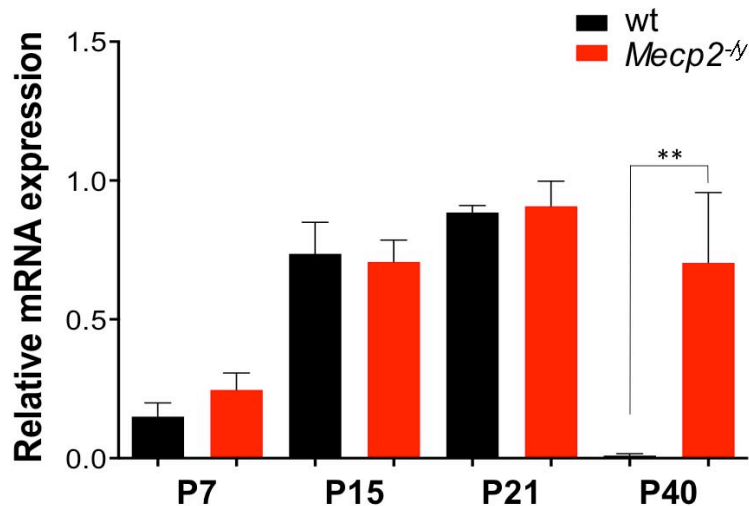

Figure 4.5. Developmental mRNA expression profile of *Htr5b* in the VRG in wt compared to *Mecp2^{-/y}* mice.

Htr5b expression level in the VRG was measured by q-PCR. The bar diagram represents mean value and SEM from n = 3 biological replicates at each development stage (P7, P15, P21, and P40) with asterisks indicating significance (** = $p \leq 0.01$; one-way ANOVA).

4.2.3. Protein expression of 5-HTR$_{5B}$

Information about the 5-HTR$_{5B}$ and its distribution throughout the brain is sparse. *In situ* hybridization revealed strong *Htr5b* mRNA expression in the intermediate layers of the entorhinal cortex, in the CA1 region and the parasubiculum of the hippocampus, and in the medial habenula. In the brainstem, *Htr5b* mRNA is abundantly expressed in the dorsal raphé nucleus and in the inferior olive (Serrats et al., 2004).

In order to verify the results of *Htr5b* mRNA expression in the VRG at the protein level and to refine the localization of the 5-HTR$_{5B}$ protein within the respiratory network, immunohistochemistry was performed using both self-made and commercially available antibodies. The homemade antibody, which was produced in

our lab, was directed against the very last 11 amino acids of the C-terminal domain of the 5-HTR$_{5B}$ protein (NH$_2$-KNYNNAFKSLFTKQR-COOH). This epitope is 100% homologous in all species including men. The antibody was tested on N1E-115 cells. 5-HTR$_{5B}$-IR was only detectable in cells transfected with *Htr5b*, whereas no signal was observed in non-transfected cells. The 5-HTR$_{5B}$ labeling was abolished by pre-incubation of the primary antibody with peptides that were used for immunization indicating specificity. Hence, it was concluded that the antibody is reliable for detection of endogenously expressed 5-HTR$_{5B}$ protein.
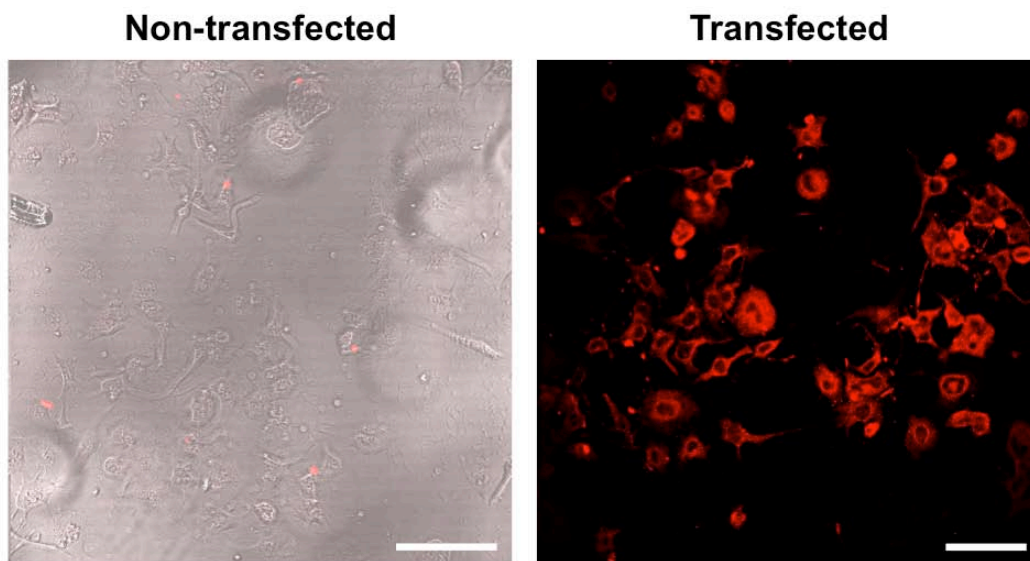

Figure 4.6. Test for specificity of the peptide specific anti-5-HT$_{5B}$R antibody.
Htr5b-transfected and non-transfected N1E-115 cells were stained with a homemade anti-5-HTR$_{5B}$ antibody followed by a secondary Atto546-conjugated anti-rabbit IgG antibody. Fluorescence was visualized using CLSM. IR was only detectable in transfected cells. Scale bars = 100 µm.

At P40 an abundant 5-HTR$_{5B}$-immunoreactivity (-IR) was detected in the inferior olive and the nucleus raphé obscurus of both wt and *Mecp2*$^{-/y}$ mice, which is in accordance with the literature describing a strong *Htr5b* mRNA expression in these regions in rat (Serrats et al., 2004). In contrast, in the pre-BötC a strong 5-HTR$_{5B}$ expression was only observed in Rett mice, whereas the protein expression in the pre-BötC of wt was rather weak, which is consistent with the q-PCR results.
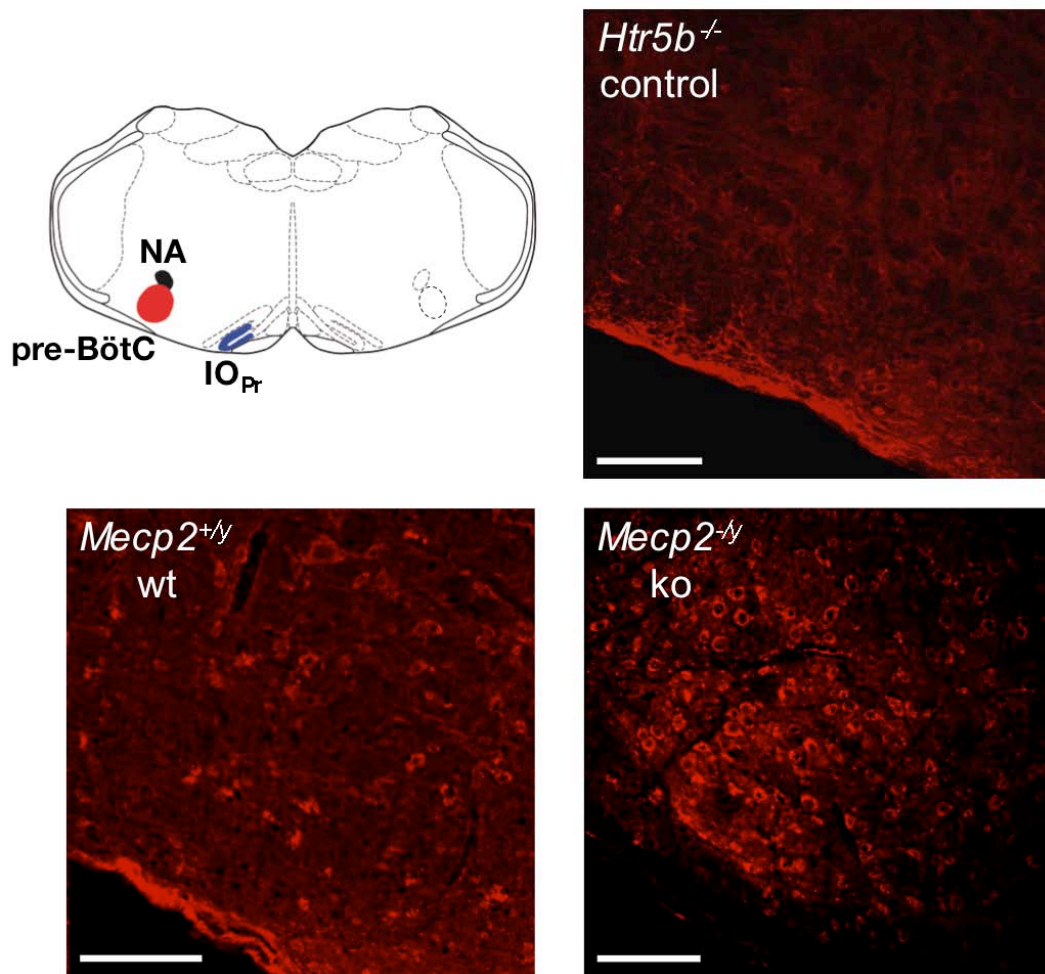
Figure 4.7. Comparison of 5-HTR$_{5B}$ protein expression in wt and Rett mice at P40.
Representative images of 5-HTR$_{5B}$ immunoreactivity in the ventrolateral medulla from wt and *Mecp2* knockout mice. Sections from *Htr5b* null mice (*Htr5b$^{-/-}$*) served as negative control. Schematic drawing shows where the sections were cut with the pre-Bötzinger complex (pre-BötC) and its anatomical landmarks such as the nucleus ambiguus (NA) and the principal nucleus of the inferior olive (IO$_{Pr}$). Scale bars = 100 µm.

4.3. Regulation of *Htr5b* expression in the VRG

MeCP2 is a transcription factor involved in epigenetical gene regulation (Guy et al., 2011). As *Htr5b* is dysregulated between wt and *Mecp2$^{-/y}$* mice in the VRG at P40, it was investigated whether MeCP2 directly causes these alterations. Recently, it has been reported that in mice experiencing social stress the *Htr5b* gene is under control of the transcription factor ATF-7 (Maekawa et al., 2010). As RTT is also accompanied with stress, we analyzed whether ATF-7 affects *Htr5b* mRNA expression in Rett mice. However, q-PCR performed from total RNA of the VRG region at P40 revealed no alterations in *Atf7* mRNA expression between wt and Rett

mouse (1.0000 ± 0.0927 vs. 0.8725 ± 0.0465; fig. 4.8A). In addition, the mRNA level of the mitogen-activated protein kinase 14 (*Mapk14*), which activates ATF-7 by phosphorylation, was not changed significantly (1.0000 ± 0.0611 vs. 0.9316 ± 0.04224; fig. 4.8A).

4.3.1. Developmental expression of *Htr5b* in the VRG

First evidence of a direct regulation of *Htr5b* by MeCP2 in the VRG was obtained from *Htr5b* mRNA expression in the VRG (fig. 4.5) when compared with MeCP2 protein expression in the brainstem at different development stages (P7, P15, P21, and P40) (fig. 4.8B). In wt mice the MeCP2 protein level gradually decreased during P7 and P28. Simultaneously *Htr5b* mRNA expression was increased from 0.1496 ± 0.0490 at P7 to 0.8839 ± 0.0255 (p ≤ 0.0001), whereas at P40 when the MeCP2 protein level turned back to high level, the *Htr5b* mRNA was again greatly suppressed (0.00921 ± 0.0074). The reciprocal developmental profiles of MeCP2 protein and *Htr5b* mRNA in wt indicated a putative direct control of the *Htr5b* gene by MeCP2.
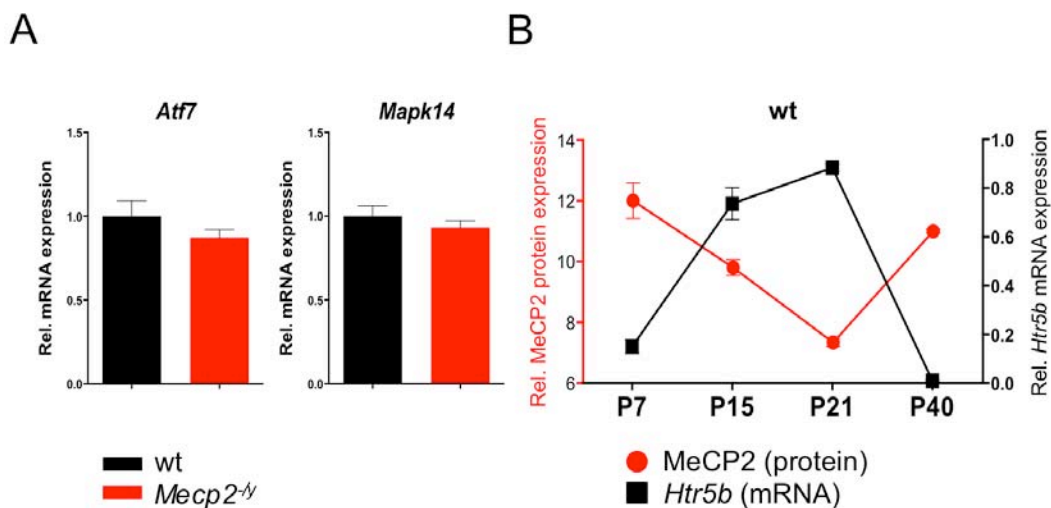
Figure 4.8. Regulation and developmental expression of *Htr5b* in wt and Rett mice.
(**A**) Messenger RNA analysis of *Atf7* and *Mapk14* in the VRG at P40 of wt and *Mecp2$^{-/y}$* mice. Bar diagrams show mean value and SEM of n = 5 biological replicates (student´s t-test). (**B**) Comparison of MeCP2 protein and *Htr5b* mRNA expression in wt mice during development stages P7, P15, P21, and P40. MeCP2 protein content was measured using ELISA procedure from brainstem lysates (n = 3). *Htr5b* mRNA expression was measured in the VRG using q-PCR (n = 3). *Htr5b* mRNA level was increased at developmental stages when MeCP2 protein concentration was reduced, whereas low level of *Htr5b* was found at P7 and P40 when MeCP2 protein was high.

4.3.2. MeCP2 binds to the *Htr5b* promoter

In order to test whether *Htr5b* is a direct target of MeCP2 we performed chromatin immunoprecipitation (ChIP) to test for putative MeCP2 binding within the proximal *Htr5b* promoter region. Therefore, protein-DNA interactions were fixed and shared into smaller fragments. MeCP2-precipitated DNA was purified and served as template in subsequent q-PCR analysis. For want of a defined putative MeCP2 DNA binding site we used 7 primer pairs, which bind along the 5.3 kb proximal *Htr5b* promoter (+5.0 kb to +0.2 kb before transcription start). At all investigated loci we found a significant difference between MeCP2 precipitated DNA using a MeCP2-specific antibody, in comparison to controls. However, the highest amount of MeCP2-precipitated DNA was detected at +4.7 kb. This was (3.6 ± 0.5)-fold compared to the IgG control, which was set to 1.0 $(1.0 \pm 0.5; p < 0.01)$, indicating an efficient MeCP2 binding to the *Htr5b* promoter (fig. 4.9A).

4.3.3. MeCP2 represses *Htr5b* expression *in vitro*

To determine whether the observed binding of MeCP2 inhibits the expression of the *Htr5b* gene directly, we co-transfected luciferase reporter constructs driven by the 4.8 kb up stream *Htr5b* promoter together with increasing amounts of *Mecp2* expression plasmid (1 or 2 µg) into N1E-115 cells. Before performing a promoter-luciferase reporter assay (fig. 4.9B), the MeCP2 expression was verified using immunoblot analysis (fig. 4.9C). Higher amount of *Mecp2* expression plasmid led to an increase of MeCP2 protein. In contrast to the MOCK control without MeCP2, luciferase activity was gradually decreased with increasing amounts of MeCP2 by approximately 30% $(p<0.01)$ or 53% $(p<0.001; n = 3;$ fig. 4.9B), respectively.
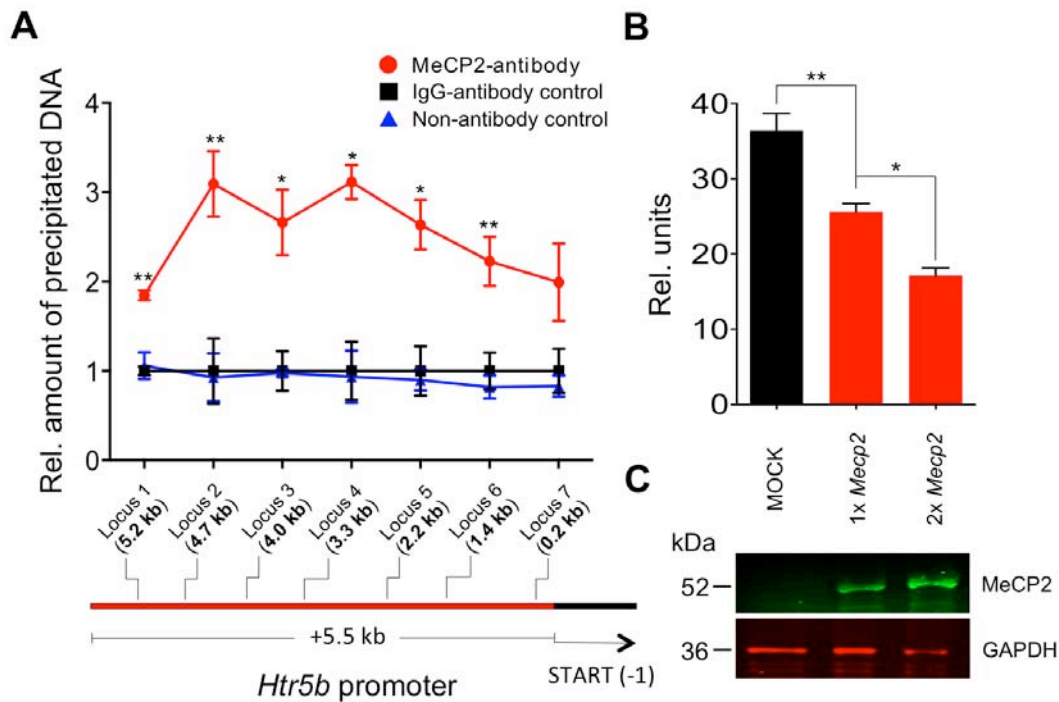
Figure 4.9. Direct regulation of *Htr5b* gene expression by MeCP2 in the VRG.
(**A**) Chromatin immunoprecipitation (ChIP) analysis was performed using an anti-MeCP2 specific antibody. DNA was isolated from the VRG of wt mice. Quantification of MeCP2-precipitated DNA followed by q-PCR using 7 different primer pairs specific for different loci of the *Htr5b* promoter (schematically shown below the diagram). (**B**) *Htr5b* promoter luciferase assay. N1E-115 cells were co-transfected with *Htr5b* promoter and increasing amounts of *Mecp2* expressions constructs. Bar diagram shows mean value and SEM of luciferase activity (n = 3). Asterisks indicate significance (* = p < 0.05; ** < 0.01; one-way ANOVA). (**C**) Representative MeCP2 immunoblot of N1E-115 cell lysates transfected with increasing amount of *Mecp2* expression constructs. Glycerinaldehyd-3-phosphat-dehydrogenase (GAPDH) served as reference protein and loading control.

4.4. 5-HTR$_{5B}$ is expressed in human

The *Htr5b* is abundantly expressed in the inferior olive of rodents (Serrats et al., 2004). The gene exists in all mammalian species with exception of men where it is described as a pseudo gene (Grailhe et al., 2001). In contrast to rodents and other mammals the human *HTR5B* open reading frame is disrupted by 3 stop codons and repeated insertion in its 5'-region, which affects the N-terminal part of the protein (fig. 4.11).

Surprisingly, immunohistochemistry of human brainstem sections using self-made anti-5-HTR$_{5B}$ antibodies (fig. 4.6), which are directed against the C-terminal domain of the protein, revealed a strong signal in the inferior olive (fig. 4.10). Furthermore, higher magnification showed an unexpected clustered expression pattern.
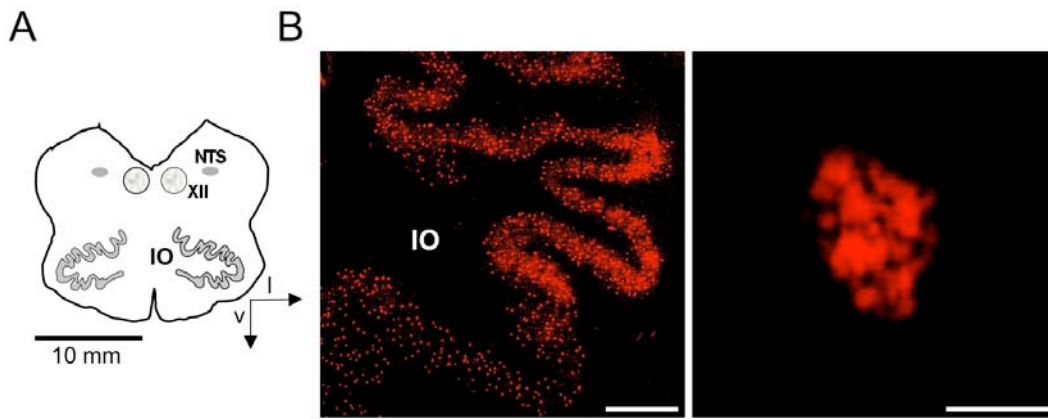
**Figure 4.10. Expression of the 5-HTR$_{5B}$ receptor in the human inferior olive.**

(**A**) Schematic representation of a human brainstem section with anatomical landmarks inferior olive (IO), nucleus of the solitary tract (NTS), and hypoglossal nucleus showing where the sections were taken from. (**B**) Representative human brainstem sections stained with anti-5-HTR$_{5B}$ antibody followed by an Atto546-conjugated secondary antibody. Immunofluorescence was finally visualized by CLSM. Strong IR was detected in the IO. Scale bars = 200 µm (overview) or 10 µm (clustered 5-HTR$_{5B}$ expression within a single cell of the human IO).

4.4.1. The serotonin receptor 5B is truncated

Depending on the unexpected result of 5-HTR$_{5B}$ expression in human tissue, DNA sequence comparisons were carried out. The rodent *Htr5b* gene, which consists of two exons, revealed highly conserved second ATG in the 5'-region within the first exon in all species (4.11B). This ATG is in frame with the coding sequence, but the corresponding translation would result in a truncated protein containing only 197 of 370 amino acids with a theoretical relative molecular mass of 22.5 kDa. Surprisingly, although the open reading frame (ORF) in rodents is not disrupted, 5-HTR$_{5B}$ immunoblot analyses of mouse and rat brainstem lysates revealed a specific band at about 23 kDa, which corresponds with the predicted truncated variant (fig. 4.11A). No signal was observed at 41 kDa, which is the expected relative molecular mass for the full-length receptor. Comparison of the truncated 5-HTR$_{5B}$ amino acids sequence starting with the methionine encoded by the second ATG reveled a high conservation, suggesting that the C-terminal part is of special functional importance. Related to mouse, rat, rabbit, and human orthologs showed 97%, 89%, or 85% homology, respectively (fig. 4.11C). Originally the 5-HTR$_{5B}$ has been classified as a member of G-protein coupled receptors, which possess seven transmembrane domains (Hoyer et al. 2002).

According to transmembrane domain analysis using *TMHMM server 2.0* (fig. 4.11D), the truncated 5-HTR$_{5B}$ lacks the first three transmembrane domains including the serotonin binding site, which is originally located in the N-terminal part of the protein (fig. 4.11E). However, the putative G-protein binding site, which comprises the last two intracellular domains (Bockaert, 1991; Strader et al., 1995), is still present.
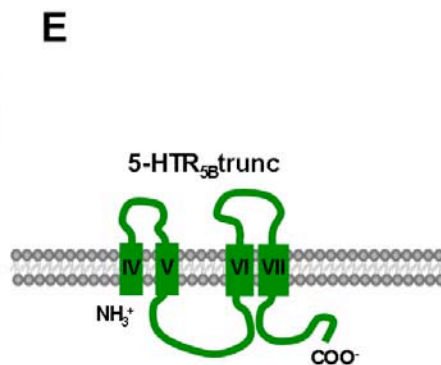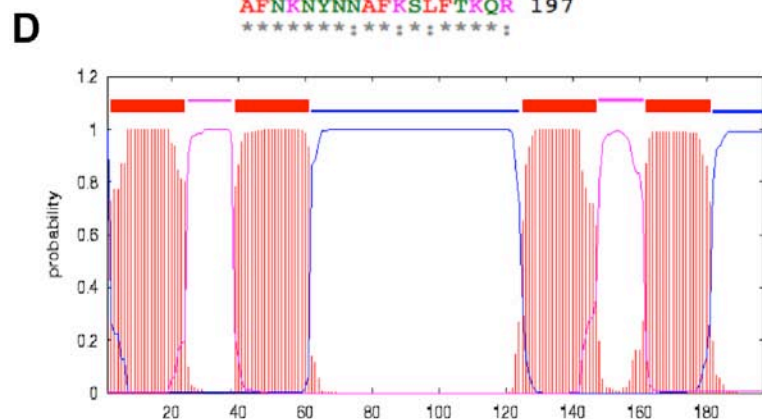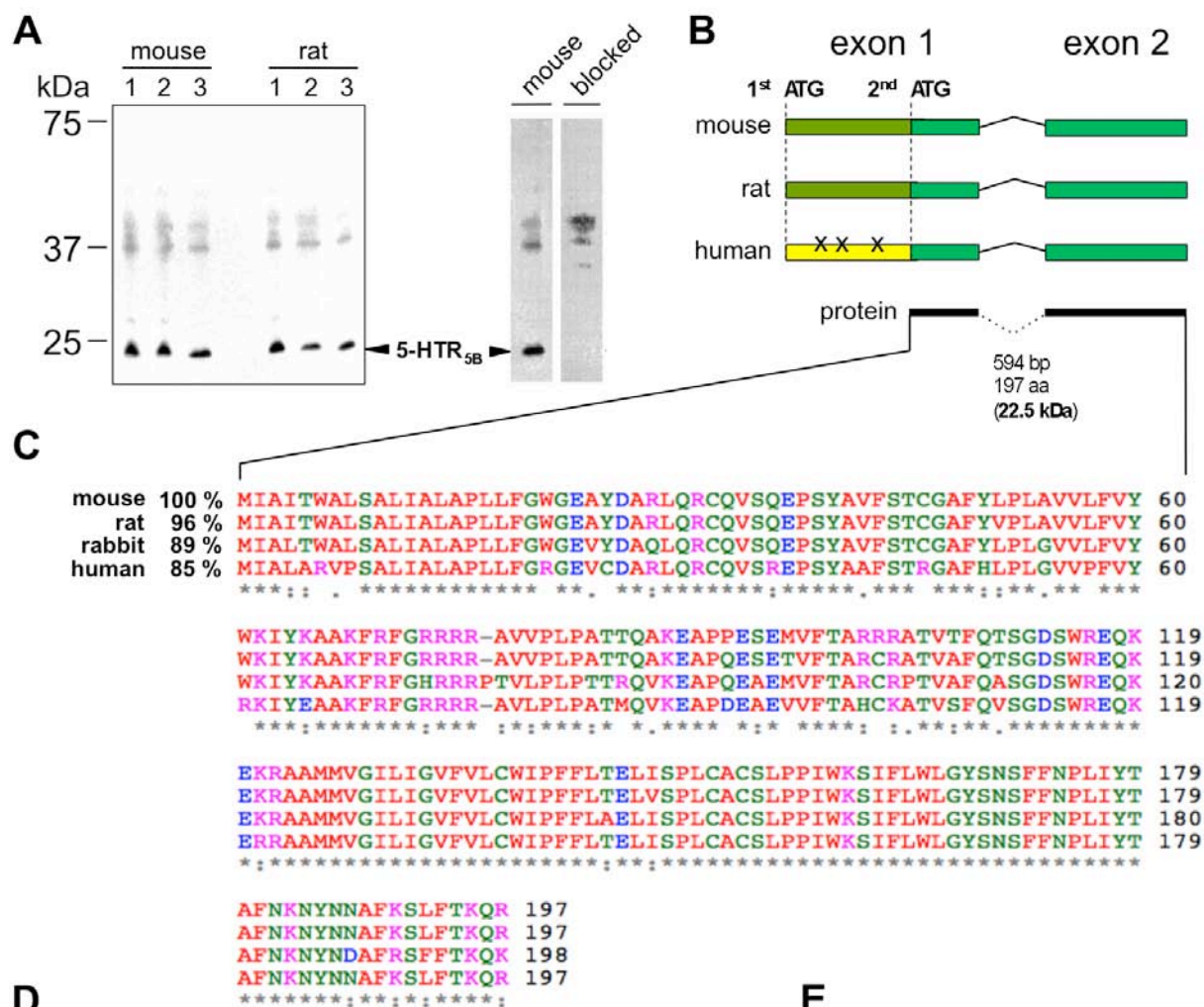
Figure 4.11. Truncation of 5-HTR$_{5B}$.

(**A**) 5-HTR$_{5B}$ immunoblot analysis of brainstem lysates (80 µg total protein per lane) from mouse and rat (n = 3) and control (antibody blockade using antigen-specific peptide) using homemade anti-5-HTR$_{5B}$ antibodies. A specific band was detected at approximately 23 kDa. (**B**) Schematic representation of the *Htr5b* gene with exon-intron structure. In men, the open reading frame is disrupted by insertion and nonsense mutations (marked as asterisks). *Htr5b* sequence comparison among species revealed a second start-ATG within the first exon. Translation would lead to a truncated protein of 197 amino acids with a predicted relative molecular mass of 22.5 kDa. (**C**) Comparison of the truncated 5-HTR$_{5B}$ amino acid sequence among 4 species using *ClustalW 2.0* revealed high homology. Percentages are related to mouse (100%). Asterisks under the amino acid mean 100% consensus. (**D**) Identification of membrane-located amino acids of the truncated 5-HTR$_{5B}$ using *TMHMM server 2.0*. Probability of 1.0 means 100% likelihood. Purple line means the domain is extracellular. Blue lines means the domain is intracellular. (**E**) shows a schematic model of the truncated 5-HTR$_{5B}$ based on the membrane prediction. The protein contains only the last 4 of naturally 7 transmembrane domains.

Overall, the expression of the protein in the human inferior olive, the immunoblot analysis of rodent brainstem lysates, and the strong phylogenetical conservation of the shortened variant of 5-HTR$_{5B}$ revealed evidence of the existence of a naturally expressed truncated GPCR.

Although there was no evidence of a full-length receptor at all, for further characterization both, the truncated and the full-length variant of 5-HTR$_{5B}$ were analyzed.

4.5. Functions of 5-HTR$_{5B}$

The truncation of the 5-HTR$_{5B}$ protein raised the question whether this protein is still functional and where it is expressed within the cell. Therefore, both 5-HTR$_{5B}$ variants were cloned from mouse brainstem cDNA, cloned into the expression plasmid pcDNA3.1(-), and fused to different fluorescent proteins.

4.5.1. Unusual endosomal localization of 5-HTR$_{5B}$ in neurons

To address the question of the 5-HTR$_{5B}$ localization, 1 - 2 µg of expression plasmid with different variants of *Htr5b* were transfected into murine neuroblastoma cells (N1E-115) and analyzed after 16 - 24 hours of incubation by confocal microscopy. In contrast to other investigated serotonin receptors, such as 5-HTR$_{1A}$ and 5-HTR$_7$, which showed an expected cell membrane expression, 5-HTR$_{5B}$ was expressed in distinct intracellular clusters no matter whether the full-length or the truncated variant was analyzed (fig. 4.12). Expression analysis in other cell lines, such as human embryonic kidney (HEK) cells or monkey kidney Cercopithecus aethiops, origin-defective SV-40 (COS-7) cells led to similar intracellular expression pattern. Interestingly, fusion constructs of *Htr5a*, which belongs to the same subclass as *Htr5b*, displayed also a clustered intracellular expression. However, contrary to *Htr5b* variants, in rare cases a surface membrane expression was observed for the *Htr5a* translated protein.
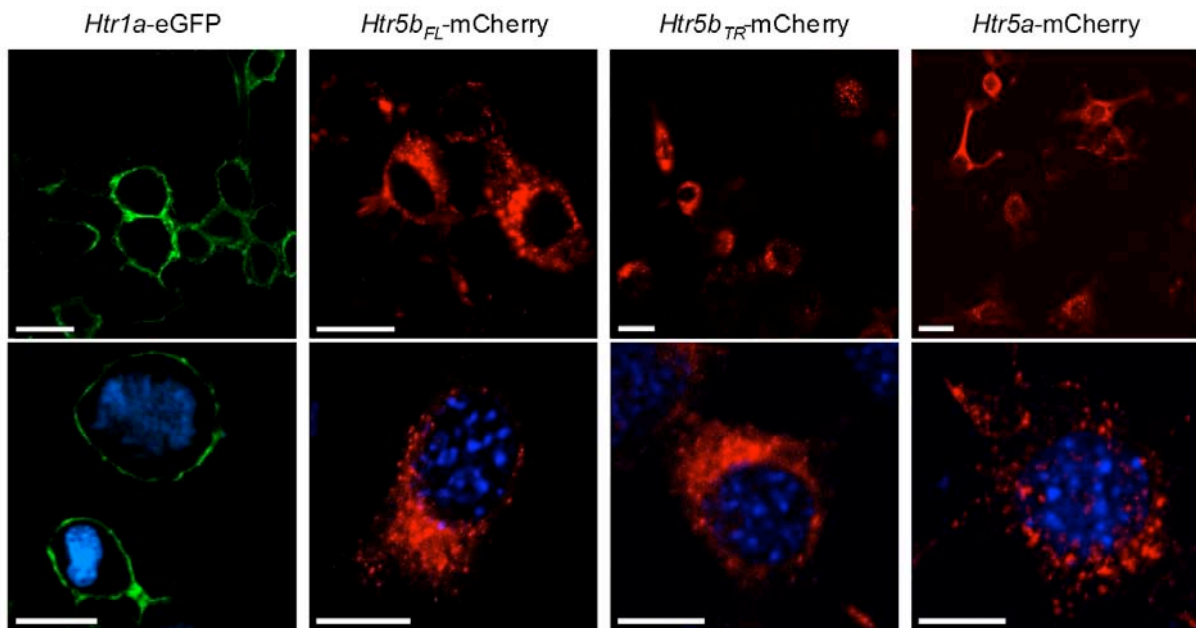
Figure 4.12. Localization of 5-HTR$_{5B}$ variants in overexpressing neuroblastoma cells.
N1E-115 cells were transiently transfected with *Htr1a*-eGFP (green), *Htr5b$_{FL}$*-mCherry, *Htr5b$_{TR}$*-mCherry, and *Htr5a*-mCherry fusion constructs (red). The lower panel shows cells at higher magnification together with DAPI nucleus staining (blue). EGFP and mCherry fluorescence were visualized directly using CLSM. Scale bars in the upper panel = 20 µm, in the lower panel = 10 µm.

For identification of the exact localization of intracellular 5-HTR$_{5B}$, fusion constructs of *Htr5b* were co-expressed in N1E-115 cells together with fluorescent marker

constructs, which are specifically located in characteristic subcellular compartments (fig. 4.13). Detailed analysis revealed a strong co-expression of 5-HTR$_{5B}$ with the endosome, but only a weak one with the lysosome or the endoplasmic reticulum. No co-expression was found for the cell membrane or mitochondria.
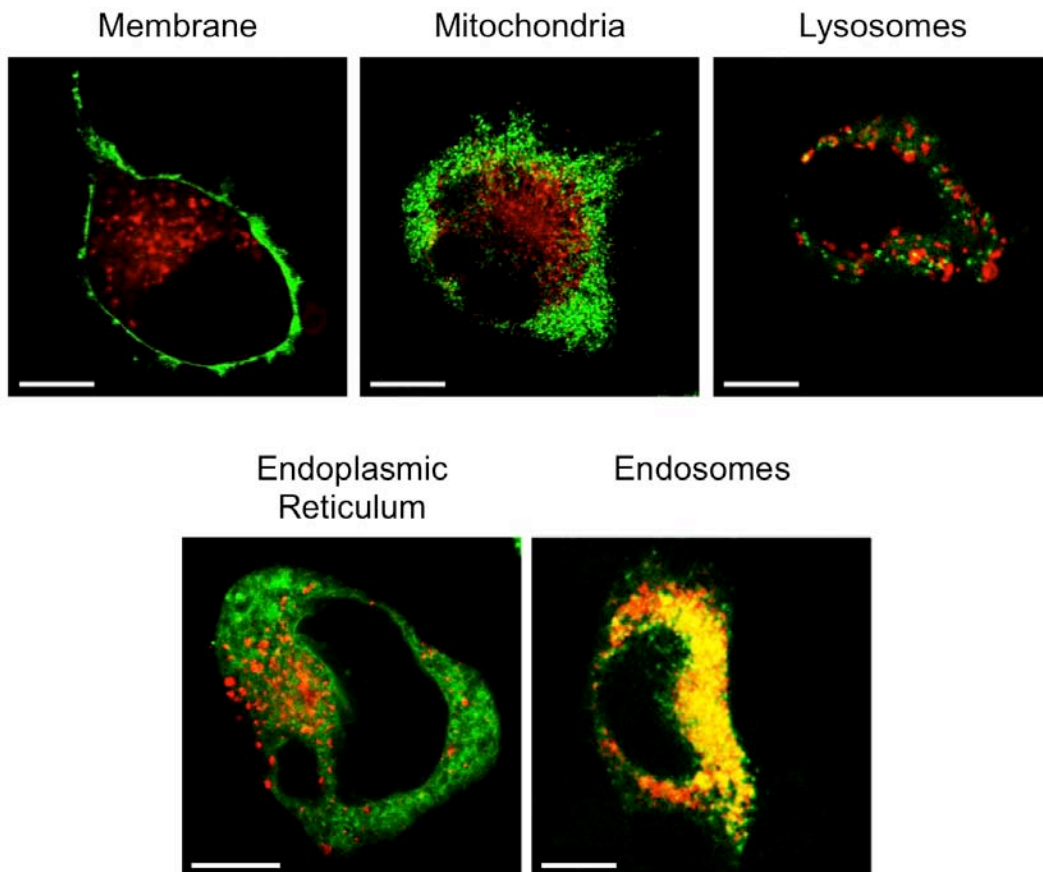
Figure 4.13. Identification of subcellular localization of 5-HTR$_{5B}$ protein *in vitro*.
Representative images of *Htr5b$_{FL}$*-mCherry (red) expressed in N1E-115 cells, which are co-transfected with fluorescent fusion constructs specific for subcellular compartments (green): pEYFP-Mem (membrane), pEYFP-Mito (mitochondria), pEYFP-Lamp1 (lysosome), pEYFP-ER (endoplasmic reticulum) and pEYFP-Rab7 (endosomes). Fluorescence was finally visualized using CLSM. Strong overlay was observed between 5-HTR$_{5B}$ and the endosomal compartment. Scale bars = 10 μm.

To exclude that these results were produced by artifacts from overexpression and to confirm the localization *in situ*, electron microscopy was performed on brainstem sections of wt mice using an anti-5-HTR$_{5B}$ antibody. A specific signal was detected in cells of the inferior olive. However, the cell surface membrane did not show any 5-HTR$_{5B}$-IR (fig. 4.14A). Detailed analysis showed a signal associated to membranes of vesicular and tubular compartments (fig. 4.14B, C).
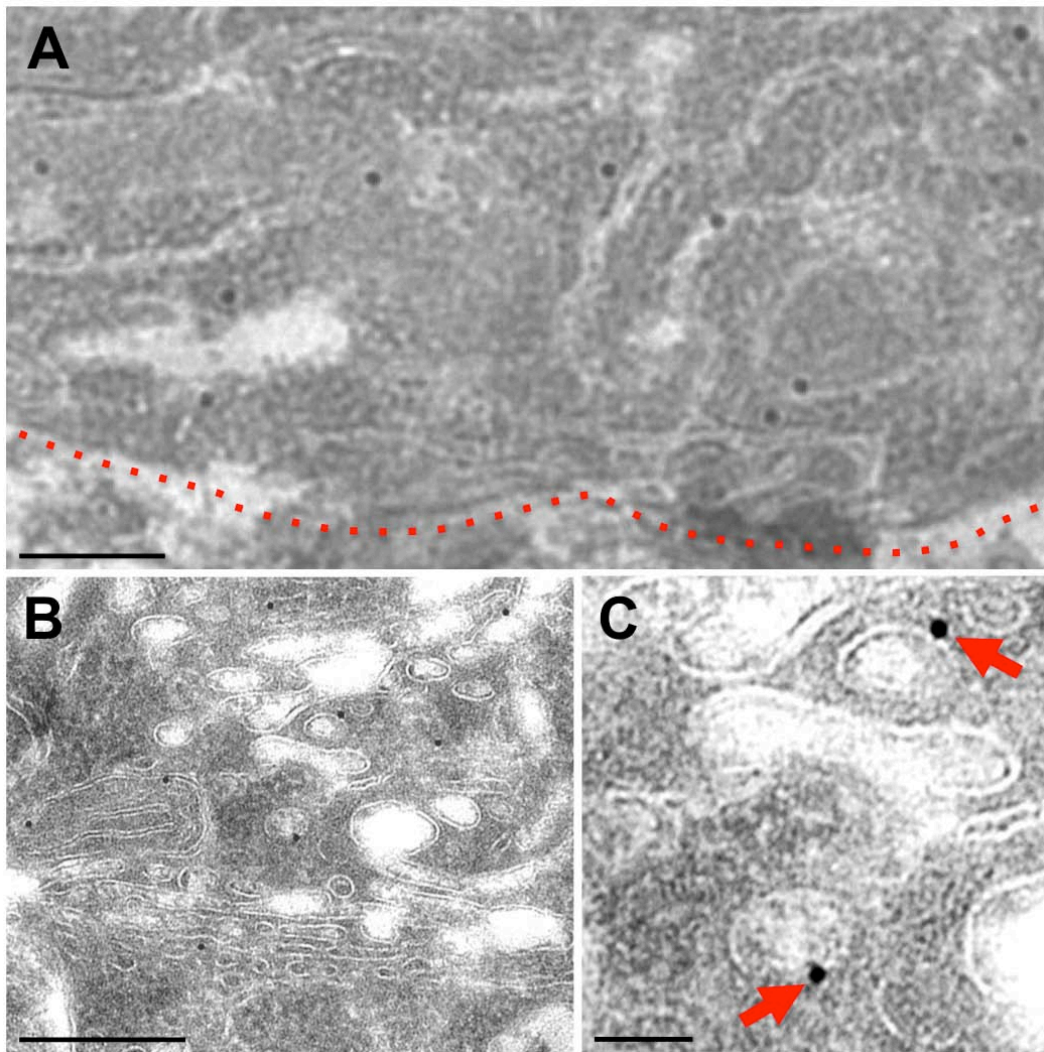
Figure 4.14. Intracellular localization of 5-HTR$_{5B}$ *in situ*.

Representative cryo-immunogold staining visualized by electron microscopy. Images of different magnification show 5-HTR$_{5B}$-IR in the inferior olive of wt mice at P40. (**A**) No 5-HTR$_{5B}$-IR was observed in the cell surface membrane (dotted red line) in contrast to strong signals in the membrane of vesicular and tubular intracellular compartments (**B**, **C**; red arrows). Scale bars = 100 nm in A; 200 nm in B; or 50 nm in C.

Furthermore, immunohistochemistry performed on brainstem sections of GFAP-transgenic mice, which express GFP under the control of the *glial fibrillary acidic protein* (*Gfap*) promoter, revealed no co-expression of 5-HTR$_{5B}$ and GFAP in the inferior olive (4.15A) and in the nucleus raphé obscurus (fig. 4.15B). Since GFAP is an established marker for astroglial cells, it was concluded that 5-HTR$_{5B}$ is expressed in neurons.
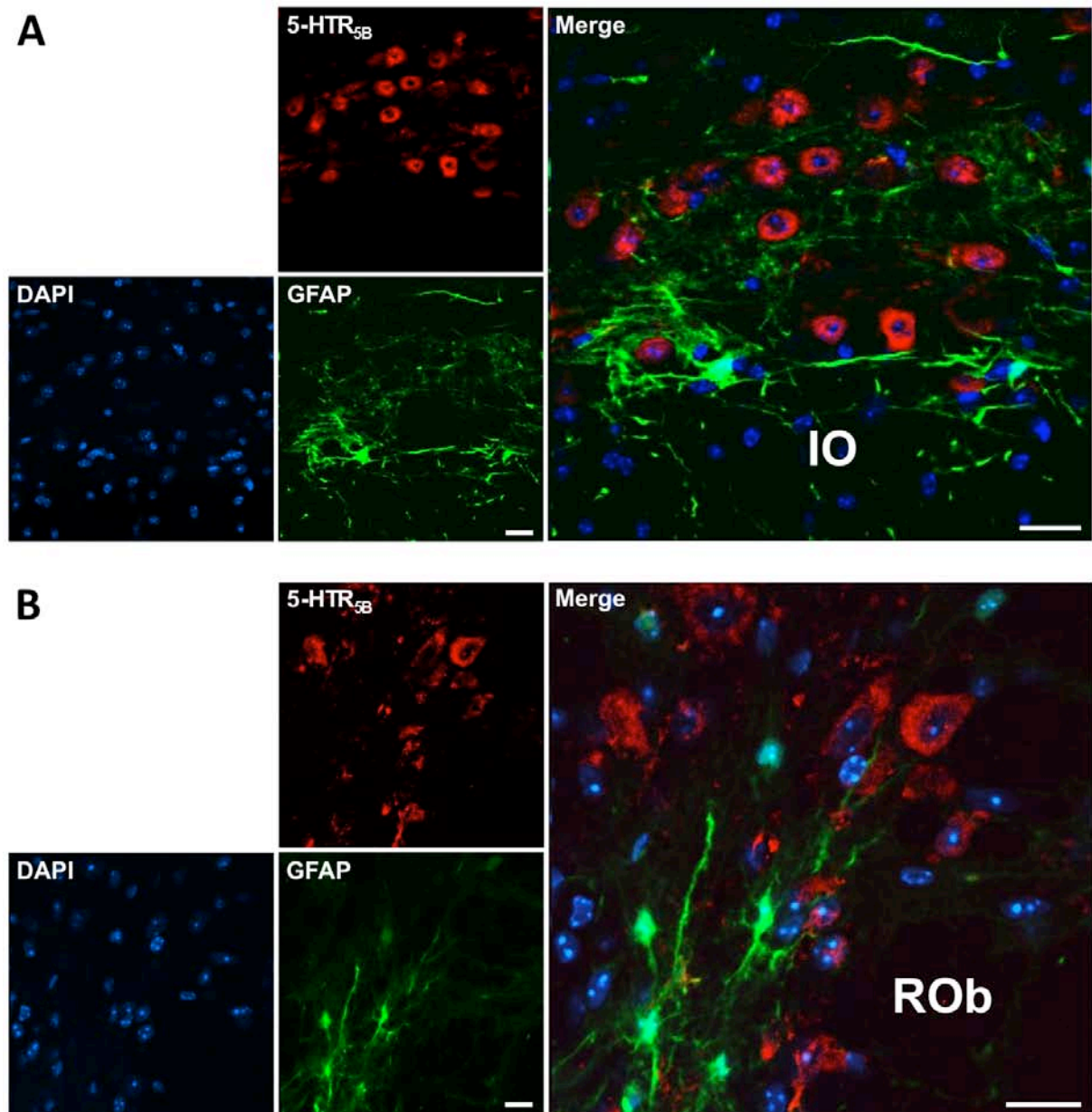
Figure 4.15. Neuronal expression of the 5-HTR$_{5B}$ protein.

Representative staining of 5-HTR$_{5B}$-IR (red) in the region of the (**A**) inferior olive (IO) and (**B**) nucleus raphé obscurus (ROb). Immunohistochemistry was performed on brainstem sections of mice, which express the green fluorescent protein (GFP) under the control of the glial fibrillary acidic protein (*Gfap*) promoter (green). DAPI nucleus staining (blue). Fluorescence was visualized using CLSM. There was no co-expression of GFAP and 5-HTR$_{5B}$. Scale bars = 20 μm.

Taken together, results of cryo-immunogold electron microscopy and CLSM of transfected cells as well as on brainstem sections using *Gfap*-transgenic mice revealed that 5-HTR$_{5B}$ is predominantly located in the membrane of intracellular vesicles. Furthermore, the truncated protein is naturally expressed in neurons but not in glial cells.

*Since the truncated receptor lost its ligand-binding site and is not expressed on the cell surface membrane this protein is renamed as **5-HT$_{5B}$** to differentiate it from ordinary metabotropic serotonin receptors.*

4.5.2. 5-HT$_{5B}$ affects localization of serotonin receptors

Originally the serotonin receptor 5B belongs to G-protein coupled receptors (Hoyer et al., 2002). Some GPCRs such as dopamine receptor D2, the muscarinic receptor m3, GABA(B) R1 and GABA(B) R2 can interact and form heterodimers (Angers et al., 2002; White et al., 1998). However, there is only little information about interactions between serotonin receptors, which seems to be rather weak (Renner et al., 2012). Confocal microscopy of 5-HTR$_{1A}$ and 5-HT$_{5B}$ co-transfected N1E-115 cells revealed a strong co-expression of both receptors (fig. 4.16).

The presence of 5-HT$_{5B}$ in 5-HTR$_{1A}$ expressing cells led to a de-localization of 5-HTR$_{1A}$ from the plasma membrane into the same compartment where 5-HT$_{5B}$ was expressed. Furthermore, the efficiency of 5-HTR$_{1A}$ translocation was only depending on the expression level of 5-HT$_{5B}$. This interaction was observed for both variants, the full-length and the truncated form of 5-HT$_{5B}$ to an equal extent. High 5-HT$_{5B}$ expression led to increased amount of intracellular 5-HTR$_{1A}$, whereas a low level of 5-HT$_{5B}$ showed only small amounts of co-expressed 5-HTR$_{1A}$ indicating that there might be a direct interaction in a certain stoichiometric ratio between both proteins. In contrast to 5-HT$_{5B}$ the 5-HTR$_{5A}$, which showed also a predominantly intracellular expression pattern (fig. 4.12), had no effect on 5-HTR$_{1A}$ localization (fig. 4.16A).

In contrast to the de-localization of 5-HTR$_{1A}$, the cell surface expression of the 5-HTR$_7$ remained unaffected when co-expressed with 5-HT$_{5B}$ variants. No co-expression of both receptors was observed (fig. 4.16B).
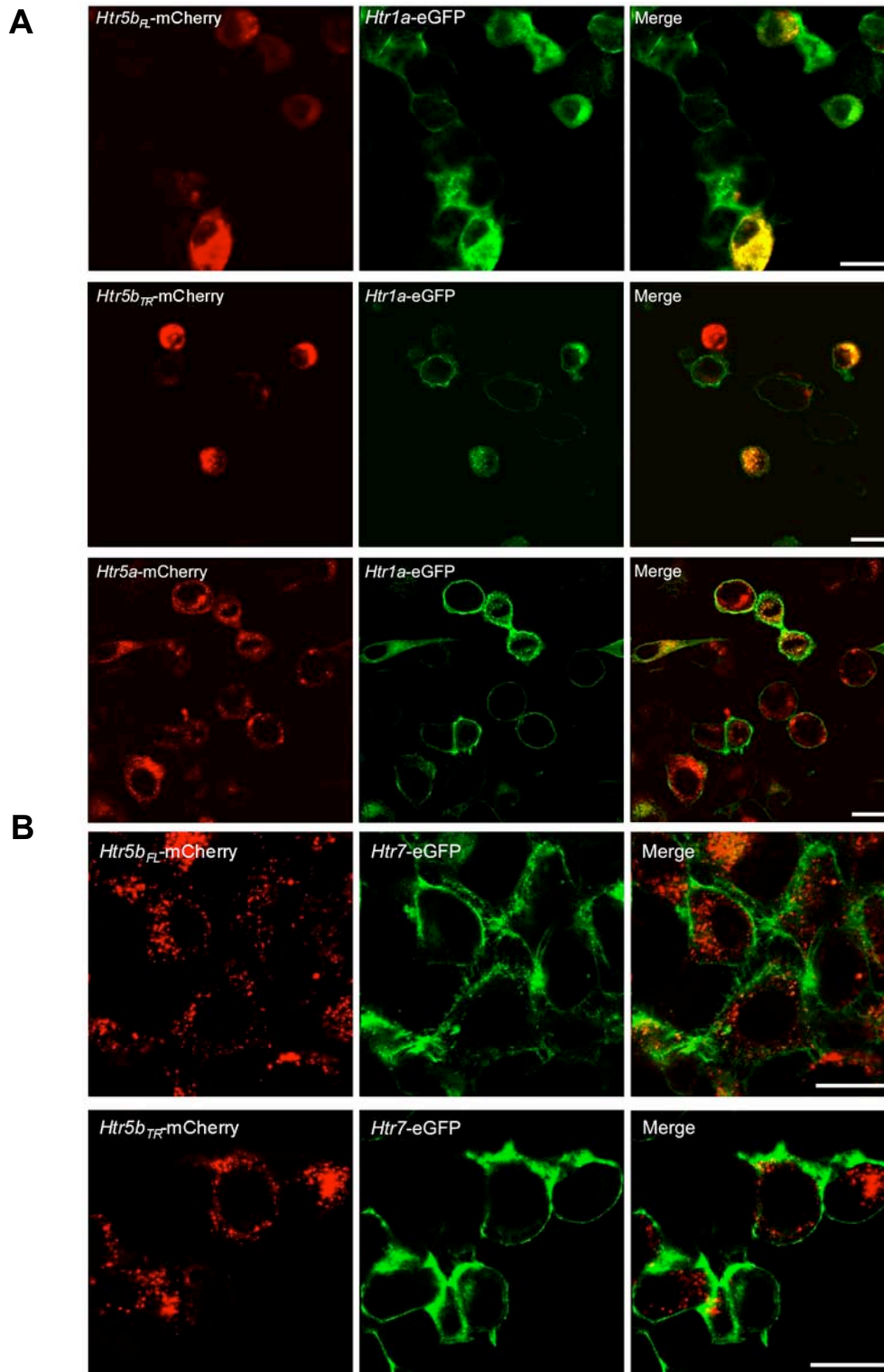
Figure 4.16. Serotonin 5B protein affects the localization of 5-HTR$_{1A}$, but not 5-HTR$_7$.

(**A**) Full-length (*Htr5b$_{FL}$*)-, truncated (*Htr5b$_{TR}$*)-, or *Htr5a*-mCherry fusion constructs (red) were co-transfected with *Htr1a*-eGFP or *Htr7*-eGFP fusion constructs (green) into N1E-115 cells. Fluorescence was analyzed after 16 - 24 hours using CLSM. 5-HTR$_{1A}$ remained intracellular in co-transfected cells and showed a strong co-expression with the 5-HT$_{5B}$ protein variants (yellow), while 5-HTR$_{5A}$ did not affect the localization of 5-HTR$_{1A}$. (**B**) In the presence of 5-HT$_{5B}$ variants the 5-HTR$_7$ cell surface expression remained unaffected. Scale bars = 20 μm.

4.5.3. Analysis of 5-HT$_{5B}$ signaling

Previous data revealed that the 5-HT$_{5B}$ protein is truncated in which its first three transmembrane domains including the serotonin-binding site are absent. Although the putative G-protein interaction domain, which comprises the last two intracellular domains (Bockaert, 1991; Strader et al., 1995), does still exist according to the hypothetical model (fig. 4.11), it was unclear whether the truncated protein is capable to bind G-proteins.

4.5.3.1. 5-HT$_{5B}$ couples to inhibitory heterotrimeric G-protein alpha 3

To test whether 5-HT$_{5B}$ is still able to bind to G-proteins as well as to identify the type of interacting G-protein, N1E-115 cells were co-transfected with the full-length 5-HT$_{5B}$ variant and different classes of G-proteins. A subsequently conducted [^{35}S]GTPγS-assay revealed that in contrast to the baseline level the GTPγS binding signal was only minor increased by 1% when 5-HT$_{5B}$ was co-expressed with the stimulatory G-protein Gα$_s$, which was similarly low in the MOCK control (2%, fig. 4.17A). However, with 220% over baseline level a strong GTPγS-binding signal was observed for Gα$_{i3}$ when co-expressed with 5-HT$_{5B}$. Only 39% was observed when Gα$_{i3}$ was expressed alone indicating that 5-HT$_{5B}$ interacts with the inhibitory G-protein Gα$_{i3}$.

4.5.3.2. 5-HT$_{5B}$ reduces cAMP *in vitro*

Due to the interaction with Gα$_{i3}$, a negative effect on the cAMP concentration was assumed. For verification, N1E-115 cells were transfected with the 5-HT$_{5B}$ variants and the cAMP concentration was measured after 16 - 24 h. Compared to the MOCK control, which was set to 100%, the intracellular cAMP concentration of 5-HT$_{5B}$TR and 5-HT$_{5B}$FL-transfected cells were decreased to 55.38 ± 5.28% (p = 0.01) or 67.03 ± 7.76% (p = 0.05) without serotonin stimulation (fig. 4.17B). A similar reduction of cAMP was observed in 5-HTR$_{1A}$ transfected cells when activated with 10 μM serotonin (68.10 ± 5.90%, p = 0.05). In contrast, non-stimulated 5-HTR$_{1A}$ cells did not reveal changes in the cAMP concentration compared to the MOCK control.
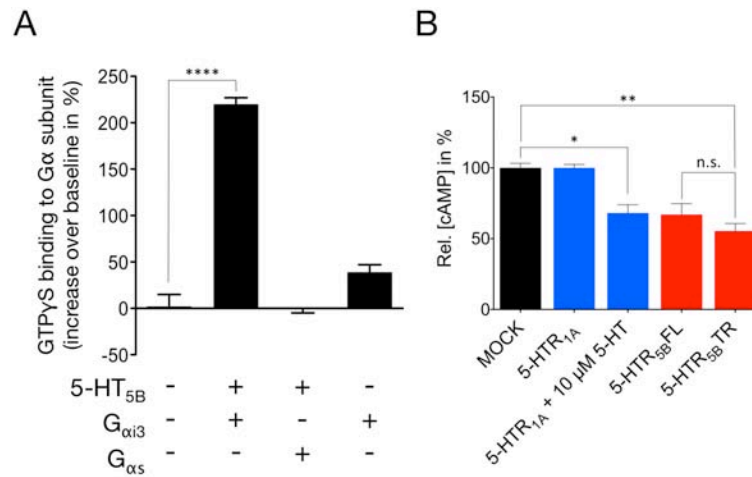
Figure 4.17. Signaling of 5-HT$_{5B}$.

(**A**) Bar diagram represents mean value and SEM of GTPγS assay from n = 3 biological replicates. N1E-115 cells were single or co-transfected with 5-HT$_{5B}$, G$_{\alpha i3}$, and G$_{\alpha s}$ expression constructs, and the level of bound GTPγS was measured by scintillation. Non-transfected cells served as control. The strongest signal was observed when 5-HT$_{5B}$ and G$_{\alpha i3}$ were co-transfected. (**B**) Effects of 5-HT$_{5B}$ variants on intracellular cAMP level. N1E-115 cells were transfected with no (MOCK) or with different serotonin receptor expression constructs and the cAMP level was activated by 10 µM of the adenylyl cyclase activator forskolin. Cyclic AMP was related to the protein content and biochemically measured in presence of 10 µM 5-HT for 5-HTR$_{1A}$ or in absence of 5-HT for both 5-HT$_{5B}$ variants. MOCK control was set to 100%. Bar diagram shows mean value and SEM of n = 3 biological replicates. Reduced cAMP levels were observed for cells transfected with 5-HT$_{5B}$ variants and serotonin-treated 5-HTR$_{1A}$ transfected cells. Asterisks indicate significance (* = $p < 0.05$; ** = $p < 0.01$; **** = $p < 0.0001$; one-way ANOVA).

4.6. Characterization of a *Mecp2$^{-/y}$;Htr5b$^{-/-}$* double-knockout mouse

To investigate the physiological consequences of the pathological strong 5-HT$_{5B}$ expression in the VRG of Rett mice, a Rett mouse additionally missing the *Htr5b* gene was generated by crossbreeding. The double-knockout mice (*Mecp2$^{-/y}$;Htr5b$^{-/-}$*, double-ko) were subsequently characterized for breathing disturbances and physical condition.

The *Htr5b* knockout mouse (*Htr5b$^{-/-}$*) did not display a conspicuous phenotype at least until an age of 400 days. Furthermore, individuals did not show any breathing irregularities between P40 and P50 (fig. 4.21).

4.6.1. 5-HT$_{5B}$ changes cAMP concentration in the VRG

Depending on the observation that 5-HT$_{5B}$ is able to reduce cAMP constitutively *in vitro* it was asked, whether the cAMP concentration in the VRG of Rett mice is changed due to the pathological strong 5-HT$_{5B}$ expression at development stage P40. Therefore, the VRG was dissected and the cAMP concentrations were measured and adjusted to the protein content. The cAMP measurements revealed a significant lower concentration of cAMP in VRG lysates of Rett mice to 73.49 ± 7.27% (p = 0.01) in comparison to wt, which was set to 100% (fig. 4.18). However, no significant change in the cAMP concentration was observed when comparing wt with double-ko mice (wt vs. *Mecp2$^{-/y}$;Htr5b$^{-/-}$*, 100 ± 4.58% vs. 98.46 ± 6.34%, n.s.).

These observations indicated that the high expression of 5-HT$_{5B}$ in the VRG of Rett mice at P40 results in a significant reduction of the cAMP concentration.
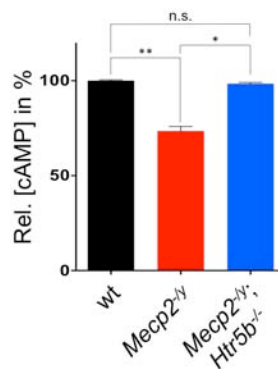
Figure 4.18. Comparison of cAMP level in the VRG at P40.

The VRG was dissected at P40 and the cAMP concentration was measured and adjusted to the protein content of the sample. The bar diagram represents mean value and SEM of n = 5 biological replicates. Cyclic AMP concentration of wild type was set to 100% and was low in the VRG of *Mecp2$^{-/y}$* mice but not changed in the *Mecp2$^{-/y}$,Htr5b$^{-/-}$* mouse. Asterisks indicate significance (* = p < 0.05; ** = p < 0.01; one-way ANOVA).

4.6.2. The genetic lack of *Htr5b* in Rett mice improves breathing

Although MeCP2 deficient mice vary in their onset of symptoms, almost all individuals display respiratory disturbances with phases of breathing arrests at P40. The most decisive question was whether the pathological sustained high expression of 5-HT$_{5B}$ in the VRG at this stage is responsible for the breathing disturbances in the Rett mouse. To address this question the double-ko mouse was characterized for breathing. Therefore, the working heart brainstem preparation (WHBP) was used to

analyze phrenic nerve activity (fig. 4.19A). As a measure for breathing irregularity the coefficient of cycle variation between consecutive rhythmic bursts was calculated (fig. 4.19B, C). As expected breathing irregularity was significantly increased in the Rett mouse in comparison to wt. The coefficient of variation increased from 7.76 ± 1.59% (wt) to 44.93 ± 12.88% ($Mecp2^{-/y}$, $p < 0.05$), but was significantly reduced in the double-ko (16.19 ± 2.35; $p < 0.05$) and always normalized compared to wt (n.s.).
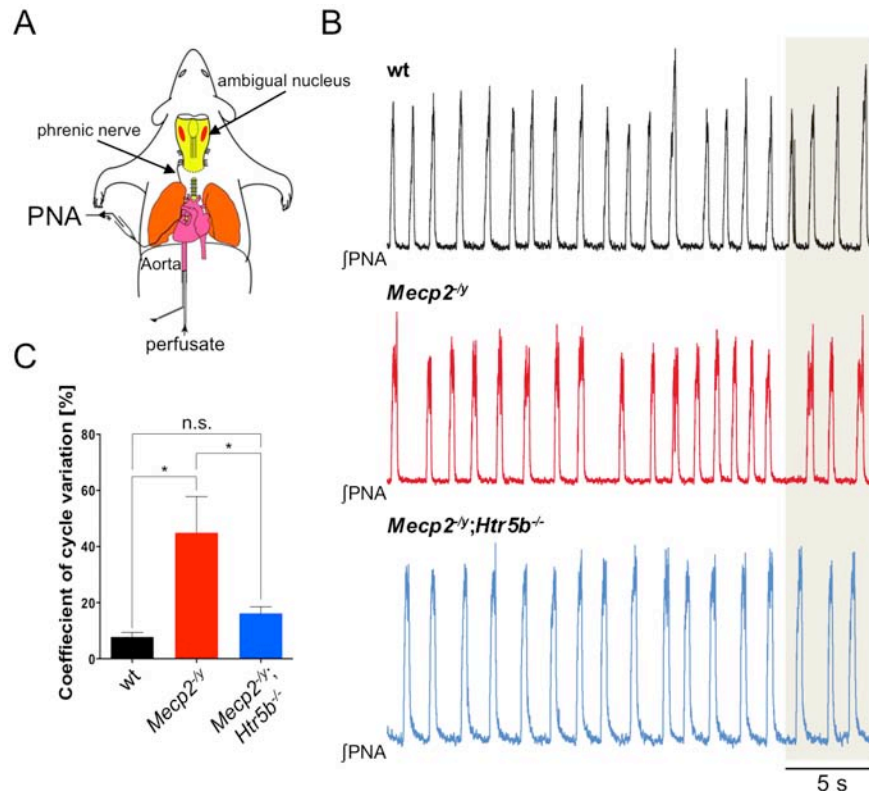
Figure 4.19. Improved breathing of double-ko mice.

(**A**) Schematic representation of the principle of the working heart brainstem preparation. (**B**) Representative recordings of integrated phrenic nerve activity (ʃPNA) of wild type (wt, black trace), $Mecp2$ knockout ($Mecp2^{-/y}$, red trace), or double-knockout ($Mecp2^{-/y};Htr5b^{-/-}$, blue trace) mice. (**C**) The bar diagram represents the coefficient of burst interval variation (CV) as a measure for breathing irregularities (n = 5). Breathing irregularities were high in the $Mecp2^{-/y}$ and low in wt and $Mecp2^{-/y};Htr5b^{-/-}$ mouse. Asterisks indicate significance (* = $p < 0.05$; one-way ANOVA).

4.6.2.1. Improvements of the breathing rhythm in double-ko mice *in vivo*

Finally, the results from WHBP studies were verified *in vivo* using plethysmography of conscious fully intact animals (fig. 4.20A). Respiratory arrests longer than 1 s, which were frequent in the Rett mouse, were reduced in the double-ko mouse ($Mecp2^{-/y}$ vs. $Mecp2^{-/y};Htr5b^{-/-}$: 5.3 ± 2.6 vs. 0.5 ± 0.4; fig. 4.20B). In wt as well as in $Htr5b^{-/-}$ no respiratory arrests were observed. The breathing frequency (4.20C), which

was reduced in the Rett mouse (4.60 ± 0.36 Hz) was significantly higher in the double-ko mouse (6.23 ± 0.41 Hz, $p < 0.05$) and normalized when compared to wt (6.69 ± 0.36 Hz, n.s.). The breathing irregularity score (fig. 4.20D) of double-ko mouse (0.33 ± 0.03) was reduced in comparison to Rett mice (0.46 ± 0.06), but was further decreased in $Htr5b^{-/-}$ (0.28 ± 0.03) and wt mice (0.24 ± 0.02).

Overall, breathing analysis *in situ* and *in vivo* revealed less irregularity in double-ko mice in comparison with Rett mice. Some of the parameters even showed normalization compared to wt, which may result in a better oxygen supply.
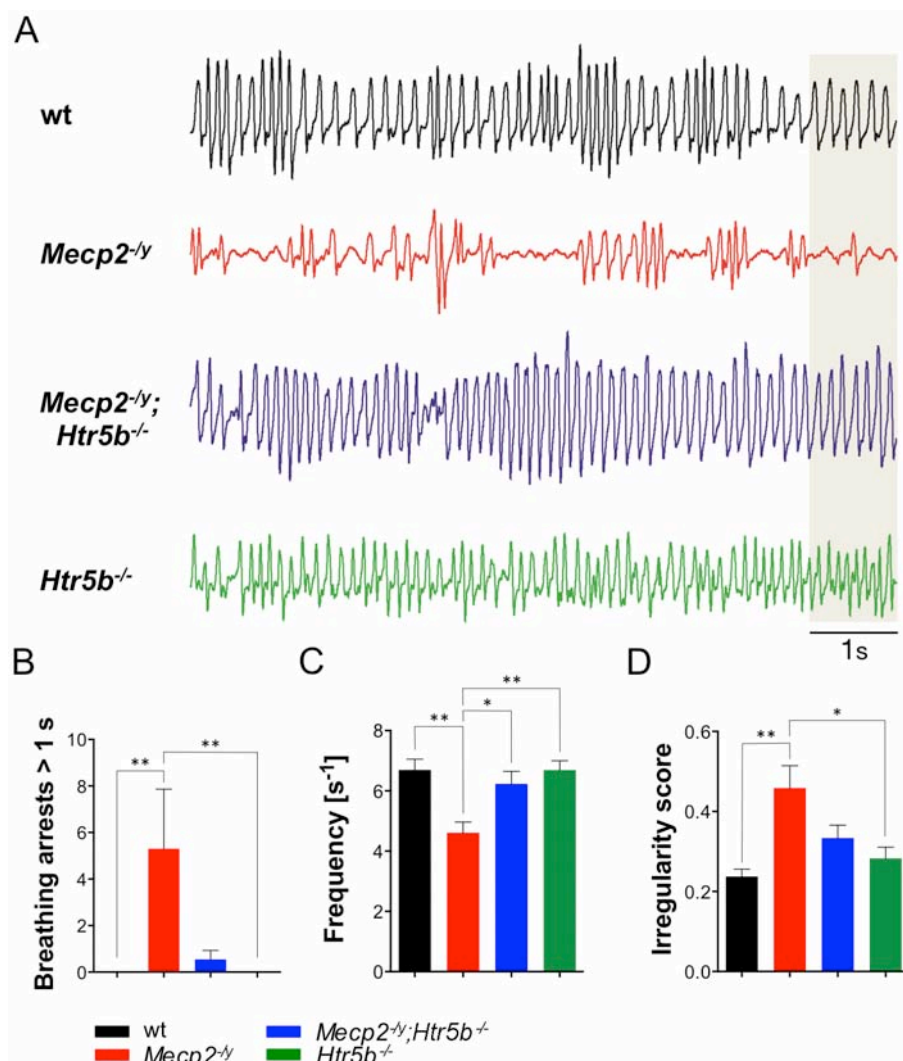
Figure 4.20. Comparison of breathing rhythm of wt, *Mecp2$^{-/y}$* and *Mecp2$^{-/y}$;Htr5b$^{-/-}$* mice *in vivo*. (**A**) Traces show representative plethysmographic recordings of conscious fully intact animal models: wt (n = 9), *Mecp2$^{-/y}$* (n = 10), *Mecp2$^{-/y}$;Htr5b$^{-/-}$* (n = 11) or *Htr5b$^{-/-}$* (n = 7) mice. Bar diagrams illustrate mean value and SEM of (**B**) breathing arrests exceeding 1 s, (**C**) breathing frequency, and (**D**) breathing irregularity. Asterisks indicate significance (* = $p < 0.05$; ** = $p < 0.01$; one-way ANOVA).

4.6.3. Improvement of physical condition of *Mecp2^{-/y};Htr5b^{-/-}* double-knockout mouse

Besides irregular breathing visible symptoms of *Mecp2^{-/y}* mice are a shorten life span, hind limb clasping, and bad generally physical condition (Guy et al., 2001), which might be a result of early onset of chronic hypoxia and ischemia. Particular physical and molecular parameters, which are known to be altered in *Mecp2^{-/y}* mice, were tested for improvement (fig. 4.21). Determination of the hematocrit value, a soft indicator for hypoxia, which is known to be increased in MeCP2 deficient mice (Fischer et al., 2009), was significantly reduced in double-ko mice (Rett vs. double-ko; 0.530 ± 0.005 l/l vs. 0.446 ± 0.016 l/l; p<0.0001) and was comparable with wt (0.435 ± 0.005 l/l). The bodyweight, which was considerably reduced in Rett mice was significantly increased in double-ko mice (Rett vs. double-ko; 12.47 ± 0.72 g vs. 17.77 ± 0.68 g, p < 0.0001) and almost normalized compared to wt (20.60 ± 0.56 g). *Htr5b^{-/-}* mice (19.06 ± 1.12 g) did not differ in their bodyweight in comparison with wt. The improved physical parameters in double-ko mice in comparison with Rett mice were accompanied by a longer survival (fig. 4.21C). The median survival of double-ko mice was as twice as high compared to Rett mice (Rett mice vs. double-ko; 40 vs. 80 days; p = 0.0006). Although most of double-ko mice displayed less gait apraxia, they still started hind limb clasping after 30 s lifting similar to Rett mice.
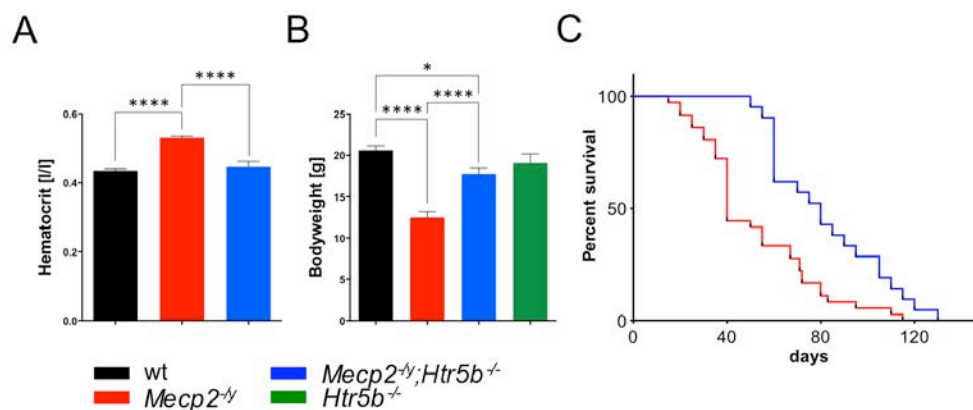
Fig 4.21. Comparison of physical parameters between Rett and double-ko mice.
(**A**) Bar diagram represents mean value and SEM of the hematocrit value from wt (n = 6), *Mecp2^{-/y}* (n = 7), and *Mecp2^{-/y};Htr5b^{-/-}* (n = 5) mice at P40 ± 2 (**** = p ≤ 0.0001; one-way ANOVA). (**B**) Bar diagram shows mean value and SEM from bodyweight measurements of wt (n = 17), *Mecp2^{-/y}* (n = 17), *Mecp2^{-/y};Htr5b^{-/-}* double-knockout mice (n = 15), and male *Htr5b^{-/-}* mice (n = 7) at P40 ± 2 (* = p ≤ 0.05; **** = p ≤ 0.0001; one-way ANOVA). (**C**) Survival plot of *Mecp2^{-/y}* (n = 37) vs. *Mecp2^{-/y};Htr5b^{-/-}* double-ko mice (n = 21) (p < 0.0006; Log-rank (Mantel-Cox) test).

Taken together, the physical condition of double-ko mice was obviously improved at P40. They were larger in their body size and appeared stronger and healthier compared to Rett mice (fig. 4.22). The improved fit was also manifested by the observation that female *Mecp2^{-/+};Htr5b^{-/-}* mice were able to rear their pups, whereas rearing of offspring of female *Mecp2^{-/+}* mice requires a nurse animal.
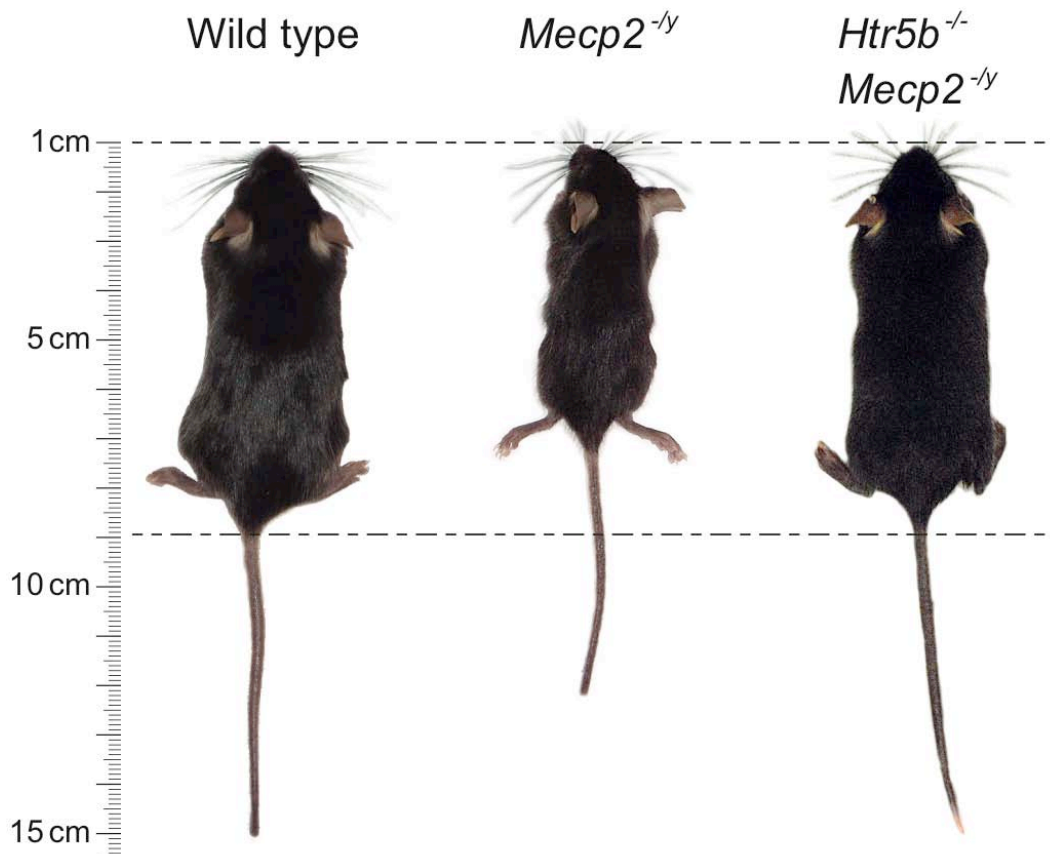
Figure 4.22. Appearance of wt, Rett, and double-ko mice.
Representative image of the body size of wt, *Mecp2^{-/y}*, and *Mecp2^{-/y};Htr5b^{-/-}* mice at P40 with scale on the left.

4.7. Pharmacological treatments

To confirm the hypothesis that low cAMP concentrations in the VRG caused by the pathological high 5-HT$_{5B}$ expression are responsible for breathing disturbances a series of pharmacological treatments were performed using the WHBP. To determine respiratory rhythm regularity again the coefficient of cycle variation (CV) was calculated.

In wt as well as in double-ko mice, a systemic cAMP reduction by administration of the protein kinase A inhibitor Rp-cAMP (0.2 - 0.4 µM) induced a disturbed Rett-like respiratory phenotype (fig. 4.23) with phases of breathing arrests. The CV of wt mice was significantly increased from 7.76 ± 1.59% to 41.12 ± 7.01%; p < 0.05). In double-ko mice the CV was elevated from 16.19 ± 2.35% to 39.52 ± 3.11%; p < 0.05.
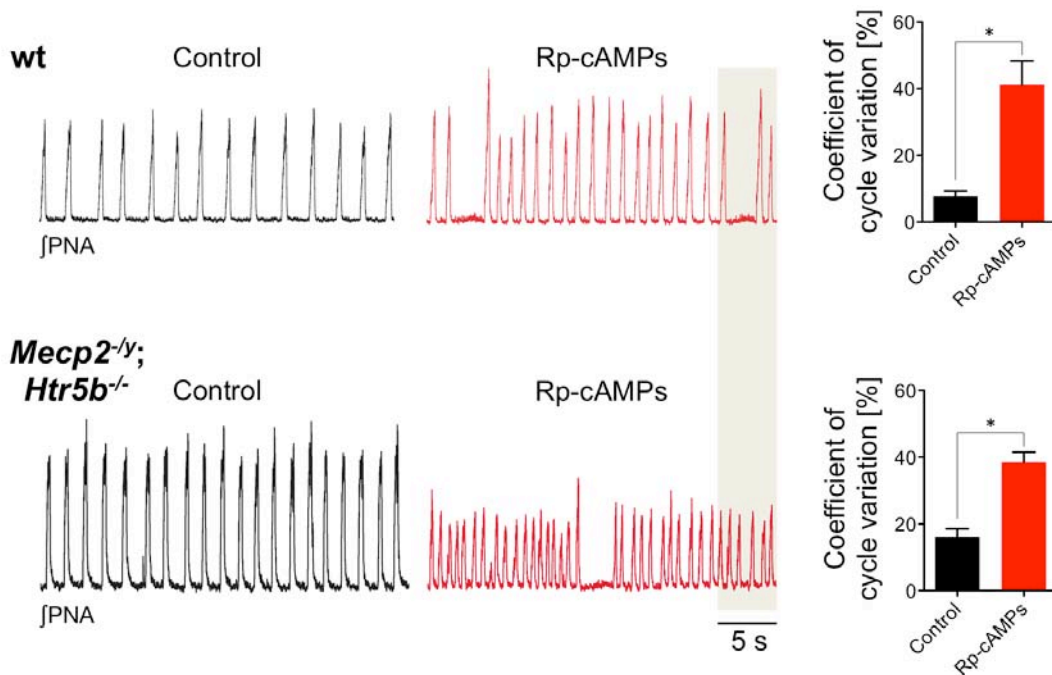
Figure 4.23. Systemic effects of cAMP reduction on the respiratory rhythm pattern.

The traces show representative recordings of integrated phrenic nerve activity (∫PNA) in wt and $Mecp2^{-/y};Htr5b^{-/-}$ mice before (control, black trace) and after systemic reduction of cAMP by application of 0.4 µM Rp-cAMPs (red trace). The bar diagrams on the right show mean value and SEM of the coefficient of cycle variation (CV) as a measure for breathing irregularity (n = 3). In both genotypes an increase of CV was observed after systemic drug application. Asterisks indicate significance (* = p < 0.05; paired t-test).

In contrast systemic augmentation of cAMP by administration of 1 µM of the adenylyl cyclase activator forskolin rescued a regular breathing rhythm in the Rett mouse (fig. 4.24). The CV between rhythmic bursts of the phrenic nerve decreased from 44.93 ± 12.88% to 12.21 ± 0.61%; p < 0.05, whereas a further decrease of cAMP by systemic application of the specific 5-HTR$_{1A}$ agonist 8-OH-DPAT even deteriorated the respiratory rhythm. The CV of consecutive bursts increased from 39.87 ± 8.75% to 68.73 ± 11.23%; p < 0.05.
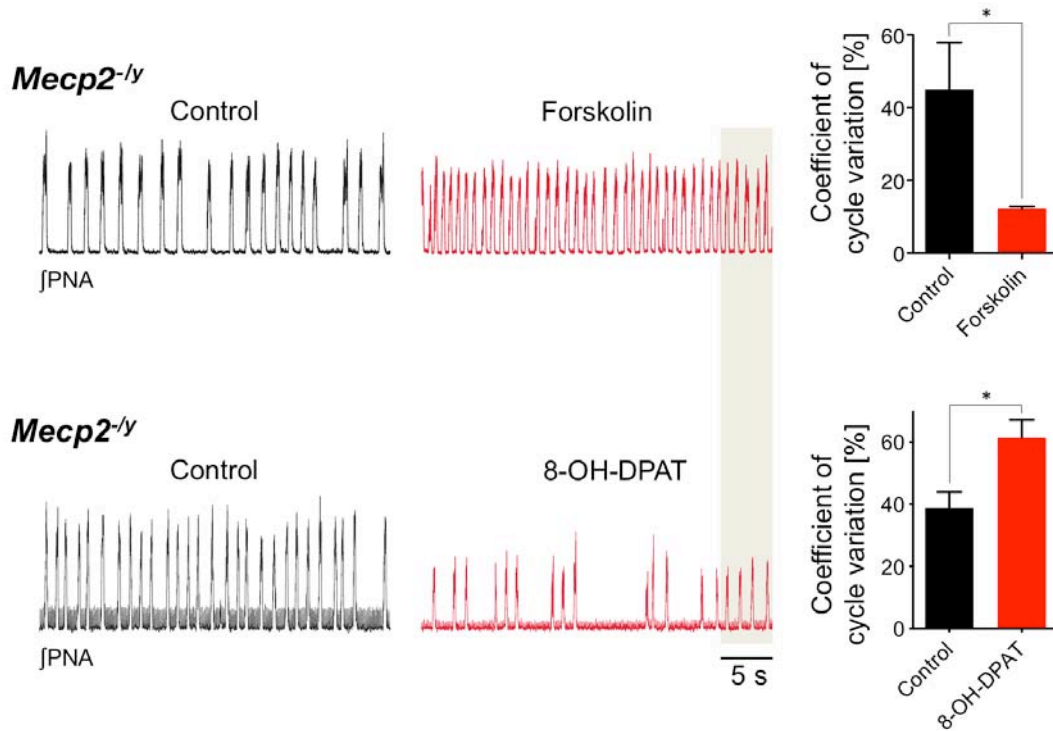
Figure 4.24. Systemic effects of cAMP on the breathing rhythm of Rett mouse.

The traces show representative recordings of integrated phrenic nerve activity (∫PNA) in *Mecp2⁻/ʸ* mice before (control, black trace) and after increase of cAMP by application of 1 µM forskolin or decrease of cAMP by treatment with 0.2 - 0.4 µM 8-OH-DPAT (red trace). The bar diagram on the right shows mean value and SEM of the coefficient of cycle variation (CV) as a measure for breathing irregularity (n = 3). Elevation of cAMP led to an improved breathing rhythm, whereas breathing irregularities were augmented after cAMP reduction (* = $p < 0.05$; paired t-test).

Augmentation of the intracellular cAMP concentration improved respiratory network activity in Rett mice, which might open novel strategies to treat breathing disturbances in RTT patients by application of cAMP-elevating drugs.

5. Discussion

Disturbed breathing is one of the most devastating symptoms of the Rett syndrome (RTT), which is caused by various mutations in the *MeCP2* gene encoding the transcription regulator Methyl-CpG binding protein 2 (MeCP2). Besides other breathing irregularities, patients suffer from recurring life threatening breathing arrests lasting longer than 45 sec, which are supposed to be responsible for up to 25% of sudden death (Kerr et al., 1997; Julu et al., 1997). Similar to human patients, mice, which carry a knockout in the *Mecp2* gene, display arrhythmic breathing with onset at approximately postnatal stage 35 (Guy et al., 2001; Viemari et al., 2005; Ogier & Katz, 2008; Roux et al., 2008; Zanella et al., 2008).

In mammals, the three-phase breathing rhythm originates from a neuronal network located in the lower brainstem, in which the pre-Bötzinger complex (pre-BötC) that belongs to the bilaterally located ventral respiratory group (VRG) is of significance for respiratory rhythm generation. Within this network, reciprocal glycinergic inhibition between antagonistically connected neurons and serotonergic modulation is relevant for the maintenance of regular breathing rhythm (Richter et al., 2003).

5.1. Altered gene expression in the VRG of MeCP2 deficient mice

5.1.1. MeCP2 expression and its role in the brainstem during development

MeCP2 is predominantly expressed in post-mitotic neurons but is also essential during embryonic development (Tate et al., 1996). The developmental gene expression patterns correlate with the time course of neuronal differentiation and is closely linked to synaptogenesis (Shahbazian et al., 2002; Jung et al., 2003; Martinowich et al., 2003; Chen et al., 2003). Detailed spatial and temporal MeCP2 expression analysis in mice brains using IHC and IF, Shahbazian and colleagues demonstrate that the protein first becomes evident at embryonic stages in distinct regions of the spinal cord and the brainstem (Shahbazian et al., 2002). In the mature brain at 19 weeks MeCP2 is expressed strongest in the cerebellum, cortex, hippocampus, and olfactory bulb.

To estimate the importance of MeCP2 on development of the brainstem and the respiratory network, the protein level was measured at P7, P15, P21, and P40 quantitatively. Additionally, mRNA level was measured specifically in the VRG. In

both cases *Mecp2* mRNA and MeCP2 protein revealed high levels at early state P7 and late state P40, whereas in intermediate states the level of mRNA and protein was significantly lower. Brainstem immaturity and developmental alterations in various neurotransmitter systems have been reported for both RTT patients as well as for MeCP2 deficient mice (Saito et al., 1999; Paterson et al., 2005; Julu et al., 1997a; Julu et al., 1997b; Kerr et al., 1999; Smeets et al., 2006). Although MeCP2 deficient mice show a reduction in their brain size, gross morphological alteration in the brainstem has not been reported so far (Ogier & Katz, 2008; Santos et al., 2010). Similar to humans, breathing irregularity in Rett mice has not been described in early periods of development, but becomes obvious not before P35, when MeCP2 returns to higher levels in wt mice. Hence, it was concluded that lack of MeCP2 has an impact on gene expression at this stage. A similar high level at P7, however, did not reveal an impact on breathing disturbances.

5.1.2. Glycinergic and serotonergic components

Developmental gene expression of the glycinergic and serotonergic systems were analyzed in the VRG using q-PCR. Gene expression of glycinergic components was not deregulated at the RNA level in the VRG of MeCP2 deficient mice, whereas three of 14 genes associated with the serotonergic system, the dopa decarboxylase (*Ddc*) and the serotonin receptors 1D (*Htr1d*) and 5B (*Htr5b*), were significantly up-regulated. This corresponds with the common concept classifying MeCP2 exclusively as a transcriptional repressor. This idea refers to the observation that MeCP2 binds to methylated cytosines inhibiting gene expression *in vitro* (Lewis et al. 1992; Meehan et al., 1992; Nan et al., 1997) and was supported by discoveries that MeCP2 is able to interact with several co-repressors including Sin3A, cSki, CoREST, and NcoR initiating heterochromatin formation by recruitment of histone deacetylases (HDACs) (Nan et al., 1998; Kokura et al., 2001; Ballas et al., 2005). The *Ddc* has been shown to be up-regulated also in other brain regions including the cortex, cerebellum, and midbrain (Urdinguio et al., 2008). Moreover, *Ddc* was identified as direct target of MeCP2 by chromatin immunoprecipitation (ChIP) assay.

In the present study, we also found the serotonin receptor (5-HTR) 2C to be repressed in MeCP2 deficiency, which may result from secondary effects. Several studies investigating global gene expression with cDNA microarray analysis found that the majority of genes were down-regulated in the absence of MeCP2, in which

most of the identified genes showed only moderate alterations (> 1.5-fold) (Jordan et al., 2007; Urdinguio et al., 2008; Ben-Shachar et al., 2009). Integrated epigenomic analysis revealed that 63% of MeCP2-bound promoters are transcriptionally active (Yasui et al., 2007). Furthermore, several genes are activated directly by MeCP2 via direct interaction with the transcriptional activator cAMP responsive element binding protein 1 (CREB1) (Chahrour et al., 2008).

Among the dysregulated genes that we identified, *Htr5b* up-regulation was strongest with 70-fold higher mRNA expression rate in the VRG of MeCP2 deficient mice in comparison with wt. Such high differences of gene expression in the VRG have not been reported so far. Immunohistochemical analysis confirmed the results at the protein level showing that the 5-HTR$_{5B}$ up-regulation particularly includes the pre-BötC, which is vital for respiratory rhythm generation in mammals.

The temporal coincidence of disturbed breathing functions and the dramatic up-regulation of *Htr5b* through missing repression by MeCP2 in Rett mice indicates that this gene is a suitable target for direct control by MeCP2 and for further investigations of its role in the control of breathing.

5.2. Epigenetic control of 5-HTR$_{5B}$ in the VRG

First evidence that MeCP2 directly represses *Htr5b* gene expression in the VRG is based on the observation that both genes showed reciprocal developmental profiles in wild type mice (fig. 4.8).

At developmental stages when MeCP2 expression was high, *Htr5b* expression was suppressed, whereas high *Htr5b* levels were observed when MeCP2 was low. However, this does not explain the results at P7 when MeCP2 is elevated. Hence, *Htr5b* should be up-regulated in MeCP2 deficient mice. In contrast to P40, however, there were no differences in *Htr5b* mRNA expression between *Mecp2$^{-/y}$* and wt mice at P7.

Moreover, with exception of the cortex, no *Htr5b* dysregulation were found in other brain regions (fig. 4.4). Comparable results have been reported for other genes, which are under direct control of MeCP2. For example, the S100 protein S100a9 was found to be up-regulated in the cortex and in the midbrain, but not in the cerebellum (Urdinguio et al., 2008).

Such regulatory differences can be explained either by developmental and brain-region specific posttranslational modifications of MeCP2 and/or by specific expression of interacting co-repressor proteins.

Several posttranslational modifications have been reported, such as phosphorylation at several serine (S) sites (e.g. S-80, S-229, and S-421), acetylation, and ubiquitylation, which affects the binding properties of MeCP2 to DNA and interaction partners, such as the co-repressors Sin3A and HP1 (Tao et al., 2009; Chen et al., 2003; Zhou et al., 2006; Gonzales et al., 2012; Cohen et al., 2011; Zocchi & Sassone-Corsi, 2012). Zhou and colleagues demonstrated that phosphorylation at serine-421 is specific for brain tissue. However, the authors did not distinguish between different regions.

As MeCP2 binds specifically to methylated DNA, another explanation is a region and developmental specific methylation pattern, which already has been shown for various genes including the serotonin receptor 2A. For this receptor the methylation pattern of the promoter is different between cortex and cerebellum (Ladd-Acosta et al., 2007).

Using ChIP procedure we demonstrated an effective binding of MeCP2 to the proximal *Htr5b* promoter in the VRG at P40 (fig. 4.9). However, we could not define a specific binding region. We rather found a ubiquitous binding throughout the +5.5 kb promoter region, which was enriched at about +4.7 kb. Before MeCP2-specific DNA precipitation, the DNA was sheared into smaller fragments between 1,000 and 1,400 bp in a random fashion, which leads to a statistical distribution of analyzed loci in a subsequent q-PCR. However, there is evidence that MeCP2 could be a more global regulator and might be able to bind abundantly to almost all single methylated CpG sites throughout the whole chromatin (Guy et al., 2011), but seems to be more effective by adjacent A/T bases rich regions (AT ≥ 4) (Klose et al., 2005). Such motifs are ubiquitously present in the *Htr5b* promoter.

By means of *Atf7$^{-/-}$* knockout mouse it has been shown that *Htr5b* is subject to epigenetic control (Maekawa et al., 2010) and was found to be strongly up-regulated specifically in the dorsal raphé nuclei of the brainstem.

However, there could not be found any information indicating *Htr5b* alteration in the VRG. Interestingly, similar to the results of this study, Maekawa and colleagues did not find any differences in mRNA expression in other brain regions, neither in the

hippocampus, the nucleus habenula, nor the nucleus olivaris inferior. The authors demonstrated that ATF-7 binds directly to cAMP responsive element (CRE) DNA sites at three places/sites in the proximal *Htr5b* promoter to inhibit gene expression by recruiting the methyltransferase HMTase that is part of the EST complex mediating methylation histone H3-K9 trimethylation. MeCP2 is able to recruit histone deacetylases (HDAC) by means of the co-repressor Sin3A, which mediates deacetylation of histones (Nan et al., 1998). Both histone modifications mediate heterochromatin formation, which is closely linked to gene silencing (Kass et al., 1997; Grunstein, 1997; Laherty et al., 1997; Hassig et al., 1997). *Atf7$^{-/-}$* null mice displayed abnormal behavior, such as anxiety-related attitude and abnormalities in the sensomotoric system (Maekawa et al., 2010). These to characteristics are common features in Rett syndrome. However, there are no breathing disturbances. Furthermore, it was demonstrated that ATF-7 became phosphorylated when mice were exposed to isolation stress. Phosphorylation by the map kinase 14 (MAPK14) led to dissociation of ATF-7 from the CRE binding site. Same effects were observed *in vitro* when cells were exposed to various kinds of stress.

In our study *Mapk14* and *Atf7* mRNA expression did not show any differences in the VRG of Rett mice. However, it is most likely that Rett mice also suffer from different kinds of stress. Both effects, lack of MeCP2 repression and stress-dependent dissociation of ATF-7 from the *Htr5b* promoter may be an explanation for the tremendous *Htr5b* up-regulation in the VRG, which could be additionally increased by CREB1 as the chromatin structure is less dense and CRE is accessible to the transcription activator CREB1 (fig. 5.1).
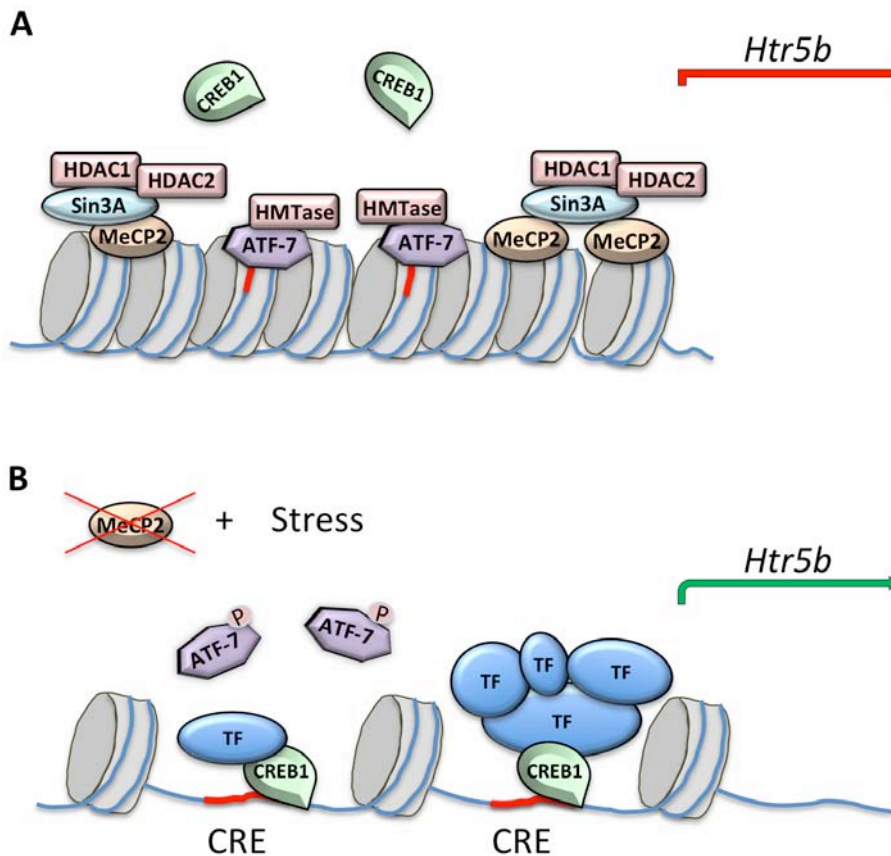
Figure 5.1. Hypothetical model of *Htr5b* regulation in the VRG

(**A**) Under normal conditions ATF-7 binds to the cAMP responsive element (CRE, marked in red) and recruits the methyltransferase HMTase, which leads to methylation of histones. MeCP2 binds methyl-CpG-dependend to various regions within the *Htr5b* promoter and recruits the histone deacetylases HDAC1 and HDAC2 by means of the co-repressor Sin3A, which results in deacetylation of histones. Both histone modifications lead to heterochromatin formation and to silencing of the *Htr5b* gene.

(**B**) The absence of the global regulator MeCP2 in Rett mice most likely results in cell stress, which leads to phosphorylation (P) and to dissociation of ATF-7 from the CRE sites. As a result the chromatin structure is opened and CRE is accessible to CREB1 and other transcription activators to induce *Htr5b* mRNA expression.

Under normal conditions of wt mice, high 5-HTR$_{5B}$ protein expression was observed in the inferior olive and in the nucleus raphé obscurus, which is in accordance with *in situ* hybridization experiments showing high level of *Htr5b* mRNA in these brainstem regions (Serrats et al., 2004; Matthes et al., 1993). Other brain regions with strong *Htr5b* mRNA expression such as the CA1 region of the hippocampal formation, the entorhinal cortex, and the habenula were not tested for protein expression.

Furthermore, in contrast to the phylogenetically related 5-HTR$_{5A}$, which has been shown to be predominantly expressed in astrocytes (Carson et al., 1996), we found 5-HT$_{5B}$ protein expression only in neurons.

To date, however, it is still unclear whether the strong up-regulation of 5-HT$_{5B}$ in the VRG also affects astrocytes.

5.3. 5-HTR$_{5B}$ - A classical serotonin receptor?

5.3.1. 5-HTR$_{5B}$ expression in men

Immunohistochemical analysis of human brainstem sections with a homemade antibody revealed strong evidence that 5-HTR$_{5B}$ is also expressed in humans, because of the strong reactivity in the inferior olive (IO), where the protein is also strongly expressed as in rodents. This is in accordance with reports describing *Htr5b* mRNA to be abundantly expressed in the IO of rat and mouse (Serrats et al., 2004; Matthes et al., 1993).

Comparison of the protein sequence indicated that the antibody epitope, which is derived from the C-terminal domain of the receptor, is 100% conserved among mouse, rat, and human. In all species the *Htr5b* gene consists of two exons. Sequence analysis of the human *HTR5B* gene, however, revealed insertions and nonsense mutations in its 5'-region after the putative start codon within the first exon, which disrupts the coding sequence (cds) failing to encode a functional protein (Grailhe et al., 2001). Nevertheless, using q-PCR the authors verified *Htr5b* mRNA expression also in human brain tissue. Sequence analysis among mouse, rat, rabbit, and human revealed a highly conserved second ATG within the last part of the second exon, which is in frame with the cds. Expression from this ATG would lead to an N-terminal-truncated protein. The applied antibody, which is directed against the very end of the C-terminal domain of the receptor, could explain the immunoreactivity in the human inferior olive. Another possibility would be the presence of an alternative first exon. However, chromosome mapping of the *HTR5B*/*Htr5b* gene by *in situ* hybridization only showed a single locus in human and mouse (Matthes et al., 1993).

5.3.2. 5-HTR$_{5B}$ is truncated

The hypothesis that 5-HTR$_{5B}$ is truncated was supported by western blot analysis. Surprisingly, the immunoblot revealed for both rat and mouse brainstem lysates a specific signal at 22.5 kDa, which was smaller than the expected relative molecular mass of 41 kDa for the full-length protein (fig. 4.11). This correlated exactly with the predicted mass of the protein encoded by the second ATG. There was no evidence for a shortened transcript. Western blot analysis did not reveal a full-length 5-HTR$_{5B}$ protein in both species, although the full-length open reading frame from brainstem cDNA could be cloned. Another evidence for the truncation was provided by sequence comparison showing that the protein sequence among species was highly conserved after the second ATG, whereas the 5'-region was not, which indicates an evolutionary preserved function. We consider that the truncation of the protein might result from the posttranslational cleavage by a protease. However, human protein expression and identification of a specific second ATG also argues for truncation as a result of expression from the alternative start codon. The exact molecular mechanism of the ATG switch could not be defined yet.

Originally, the 5-HTR$_{5B}$ groups with the 5-HTR$_{5A}$ to a distinct subclass of G-protein coupled serotonin receptors (GPCRs). Both receptors share 70% sequence homology (Hoyer et al., 2002), but only 23 - 34% homology to other 5-HT receptors (Plassat et al., 1992). Detailed protein analysis revealed that the shortened 5-HTR$_{5B}$ is truncated by the first 3 of 7 transmembrane domains (TM) including the serotonin-binding site. The missing ligand-binding site of 5-HTR$_{5B}$ could explain the results of a pharmacological study using radio-ligand binding assay (Matthes et al., 1993), in which there was no binding of various serotonergic radio-ligands, such as [^{3}H]5-HT, [^{3}H]8-OH-DPAT, or ^{125}I-cyanopindolol, in membrane fractions of *Htr5b* (full-length) transfected COS-7 cells were detectable. However, they found a binding of ^{125}I-LSD, a well-known activator of serotonin receptors, which might be a result of an unspecific binding to the C-terminal part of the protein.

5.3.3. *Htr5* group show partially unusual protein localization

Overexpression of fusion constructs in murine N1E-115 neuroblastoma cells showed an unexpected clustered intracellular expression pattern for both variants (4.12), which resembled the 5-HTR$_{5B}$ immunoreactivity observed in human tissue (fig. 4.10). Contrary to 5-HTR$_{5B}$, 5-HTR$_{1A}$ and 5-HTR$_7$ showed an expected strong cell membrane expression pattern (fig. 4.12 and 4.16). As N1E-115 cells were transfected under identical conditions, and all fusion constructs were generated in an identical manner, the unusual intracellular expression of 5-HTR$_{5B}$ does not seem to result from overexpression.

Trafficking and stability of cell membrane localization of GPCRs is affected by various posttranslational modifications such as palmitoylation and glycosylation (Goddard and Watts, 2012). Recently, it has been shown that cell surface expression of the related 5-HTR$_{5A}$ is affected by specific N-glycosylation on asparagine-6 and asparagine-21 in the N-terminal part of the protein (Dutton et al., 2008). The receptor remained intracellular either when both asparagine residues were deleted, or N-glycosylation was inhibited by tunicamycin.

The putative full-length 5-HT$_{5B}$ protein contains an asparagine residue on position 5 in its amino acid sequence, which is absent in the truncated protein. However, expression of the full-length 5-HTR$_{5B}$ exhibited the same intracellular localization as the truncated form.

Dutton and co-workers also observed that a large percentage of the non-mutated 5-HTR$_{5A}$ was located intracellularly, which is in accordance with our findings for this receptor subtype.

Cell surface expression can also be affected by many co-factors, such as cytoplasmic PDZ proteins [named for its structural domain shared by the postsynaptic density protein (PSD95)] (Romero et al., 2011), GPCR-associated sorting proteins (GASPs) (Magalhaes et al., 2012), Homer proteins (Kammermeier & Worley, 2007), regulator of G-protein signaling (RGS) (Sethakorn et al., 2010), and also small G-proteins such as Rab GTPases (Magalhaes et al., 2012).

This is only a selected number of protein classes, which have either direct or indirect influence on retaining GPCRs at the cell membrane. For example, the C-terminal region of 5-HTR$_{2A}$ has been shown to interact with the multiple PDZ protein-1 MUPP1, which effectively affects 5-HTR$_{2A}$ localization in spines and dendrites (Xia et al., 2003; Jones et al., 2009). Interaction between 5-HTR$_{2C}$ and MAGUK p55

subfamily member 3 (MPP3) increased cell membrane stability, whereas PSD-95 showed opposite effects (Gavarini et al., 2006). Specific interaction partner of 5-HTR$_{5B}$ may be absent in N1E-115 cells, which could avoid effective trafficking to the cell membrane. However, electron microscopy of 5-HTR$_{5B}$-immunogold staining on brainstem sections of wild type mice confirmed the results of *in vitro* experiments as we detected strong signals associated with membranes of vesicular and tubular structures, whereas cell membrane expression was not observed (fig. 4.14).

Even though we cannot fully exclude that 5-HTR$_{5B}$ is expressed on the cell surface in other brain regions, we propose that the truncated 5-HTR$_{5B}$ has lost its function as a classical serotonin receptor. Hence, we renamed the protein to 5-HT$_{5B}$.

The secretory pathway of GPCRs to their destination on the cell membrane begins with the co-translational integration into the endoplasmic reticulum (ER) membrane, which either occurs in a signal-dependent or independent manner by means of the signal recognition particle (SRP) and the translocon (mainly consisting of the protein-conducting channel protein Sec61) (Alken et al., 2005). The latter is the case for the majority of GPCRs (90 - 95%) (Wallin & von Heijne, 1995). The ER plays important role in the correct folding of proteins. 50% of all newly synthesized proteins are retained in the ER due to failing of quality control criteria (Ellgaard et al., 1999).
A major part of meanwhile identified truncated GPCRs, which are mostly splice variants of their wt receptor form, are also retained predominantly in the ER (tab. 5.1).
5-HT$_{5B}$ seemed to pass the ER because the majority of 5-HT$_{5B}$ protein is co-localized with RAB7, which is a marker for the (late) endosomal compartment. We did not observe any differences in the localization of both 5-HT$_{5B}$ variants. Hence, it was concluded that lack of the N-terminal part in the truncated protein cannot be causative for the endosomal localization. The (late) endosomal compartment seems to be rather associated with desensitization, which describes the β-arrestin-mediated internalization of GPCRs after activation. This is a common mechanism to switch off the signaling cascade. From the (late) endosomal compartment, GPCRs are either degraded in the lysosome by compartment fusion or recycled and restored to the cell membrane (Hanyaloglu & von Zastrow, 2008).

Table 5.1. Selection of identified truncated GPCRs with localization and their influence of corresponding wild type receptors.

The truncated variant of receptors often dominates (dom) the localization of the wild type form.

Receptor	Name/truncation	Localization	Dom/neg	Reference
α_{1A}-adrenoceptor	6TM	ER	Yes	Seck et al., 2005
Chemokine receptor 5	Ccr5Δ32, 5TM	ER	Yes	Benkirane et al., 1997
Dopamine receptor (D_3)	D3nf, 5TM	ER	Yes	Karpa et al., 2000
Gastric inhibitory polypeptide receptor	4TM	ER	Yes	Harada et al., 2008
Ghrelin receptor	GHS-R1b, 5TM	ER	Yes	Leung et al., 2007
Gonadotropin-releasing hormone receptor	5TM		Yes	Grosse et al., 1997
Histamine receptor	rH$_3$R		Yes	Bakker et al., 2006
Nociceptin receptor	4TM	CM	Yes	Xie et al., 2000
Somatostatin receptor 5	4TM	?	No	Cordoba-Chacon et al., 2010
Vasopressin receptor V_2	6TM	ER	Yes	Gonzales et al., 2011

5.4. The physiological role of 5-HT$_{5B}$

The role of the resident localization of 5-HT$_{5B}$ into endosomes remains obscure. Based on further findings we propose two hypotheses regarding interaction of 5-HT$_{5B}$ with other 5-HT receptors and influence of 5-HT$_{5B}$ on cAMP signaling.

5.4.1. 5-HT$_{5B}$ proteins affect localization of serotonin receptors

In the past two decades numerous studies were set up, which described homo-, hetero-, and oligomerization of GPCRs. A well-known example is the GABA$_B$ receptor, which is selectively activated by the inhibitory transmitter γ-aminobutyric acid (GABA). The receptor is active only as heterodimer consisting of GABA$_B$R1 and GABA$_B$R2 monomers (Angers et al., 2002; White et al. 1998; Kaupmann et al., 1998). In rare cases hetero- and homodimerization were also found for serotonin receptors, e.g. homodimerization of the G$_{\alpha q}$-coupled 5-HTR$_{2C}$ has been reported to be important for its signaling function (Herrick-Davis et al., 2005). Homo- and dimerization have been described also for other serotonin receptors, but

preferentially for class 1, such as 5-HTR$_{1B}$, 5-HTR$_{1D}$, and 5-HTR$_{1A}$ (Xie et al., 1999; Renner et al., 2012; Lukasiewicz et al., 2007). 5-HTR$_{1A}$ is able to form homodimers and heterodimers with 5-HTR$_7$ and even with the adenosine A$_{2A}$ receptor (Renner et al., 2012; Lukasiewicz et al., 2007). However, there was no information about interaction of 5-HT receptors with 5-HT$_B$ proteins. Our cell experiments showed that a major part of the 5-HTR$_{1A}$ was removed from the cell membrane and retained within the cell in presence of 5-HT$_{5B}$. This effect on 5-HTR$_{1A}$ was equal for both variants of 5-HT$_{5B}$ (fig. 4.16A). However, we cannot exclude, that this finding was an artifact due to overexpression. We did not observe such effect concerning 5-HTR$_7$ (fig. 4.16B). Otherwise, no co-localization was observed when 5-HTR$_{1A}$ and 5-HTR$_{5A}$ were co-expressed (fig. 4.16A). Therefore, we assume that 5-HTR$_{1A}$-5-HT$_{5B}$ interaction is specific. For clarification we plan further experiments, such as co-immunoprecipitation, Förster resonance energy transfer (FRET), or surface plasmon resonance (SPR), which might provide more evidence for the observed phenomenon.

Similar effects were reported recently for the ghrelin receptor (GH-R1a). Due to direct interaction with a naturally occurring truncated splice variant (TM-I - TM-V), the receptor is retained within the ER (Howard et al., 1996; Leung et al., 2007; Chow et al., 2012). Other examples are listed in table 5.1. Similar to our data, most of the identified truncated GPCRs show a dominant-negative effect on the localization of their corresponding wild type forms. Thus, truncated receptors may play an important role in the regulation of GPCR activity and the signaling process (Magalhaes et al., 2012; Milligan, 2010).

5.4.2. 5-HT$_{5B}$ and its role in cAMP signaling

Activation of GPCRs results in a conformational change of the bound heterotrimeric G-protein induced by a nucleotide exchange, in which GDP is replaced by a GTP in the G$_\alpha$-subunit. This leads to a dissociation of the G$_\alpha$-subunit from the G$_{\beta\gamma}$-dimer. Depending on the class of the Gα-protein various pathways can be switched on. Using [^{35}S]GTP$_\gamma$S binding assay, we identified the inhibitory G$_{\alpha i3}$-protein, which couples to the phylogenetically related 5-HTR$_{5A}$ (Francken et al., 1998), as the preferred G-protein binding partner of 5-HT$_{5B}$. G$_{\alpha i3}$-proteins inhibit adenylyl cyclases (ACs) occluding cAMP formation. This is in accordance with our results showing that in *Htr5b* transfected N1E-115 cells, cAMP-concentration was reduced by 50%

compared to MOCK control. For this effect no serotonin stimulation was needed, which indicates that there is an intrinsic constitutive activity of 5-HT$_{5B}$. However, an additional contribution of other co-factors cannot be excluded.

The cAMP-reducing properties of 5-HT$_{5B}$-proteins were also demonstrated in *in vivo*. The pathologically strong expression of 5-HT$_{5B}$ in the VRG of MeCP2 deficient mice at P40 was accompanied with low level of cAMP in this region. This is in line with recent studies showing a decreased level of *in vitro*-cultured brainstem slices including the pre-BötC (Mironov et al., 2011). A consistent finding was that double-ko (*Mecp2$^{-/y}$;Htr5b$^{-/-}$*) mice at P40 showed a normalized cAMP level, which demonstrated that 5-HT$_{5B}$-proteins were responsible for the reduction.

The observation of the putative constitutive activity of 5-HT$_{5B}$ and the predominantly endosomal localization raises the question of the physiological role, which is closely linked with potential regulatory targets.

Cyclic AMP is produced by adenylyl cyclases after stimulation via G$_{\alpha s}$-proteins through GPCRs. To date, in mammals at least 10 different AC isoforms have been identified (Billington & Hall, 2012). Nine of them represent large membrane integrated proteins (AC$_{tm}$) with a relative molecular mass of 120 to 140 kDa. Another soluble isoform (AC$_s$) has been isolated first from cytosolic extract of rat testis, but is also present in other tissues including the brain (Braun & Dods, 1975; Sinclair et al., 2000). Cyclic AMP is the classical second messenger regulating a vast number of signaling processes either directly in case of cyclic nucleotide-gated channels (CNGs) or mediated by cAMP-dependent protein kinase A (PKA). Uncountable target proteins of PKA have been reported. Hence, cAMP is directly and indirectly involved in almost all physiological cell processes including cell excitability, metabolism, gene regulation, cell division, differentiation, and apoptosis (Francis & Corbin, 1994).

Therefore, it is important for cells to keep different cAMP signaling pathways separated. This is maintained by scaffold and anchor proteins, which cohere proteins involved in the same pathway, and separation by lipid raft microdomains. However, cAMP is soluble and diffusible. If cAMP signals remain uncontrolled and cAMP concentrations increase rapidly, all pools of cAMP effectors would have the same chance of being activated, which could result in uncoordinated simultaneous activation of different pathways. To this end, cells express a defined subset of phosphodiesterases (PDEs) that rapidly degrade cAMP, which is an important function in the arising concept of cAMP microdomains (Tresguerres et al., 2011).

Endosomal $G_{\alpha i3}$-coupled 5-HT$_{5B}$ might be engaged in the inactivation of co-internalized ACs together with GPCRs, and keeping ACs in an inactive state until they are restored at the cell membrane. Thus, 5-HT$_{5B}$ proteins might be involved in the maintenance of cAMP microdomains (fig. 5.2).
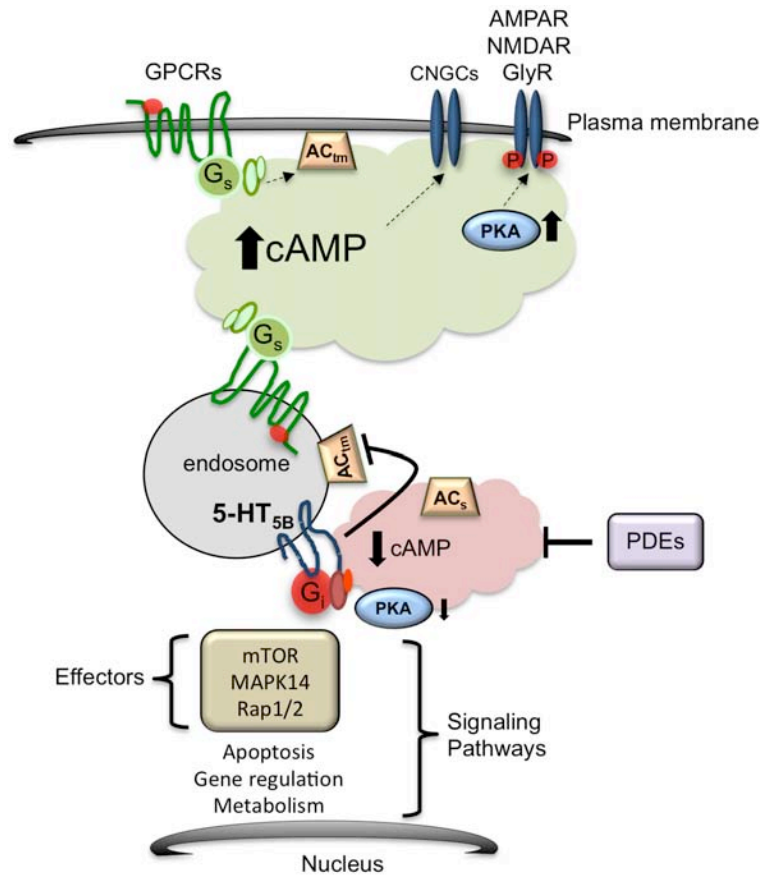
Figure 5.2. Schematic representation of the putative function of 5-HT$_{5B}$ in cAMP signaling.
Cyclic 3′,5′-adenosine monophosphate (cAMP) is produced by $G_{\alpha s}$-activated adenylyl cyclases (ACs) upon G-protein coupled receptor (GPCR) stimulation. Cyclic AMP acts directly on cyclic nucleotide-gated channels (CNGCs) or is indirectly involved, mediated by protein kinase A, in almost all physiological processes, such as gene regulation, metabolism, or apoptosis via diverse effectors, such as mammalian target of rapamycin (mTOR), mitogen-activated protein kinase 14 (MAK14), or Ras related proteins (Rap1/2). To avoid cross-reactions between different cAMP-mediated signaling pathways, cAMP is regulated strongly to maintain cAMP microdomains. Therefore, cAMP is degraded by soluble phosphodiesterases (PDEs), whereas endosomal 5-HT$_{5B}$ proteins are involved in switching off AC activity.

5.5. Pathophysiological consequences of 5-HT$_{5B}$-induced cAMP depression

Almost all $Mecp2^{-/y}$ mice displayed irregular breathing at P40 in the *in situ* working heart brainstem preparation as well as in *in vivo*, which was in accordance with previous studies of this mouse model (Guy et al., 2001; Stettner et al., 2007; Abdala et al., 2010). We demonstrated that the pathologically strong expression in the VRG at P40 plays a crucial role in the onset of arrhythmic breathing. *In situ* and *in vivo* experiments showed a clear improvement of breathing in double-ko mice. There are suggestions that the breathing phenotype of $Mecp2^{-/y}$ mice may result from impaired synaptic plasticity of the respiratory network caused by altered developmental gene expression (Julu et al., 1997; Stettner et al., 2007; Medrihan et al., 2008; Abdala et al., 2010). Although expression of GABA receptors is dysregulated at early development stage P7, plethysmographic recordings did not show any abnormalities in resting ventilation (Medrihan et al., 2008). Additionally, breathing disturbances also occurred in mice after *Mecp2* was switched off at a later postnatal stage (> P60), when the respiratory network is already completely matured (McGraw et al., 2011), or were diminished when *Mecp2* expression was switched on after P28 (Guy et al., 2007). The coincidence of the strong dysregulation of 5-HT$_{5B}$ in the VRG together with the onset of disturbed breathing in Rett mice was a strong indication for the involvement of this protein, which was proved using $Mecp2^{-/y},Htr5b^{-/-}$ double-ko mice.

Regular breathing (eupnoea) depends on a coordinated respiratory network activity to accurately shape the firing pattern and to control burst termination and phase transitions (Richter, 1996; Richter & Spyer 2001). The respiratory network operates with a reciprocal organization of antagonistic groups of glutamatergic, GABA-ergic, and glycinergic interneurons (Richter et al., 1996), in which the glycinergic control is vital for respiratory phase termination (Pierrefiche et al., 1998). A disturbed glycinergic transmission is able to cause several breathing abnormalities like hypoxia (Richter et al., 1991) and hyperekplexia (Büsselberg et al., 2001). However, in $Mecp2^{-/y}$ mice the expression of glycine receptors and transporters at the RNA level was not altered in comparison with wt mice at P40, when the respiratory phenotype is entirely developed (fig. 4.2). One explanation for the disturbed network function might be the coincidence of down-regulation of glycine receptor alpha 3 (GlyRα3), which is important for rhythmic breathing and target for G$_{\alpha i3}$-dependent phosphorylation (Manzke et al., 2010), and up-regulation of 5-HT$_{5B}$, which also couples to G$_{\alpha i3}$-protein reducing intracellular cAMP concentration. This presumed involvement of gylcine

receptors corresponds with comparable breathing disturbances occurring at the end of the 3rd postnatal week in the *Oscillator* mouse model for hyperekplexia, in which a deficient GlyRα1 is expressed (Markstahler et al., 2002; Büsselberg et al., 2001).

However, to explain the arrhythmic breathing pattern on network level in detail, it is indispensable to collect further information about the physiological role of 5-HT$_{5B}$ within the cell, its expression in electro-physiologically identified respiratory neurons and its effect on signaling pathways. Although the exact mechanism still is unknown, the reduced cAMP level in the VRG at P40 is obviously causative for the disturbed breathing in *Mecp2$^{-/y}$* mice.

Systemic application of the protein kinase A inhibitor Rp-cAMPs induced a Rett-like respiratory phenotype in working heart brainstem preparations (fig. 4.23), whereas administration of forskolin, an adenylyl cyclase activator elevating intracellular cAMP concentration, rescued a regular central respiratory rhythm in *Mecp2$^{-/y}$* mice (fig. 4.24). The definitive proof that 5-HT$_{5B}$ is truly causal for the respiratory dysfunction in *Mecp2$^{-/y}$* mice, was demonstrated by means of double-ko mice (*Mecp2$^{-/y}$;Htr5b$^{-/-}$*), in which *Htr5b* was additionally knocked out. It is noteworthy that *Htr5b$^{-/-}$* ko-mice, which were used for crossbreeding, did not show any respiratory disturbances (fig. 4.20).

In contrast to *Mecp2$^{-/y}$* mice, double-ko mice, which showed a normal cAMP concentration in the VRG (fig. 4.18), displayed regular phrenic nerve output activity of the respiratory network (fig. 4.19). These findings were confirmed by plethys-mographic recordings in conscious fully intact animals (fig. 4.20).

Based on breathing irregularities accompanied with breathing arrests, MeCP2 deficient mice may be chronically hypoxic and ischemic, which is displayed e.g. by an up-regulation of the hypoxia-inducible factor 1 alpha (HIF1α) and an increased hematocrit value, which was previously reported (Fischer et al., 2009), and which is in accordance with our data. These hypoxic conditions might be reasonable for the bad physical condition and the shortened lifespan. This hypothesis is supported by double-ko mice exhibiting an almost normalized hematocrit value in comparison with wt mice that might be caused by improved oxygen supply.

Overall, double-ko mice appeared healthier compared to *Mecp2* ko mice (fig. 4.22). In particular, hematocrit and body weight returned to wild type levels (fig. 4.21), and double-ko mice lived up to 40 days longer than *Mecp2* ko mice (fig. 4.21).

5.6. Pharmacological strategies

The research for the cause of the origin of breathing disturbances goes hand in hand with the development of a potential pharmacotherapy to overcome life-threatening breathing arrests in RTT patients.

Basically, serotonin receptors are potential targets to treat several diseases, such as irritable bowel syndrome, anxiety, and depression. However, a treatment directly targeting $5-HT_{5B}$ should be difficult due to its truncation and intracellular localization.

Activation of $5-HTR_{1A}$, e.g. with 8-OH-DPAT or the clinically approved anxiolyticum buspirone, is an established strategy to overcome apneustic breathing in several diseases, spinal cord injury (SCI), or after pharmacological treatment with opiates (El-Khatib et al., 2003; Wilken et al., 1997; Lalley et al., 1994; Richter et al., 1994; Dutschmann et al., 2009; Sahibzada et al., 2000; Teng et al., 2003).

The supposed molecular mechanism begins with cAMP reduction through activation of inhibitory G-proteins $G_{i\alpha3}$, which results in dephosphorylation of the glycine receptor subunit α3 due to diminished PKA activity (Manzke et al., 2010). Resultant potentiation of glycinergic synaptic inhibition of inspiratory neurons mediated by post-I-neurons terminates inspiration. Such potentiation of glycinergic synaptic inhibition is beneficial during early development of MeCP2 deficient mice, but fades despite low cAMP levels when the cAMP-PKA sensitive GlyRα3 is downregulated, a further depression of cAMP through activation of $5-HTR_{1A}$ would remain ineffective. Hence, we propose a cAMP-elevating strategy, which is supported by experiments showing that systemic cAMP elevation in *in vivo*-like preparations rescued regular breathing.

Therefore, it is surprising that treatment with 8-OH-DPAT led to improvement of breathing in *Mecp2*$^{-/y}$ and *Mecp2*$^{-/+}$ mice (Abdala et al., 2010). However, this is in contrast to our data. We found that apneas in *Mecp2*$^{-/y}$ mice even become more frequent, and the phrenic nerve activity undergoes a dramatic decline after lowering cAMP upon systemic $5-HTR_{1A}$ activation by 8-OH-DPAT. To date, we cannot eradicate this contradiction.

Alternative approaches to improve respiration in Rett mice are summarized in the following table 5.2.

Table 5.2. Pharmacological treatment of breathing disturbances in mouse models for the Rett syndrome

IP = intraperitoneal, Tyrosine kinase receptor B (TrkB), Insulin-like growth factor 1 (IGF-1)

Substance/drug	Application form	Mouse model	Target	Effect	Reference
Desipramine	oral	$Mecp2^{-/y}$	norepinephrine reuptake blocker	Yes	Zanella et al., 2008
Desipramine	IP injection	$Mecp2^{-/y}$	norepinephrine reuptake-blocker	Yes	Roux et al., 2007
Ampakine	IP injection	$Mecp2^{-/y}$	AMPA receptor agonist	Yes	Ogier et al., 2007
LM22A-4	IP injection	$Mecp2^{+/-}$	(TrkB) agonist	Yes	Schmid et al., 2012
Active peptide of IGF-1	IP injection	$Mecp2^{-/y}$	IGF-1 receptor	Yes	Tropea et al., 2009
NO-711	IP by transplanted pump	$Mecp2^{-/y}$ $Mecp2^{+/-}$	GABA reuptake blocker	Yes	Abdala et al., 2010
8-OH-DPAT	IP by transplanted pump	$Mecp2^{-/y}$ $Mecp2^{+/-}$	5-HTR_{1A} agonist	Yes	Abdala et al., 2010

Despite diverse approaches, which seemed to be more or less effective to overcome respiratory disturbances in mouse models for the Rett syndrome, there is no reliable pharmacotherapy in men.

6. Conclusion

The present work shows that breathing disturbances in a mouse model for Rett syndrome (RTT) arises mainly by dysregulation of a single gene, which encodes for the orphan serotonin receptor 5B (5-HTR$_{5B}$). The lack of MeCP2 repression, which is causal for RTT, results directly in high levels of 5-HTR$_{5B}$ in the VRG and adjacent regions important for respiratory rhythm generation at postnatal stage 40, which coincides with the onset of breathing disturbances in MeCP2 deficient mice. In this thesis, it is demonstrated that the receptor is naturally truncated and attached to the membrane of endosomes, but retains its ability to bind inhibitory G-proteins G$_{\alpha i3}$ that reduces intracellular cAMP in a constitutive manner. The pathologically strong 5-HT$_{5B}$-protein expression in the VRG of MeCP2 deficient mice results in a persistent low cAMP level, which obviously disturbs central breathing rhythm.

The second messenger cAMP affects a broad range of signal transduction cascades ranging from alteration of membrane excitability by direct influence on ion channels right up to the influence on regulation of gene expression. Accompanied with the molecular behavior and peculiar localization of the 5-HT$_{5B}$ protein in endosomes, we currently could not identify molecular targets affected by persistent low cAMP concentration to explain the breathing disturbances on respiratory network level in detail.

This is complicated by the observation that 5-HT$_{5B}$ proteins affect the localization of the serotonin receptor 1A, which plays an important role for the modulation of the respiratory rhythm.

However, showing successful treatment by cAMP elevation in *in situ* together with the proof of 5-HT$_{5B}$ expression in men provide new pharmacological strategies to treat respiratory disturbances in Rett patients.

7. References

Alken, M., Rutz, C., Köchl, R., Donalies, U., Oueslati, M., Furkert, J., Wietfeld, D., et al. (2005). The signal peptide of the rat corticotropin-releasing factor receptor 1 promotes receptor expression but is not essential for establishing a functional receptor. *The Biochemical journal*, *390*(Pt 2), 455–64.

Amano, K., Nomura, Y., Segawa, M., & Yamakawa, K. (2000). Mutational analysis of the MECP2 gene in Japanese patients with Rett syndrome. *Journal of human genetics*, *45*(4), 231–6.

Amano, T., Richelson, E., & Nirenberg, M. (1972). Neurotransmitter synthesis by neuroblastoma clones (neuroblast differentiation-cell culture-choline acetyltransferase-acetylcholinesterase-tyrosine hydroxylase-axons-dendrites). *Proceedings of the National Academy of Sciences of the United States of America*, *69*(1), 258–63.

Amir, R. E., Van den Veyver, I. B., Wan, M., Tran, C. Q., Francke, U., & Zoghbi, H. Y. (1999). Rett syndrome is caused by mutations in X-linked MECP2, encoding methyl-CpG-binding protein 2. *Nature genetics*, *23*(2), 185–8.

Angers, S., Salahpour, A., & Bouvier, M. (2002). Dimerization: an emerging concept for G protein-coupled receptor ontogeny and function. *Annual review of pharmacology and toxicology*, *42*, 409–35.

Archer, H. L., Whatley, S. D., Evans, J. C., Ravine, D., Huppke, P., Kerr, A., Bunyan, D., et al. (2006). Gross rearrangements of the MECP2 gene are found in both classical and atypical Rett syndrome patients. *Journal of medical genetics*, *43*(5), 451–6.

Azim, S., Banday, A. R., & Tabish, M. (2012). Identification of alternatively spliced multiple transcripts of 5-hydroxytryptamine receptor in mouse. *Brain research bulletin*, *87*(2-3), 250–8.

Azmitia, E. C. (2001). Modern views on an ancient chemical: serotonin effects on cell proliferation, maturation, and apoptosis. *Brain research bulletin*, *56*(5), 413–24.

Bailer, U. F., & Kaye, W. H. (2011). Serotonin: imaging findings in eating disorders. *Current topics in behavioral neurosciences*, *6*, 59–79.

Bakker, R. A., Lozada, A. F., van Marle, A., Shenton, F. C., Drutel, G., Karlstedt, K., Hoffmann, M., et al. (2006). Discovery of naturally occurring splice variants of the rat histamine H3 receptor that act as dominant-negative isoforms. *Molecular pharmacology*, *69*(4), 1194–206.

Ballas, N., Grunseich, C., Lu, D. D., Speh, J. C., & Mandel, G. (2005). REST and its corepressors mediate plasticity of neuronal gene chromatin throughout neurogenesis. *Cell*, *121*(4), 645–57.

Ballas, N., Lioy, D. T., Grunseich, C., & Mandel, G. (2009). Non-cell autonomous influence of MeCP2-deficient glia on neuronal dendritic morphology. *Nature neuroscience*, *12*(3), 311–7.

Bartlett, D., & Tenney, S. M. (1970). Control of breathing in experimental anemia. *Respiration physiology*, *10*(3), 384–95.

Ben-Shachar, S., Chahrour, M., Thaller, C., Shaw, C. a, & Zoghbi, H. Y. (2009). Mouse models of MeCP2 disorders share gene expression changes in the cerebellum and hypothalamus. *Human molecular genetics*, *18*(13), 2431–42.

Benkirane, M., Jin, D. Y., Chun, R. F., Koup, R. A., & Jeang, K. T. (1997). Mechanism of transdominant inhibition of CCR5-mediated HIV-1 infection by ccr5delta32. *The Journal of biological chemistry*, *272*(49), 30603–6.

REFERENCES

Berger, M., Gray, J. a, & Roth, B. L. (2009). The expanded biology of serotonin. *Annual review of medicine*, *60*, 355–66.

Bianchi, A. L., Denavit-Saubié, M., & Champagnat, J. (1995). Central control of breathing in mammals: neuronal circuitry, membrane properties, and neurotransmitters. *Physiological reviews*, *75*(1), 1–45.

Bienvenu, T, Carrié, A., de Roux, N., Vinet, M. C., Jonveaux, P., Couvert, P., Villard, L., et al. (2000). MECP2 mutations account for most cases of typical forms of Rett syndrome. *Human molecular genetics*, *9*(9), 1377–84.

Bienvenu, Thierry, & Chelly, J. (2006). Molecular genetics of Rett syndrome: when DNA methylation goes unrecognized. *Nature reviews. Genetics*, *7*(6), 415–26.

Billington, C. K., & Hall, I. P. (2012). Novel cAMP signalling paradigms: therapeutic implications for airway disease. *British journal of pharmacology*, *166*(2), 401–10.

Birnboim, H. C., & Doly, J. (1979). A rapid alkaline extraction procedure for screening recombinant plasmid DNA. *Nucleic acids research*, *7*(6), 1513–23.

Blondel, O., Gastineau, M., Dahmoune, Y., Langlois, M., & Fischmeister, R. (1998). Cloning, expression, and pharmacology of four human 5-hydroxytryptamine 4 receptor isoforms produced by alternative splicing in the carboxyl terminus. *Journal of neurochemistry*, *70*(6), 2252–61.

Bockaert, J., Claeysen, S., Bécamel, C., Dumuis, A., & Marin, P. (2006). Neuronal 5-HT metabotropic receptors: fine-tuning of their structure, signaling, and roles in synaptic modulation. *Cell and tissue research*, *326*(2), 553–72.

Bou-Flores, C., Lajard, A. M., Monteau, R., De Maeyer, E., Seif, I., Lanoir, J., & Hilaire, G. (2000). Abnormal phrenic motoneuron activity and morphology in neonatal monoamine oxidase A-deficient transgenic mice: possible role of a serotonin excess. *The Journal of neuroscience : the official journal of the Society for Neuroscience*, *20*(12), 4646–56.

Boyes, J., & Bird, A. (1991). DNA methylation inhibits transcription indirectly via a methyl-CpG binding protein. *Cell*, *64*(6), 1123–34.

Braun, T., & Dods, R. F. (1975). Development of a Mn-2+-sensitive, "soluble" adenylate cyclase in rat testis. *Proceedings of the National Academy of Sciences of the United States of America*, *72*(3), 1097–101.

Braunschweig, D., Simcox, T., Samaco, R. C., & LaSalle, J. M. (2004). X-Chromosome inactivation ratios affect wild-type MeCP2 expression within mosaic Rett syndrome and Mecp2-/+ mouse brain. *Human molecular genetics*, *13*(12), 1275–86.

Budden, S. S., Dorsey, H. C., & Steiner, R. D. (2005). Clinical profile of a male with Rett syndrome. *Brain & development*, *27 Suppl 1*, S69–S71.

Burns, C. M., Chu, H., Rueter, S. M., Hutchinson, L. K., Canton, H., Sanders-Bush, E., & Emeson, R. B. (1997). Regulation of serotonin-2C receptor G-protein coupling by RNA editing. *Nature*, *387*(6630), 303–8.

Büsselberg, D., Bischoff, a. M., Paton, J. F. R., & Richter, D. W. (2001). Reorganisation of respiratory network activity after loss of glycinergic inhibition. *Pflügers Archiv European Journal of Physiology*, *441*(4), 444–449.

Carson, M. J., Thomas, E. A., Danielson, P. E., & Sutcliffe, J. G. (1996). The 5HT5A serotonin receptor is expressed predominantly by astrocytes in which it inhibits cAMP accumulation: a mechanism for neuronal suppression of reactive astrocytes. *Glia*, *17*(4), 317–26.

REFERENCES

Chahrour, M., Jung, S. Y., Shaw, C., Zhou, X., Wong, S. T. C., Qin, J., & Zoghbi, H. Y. (2008). MeCP2, a key contributor to neurological disease, activates and represses transcription. *Science (New York, N.Y.)*, *320*(5880), 1224–9.

Chahrour, M., & Zoghbi, H. Y. (2007). The story of Rett syndrome: from clinic to neurobiology. *Neuron*, *56*(3), 422–37.

Charman, T., Neilson, T. C. S., Mash, V., Archer, H., Gardiner, M. T., Knudsen, G. P. S., McDonnell, A., et al. (2005). Dimensional phenotypic analysis and functional categorisation of mutations reveal novel genotype-phenotype associations in Rett syndrome. *European journal of human genetics : EJHG*, *13*(10), 1121–30.

Cheadle, J. P., Gill, H., Fleming, N., Maynard, J., Kerr, a, Leonard, H., Krawczak, M., et al. (2000). Long-read sequence analysis of the MECP2 gene in Rett syndrome patients: correlation of disease severity with mutation type and location. *Human molecular genetics*, *9*(7), 1119–29.

Chen, R. Z., Akbarian, S., Tudor, M., & Jaenisch, R. (2001). Deficiency of methyl-CpG binding protein-2 in CNS neurons results in a Rett-like phenotype in mice. *Nature genetics*, *27*(3), 327–31.

Chen, W. G., Chang, Q., Lin, Y., Meissner, A., West, A. E., Griffith, E. C., Jaenisch, R., et al. (2003). Derepression of BDNF transcription involves calcium-dependent phosphorylation of MeCP2. *Science (New York, N.Y.)*, *302*(5646), 885–9.

Choudhury, A., Dominguez, M., Puri, V., Sharma, D. K., Narita, K., Wheatley, C. L., Marks, D. L., et al. (2002). Rab proteins mediate Golgi transport of caveola-internalized glycosphingolipids and correct lipid trafficking in Niemann-Pick C cells. *The Journal of clinical investigation*, *109*(12), 1541–50.

Chow, K. B. S., Sun, J., Chu, K. M., Tai Cheung, W., Cheng, C. H. K., & Wise, H. (2012). The truncated ghrelin receptor polypeptide (GHS-R1b) is localized in the endoplasmic reticulum where it forms heterodimers with ghrelin receptors (GHS-R1a) to attenuate their cell surface expression. *Molecular and cellular endocrinology*, *348*(1), 247–54.

Ciarleglio, C. M., Resuehr, H. E. S., & McMahon, D. G. (2011). Interactions of the serotonin and circadian systems: nature and nurture in rhythms and blues. *Neuroscience*, *197*, 8–16.

Cohen, S., Gabel, H. W., Hemberg, M., Hutchinson, A. N., Sadacca, L. A., Ebert, D. H., Harmin, D. A., et al. (2011). Genome-wide activity-dependent MeCP2 phosphorylation regulates nervous system development and function. *Neuron*, *72*(1), 72–85.

Coleman, M., Naidu, S., Murphy, M., Pines, M., & Bias, W. (1987). A set of monozygotic twins with Rett syndrome. *Brain & development*, *9*(5), 475–8.

Connelly, C A, Ellenberger, H. H., & Feldman, J. L. (1989). Are there serotonergic projections from raphe and retrotrapezoid nuclei to the ventral respiratory group in the rat? *Neuroscience letters*, *105*(1-2), 34–40.

Connelly, Caroline A., Dobbins, E. G., & Feldman, J. L. (1992). Pre-Bötzinger complex in cats: respiratory neuronal discharge patterns. *Brain Research*, *590*(1-2), 337–340.

Córdoba-Chacón, J., Gahete, M. D., Duran-Prado, M., Pozo-Salas, A. I., Malagón, M. M., Gracia-Navarro, F., Kineman, R. D., et al. (2010). Identification and characterization of new functional truncated variants of somatostatin receptor subtype 5 in rodents. *Cellular and molecular life sciences : CMLS*, *67*(7), 1147–63.

DRORBAUGH, J. E., & FENN, W. O. (1955). A barometric method for measuring ventilation in newborn infants. *Pediatrics*, *16*(1), 81–7.

REFERENCES

Dahlström, A., & Fuxe, K. (1964). Localization of monoamines in the lower brain stem. *Experientia*, *20*(7), 398–9.

Dani, V. S., Chang, Q., Maffei, A., Turrigiano, G. G., Jaenisch, R., & Nelson, S. B. (2005). Reduced cortical activity due to a shift in the balance between excitation and inhibition in a mouse model of Rett syndrome. *Proceedings of the National Academy of Sciences of the United States of America*, *102*(35), 12560–5.

Dayer, A. G., Bottani, A., Bouchardy, I., Fluss, J., Antonarakis, S. E., Haenggeli, C.-A., & Morris, M. a. (2007). MECP2 mutant allele in a boy with Rett syndrome and his unaffected heterozygous mother. *Brain & development*, *29*(1), 47–50.

Depuy, S. D., Kanbar, R., Coates, M. B., Stornetta, R. L., & Guyenet, P. G. (2011). Control of breathing by raphe obscurus serotonergic neurons in mice. *The Journal of neuroscience : the official journal of the Society for Neuroscience*, *31*(6), 1981–90.

Di Pasquale, E., Lindsay, A., Feldman, J., Monteau, R., & Hilaire, G. (1997). Serotonergic inhibition of phrenic motoneuron activity: an in vitro study in neonatal rat. *Neuroscience letters*, *230*(1), 29–32.

Dinan, T. G. (1996). Serotonin and the regulation of hypothalamic-pituitary-adrenal axis function. *Life sciences*, *58*(20), 1683–94.

Dutschmann, M., Waki, H., Manzke, T., Simms, A. E., Pickering, A. E., Richter, D. W., & Paton, J. F. R. (2009). The potency of different serotonergic agonists in counteracting opioid evoked cardiorespiratory disturbances. *Philosophical transactions of the Royal Society of London. Series B, Biological sciences*, *364*(1529), 2611–23.

Dutton, A. C., Massoura, A. N., Dover, T. J., Andrews, N. A., & Barnes, N. M. (2008). Identification and functional significance of N-glycosylation of the 5-ht5A receptor. *Neurochemistry international*, *52*(3), 419–25.

D'Esposito, M., Quaderi, N. a, Ciccodicola, a, Bruni, P., Esposito, T., D'Urso, M., & Brown, S. D. (1996). Isolation, physical mapping, and northern analysis of the X-linked human gene encoding methyl CpG-binding protein, MECP2. *Mammalian genome : official journal of the International Mammalian Genome Society*, *7*(7), 533–5.

El-Khatib, M. F., Kiwan, R. A., & Jamaleddine, G. W. (2003). Buspirone treatment for apneustic breathing in brain stem infarct. *Respiratory care*, *48*(10), 956–8.

Elian, M., & Rudolf, N. D. (1991). EEG and respiration in Rett syndrome. *Acta neurologica Scandinavica*, *83*(2), 123–8.

Ellgaard, L., Molinari, M., & Helenius, A. (1999). Setting the standards: quality control in the secretory pathway. *Science (New York, N.Y.)*, *286*(5446), 1882–8.

España, R. a, & Scammell, T. E. (2011). Sleep neurobiology from a clinical perspective. *Sleep*, *34*(7), 845–58.

Ezure, K. (1990). Synaptic connections between medullary respiratory neurons and considerations on the genesis of respiratory rhythm. *Progress in Neurobiology*, *35*(6), 429–450.

Fallert, M., Böhmer, G., Dinse, H. R., Sommer, T. J., & Bittner, A. (1979). Microelectrophoretic application of putative neurotransmitters onto various types of bulbar respiratory neurons. *Archives italiennes de biologie*, *117*(1), 1–12

Fehr, S., Bebbington, A., Nassar, N., Downs, J., Ronen, G. M., DE Klerk, N., & Leonard, H. (2011). Trends in the diagnosis of Rett syndrome in Australia. *Pediatric research*, *70*(3), 313–9.

REFERENCES

Feldmann, A., Amphornrat, J., Schönherr, M., Winterstein, C., Möbius, W., Ruhwedel, T., Danglot, L., et al. (2011). Transport of the major myelin proteolipid protein is directed by VAMP3 and VAMP7. *The Journal of neuroscience : the official journal of the Society for Neuroscience*, *31*(15), 5659–72.

Fischer, M., Reuter, J., Gerich, F. J., Hildebrandt, B., Hägele, S., Katschinski, D., & Müller, M. (2009). Enhanced hypoxia susceptibility in hippocampal slices from a mouse model of rett syndrome. *Journal of neurophysiology*, *101*(2), 1016–32.

Fliegel, L., Burns, K., MacLennan, D. H., Reithmeier, R. A., & Michalak, M. (1989). Molecular cloning of the high affinity calcium-binding protein (calreticulin) of skeletal muscle sarcoplasmic reticulum. *The Journal of biological chemistry*, *264*(36), 21522–8.

Forlani, G., Giarda, E., Ala, U., Di Cunto, F., Salani, M., Tupler, R., Kilstrup-Nielsen, C., et al. (2010). The MeCP2/YY1 interaction regulates ANT1 expression at 4q35: novel hints for Rett syndrome pathogenesis. *Human molecular genetics*, *19*(16), 3114–23.

Francis, S. H., & Corbin, J. D. (1994). Structure and function of cyclic nucleotide-dependent protein kinases. *Annual review of physiology*, *56*, 237–72.

Francken, B. J., Jurzak, M., Vanhauwe, J. F., Luyten, W. H., & Leysen, J. E. (1998). The human 5-ht5A receptor couples to Gi/Go proteins and inhibits adenylate cyclase in HEK 293 cells. *European journal of pharmacology*, *361*(2-3), 299–309.

Fredriksson, R., Lagerström, M. C., Lundin, L.-G., & Schiöth, H. B. (2003). The G-protein-coupled receptors in the human genome form five main families. Phylogenetic analysis, paralogon groups, and fingerprints. *Molecular pharmacology*, *63*(6), 1256–72.

Fritschy, J.-M., Harvey, R. J., & Schwarz, G. (2008). Gephyrin: where do we stand, where do we go? *Trends in neurosciences*, *31*(5), 257–64.

Fuks, F., Hurd, P. J., Wolf, D., Nan, X., Bird, A. P., & Kouzarides, T. (2003). The methyl-CpG-binding protein MeCP2 links DNA methylation to histone methylation. *The Journal of biological chemistry*, *278*(6), 4035–40.

Garner, S. J., Eldridge, F. L., Wagner, P. G., & Dowell, R. T. (1989). Buspirone, an anxiolytic drug that stimulates respiration. *The American review of respiratory disease*, *139*(4), 946–50.

Gaultier, C., & Gallego, J. (2008). Neural control of breathing: insights from genetic mouse models. *Journal of applied physiology (Bethesda, Md. : 1985)*, *104*(5), 1522–30.

Gavarini, S., Bécamel, C., Altier, C., Lory, P., Poncet, J., Wijnholds, J., Bockaert, J., et al. (2006). Opposite effects of PSD-95 and MPP3 PDZ proteins on serotonin 5-hydroxytryptamine2C receptor desensitization and membrane stability. *Molecular biology of the cell*, *17*(11), 4619–31.

Gehring, C. (2010). Adenyl cyclases and cAMP in plant signaling - past and present. *Cell communication and signaling : CCS*, *8*(1), 15.

Geldenhuys, W. J., & Van der Schyf, C. J. (2011). Role of serotonin in Alzheimer's disease: a new therapeutic target? *CNS drugs*, *25*(9), 765–81.

Gillberg, C. (1986). Autism and Rett syndrome: some notes on differential diagnosis. *American journal of medical genetics. Supplement*, *1*, 127–31.

Glaze, D. G., Frost, J. D., Zoghbi, H. Y., & Percy, a K. (1987). Rett's syndrome: characterization of respiratory patterns and sleep. *Annals of neurology*, *21*(4), 377–82.

REFERENCES

Goddard, A. D., & Watts, A. (2012). Regulation of G protein-coupled receptors by palmitoylation and cholesterol. *BMC biology*, *10*, 27.

Goffin, D., Allen, M., Zhang, L., Amorim, M., Wang, I.-T. J., Reyes, A.-R. S., Mercado-Berton, A., et al. (2012). Rett syndrome mutation MeCP2 T158A disrupts DNA binding, protein stability and ERP responses. *Nature neuroscience*, *15*(2), 274–83.

Gonzales, M. L., Adams, S., Dunaway, K. W., & Lasalle, J. M. (2012). Phosphorylation of Distinct Sites in MeCP2 Modifies Cofactor Associations and the Dynamics of Transcriptional Regulation. *Molecular and cellular biology*, *32*(14), 2894–903.

Gonzalez, A., Borquez, M., Trigo, C. A., Brenet, M., Sarmiento, J. M., Figueroa, C. D., Navarro, J., et al. (2011). The splice variant of the V2 vasopressin receptor adopts alternative topologies. *Biochemistry*, *50*(22), 4981–6.

Grailhe, R, Grabtree, G. W., & Hen, R. (2001). Human 5-HT(5) receptors: the 5-HT(5A) receptor is functional but the 5-HT(5B) receptor was lost during mammalian evolution. *European journal of pharmacology*, *418*(3), 157–67.

Grailhe, Régis, Grabtree, G. W., & Hen, R. (2001). Human 5-HT5 receptors: the 5-HT5A receptor is functional but the 5-HT5B receptor was lost during mammalian evolution. *European Journal of Pharmacology*, *418*(3), 157–167.

Grosse, R., Schöneberg, T., Schultz, G., & Gudermann, T. (1997). Inhibition of gonadotropin-releasing hormone receptor signaling by expression of a splice variant of the human receptor. *Molecular endocrinology (Baltimore, Md.)*, *11*(9), 1305–18.

Grunstein, M. (1997). Histone acetylation in chromatin structure and transcription. *Nature*, *389*(6649), 349–52.

Guy, J, Hendrich, B., Holmes, M., Martin, J. E., & Bird, a. (2001). A mouse Mecp2-null mutation causes neurological symptoms that mimic Rett syndrome. *Nature genetics*, *27*(3), 322–6.

Guy, Jacky, Cheval, H., Selfridge, J., & Bird, A. (2011). The role of MeCP2 in the brain. *Annual review of cell and developmental biology*, *27*, 631–52.

Guy, Jacky, Gan, J., Selfridge, J., Cobb, S., & Bird, A. (2007). Reversal of neurological defects in a mouse model of Rett syndrome. *Science (New York, N.Y.)*, *315*(5815), 1143–7.

Hagberg, B. (1985). Rett's syndrome: prevalence and impact on progressive severe mental retardation in girls. *Acta paediatrica Scandinavica*, *74*(3), 405–8.

Hagberg, B. (2005). Rett Syndrome: Long-Term Clinical Follow-Up Experiences Over Four Decades. *Journal of Child Neurology*, *20*(9), 722–727.

Hagberg, B., Aicardi, J., Dias, K., & Ramos, O. (1983). A progressive syndrome of autism, dementia, ataxia, and loss of purposeful hand use in girls: Rett's syndrome: report of 35 cases. *Annals of neurology*, *14*(4), 471–9.

Hampson, K., Woods, C. G., Latif, F., & Webb, T. (2000). Mutations in the MECP2 gene in a cohort of girls with Rett syndrome. *Journal of medical genetics*, *37*(8), 610–2.

Hannon, J., & Hoyer, D. (2008). Molecular biology of 5-HT receptors. *Behavioural brain research*, *195*(1), 198–213.

Hanyaloglu, A. C., & von Zastrow, M. (2008). Regulation of GPCRs by endocytic membrane trafficking and its potential implications. *Annual review of pharmacology and toxicology*, *48*, 537–68.

REFERENCES

Harada, N., Yamada, Y., Tsukiyama, K., Yamada, C., Nakamura, Y., Mukai, E., Hamasaki, A., et al. (2008). A novel GIP receptor splice variant influences GIP sensitivity of pancreatic beta-cells in obese mice. *American journal of physiology. Endocrinology and metabolism*, *294*(1), E61–8.

Harikrishnan, K. N., Chow, M. Z., Baker, E. K., Pal, S., Bassal, S., Brasacchio, D., Wang, L., et al. (2005). Brahma links the SWI/SNF chromatin-remodeling complex with MeCP2-dependent transcriptional silencing. *Nature genetics*, *37*(3), 254–64.

Hassig, C. A., Fleischer, T. C., Billin, A. N., Schreiber, S. L., & Ayer, D. E. (1997). Histone deacetylase activity is required for full transcriptional repression by mSin3A. *Cell*, *89*(3), 341–7. R

Heidmann, D. E., Metcalf, M. A., Kohen, R., & Hamblin, M. W. (1997). Four 5-hydroxytryptamine7 (5-HT7) receptor isoforms in human and rat produced by alternative splicing: species differences due to altered intron-exon organization. *Journal of neurochemistry*, *68*(4), 1372–81.

Henikoff, S. (2000). Heterochromatin function in complex genomes. *Biochimica et biophysica acta*, *1470*(1), O1–8.

Herrick-Davis, K., Grinde, E., Harrigan, T. J., & Mazurkiewicz, J. E. (2005). Inhibition of serotonin 5-hydroxytryptamine2c receptor function through heterodimerization: receptor dimers bind two molecules of ligand and one G-protein. *The Journal of biological chemistry*, *280*(48), 40144–51.

Hilaire, G, Morin, D., Lajard, A. M., & Monteau, R. (1993). Changes in serotonin metabolism may elicit obstructive apnoea in the newborn rat. *The Journal of physiology*, *466*, 367–81.

Hilaire, Gérard, Voituron, N., Menuet, C., Ichiyama, R. M., Subramanian, H. H., & Dutschmann, M. (2010). The role of serotonin in respiratory function and dysfunction. *Respiratory physiology & neurobiology*, *174*(1-2), 76–88.

Holtman, J. R. (1988). Immunohistochemical localization of serotonin- and substance P-containing fibers around respiratory muscle motoneurons in the nucleus ambiguus of the cat. *Neuroscience*, *26*(1), 169–78.

Hornung, J.-P. (2003). The human raphe nuclei and the serotonergic system. *Journal of Chemical Neuroanatomy*, *26*(4), 331–343.

Howard, A. D., Feighner, S. D., Cully, D. F., Arena, J. P., Liberator, P. A., Rosenblum, C. I., Hamelin, M., et al. (1996). A receptor in pituitary and hypothalamus that functions in growth hormone release. *Science (New York, N.Y.)*, *273*(5277), 974–7.

Hoyer, D, Clarke, D. E., Fozard, J. R., Hartig, P. R., Martin, G. R., Mylecharane, E. J., Saxena, P. R., et al. (1994). International Union of Pharmacology classification of receptors for 5-hydroxytryptamine (Serotonin). *Pharmacological reviews*, *46*(2), 157–203.

Hoyer, Daniel, Hannon, J. P., & Martin, G. R. (2002). Molecular, pharmacological and functional diversity of 5-HT receptors. *Pharmacology, biochemistry, and behavior*, *71*(4), 533–54.

Ishii, T., Makita, Y., Ogawa, A., Amamiya, S., Yamamoto, M., Miyamoto, A., & Oki, J. (2001). The role of different X-inactivation pattern on the variable clinical phenotype with Rett syndrome. *Brain & development*, *23 Suppl 1*, S161–4.

Jacobs, B. L., & Azmitia, E. C. (1992). Structure and function of the brain serotonin system. *Physiological reviews*, *72*(1), 165–229.

Jan, M. M., Dooley, J. M., & Gordon, K. E. (1999). Male Rett syndrome variant: application of diagnostic criteria. *Pediatric neurology*, *20*(3), 238–40.

REFERENCES

Jian, L., Archer, H. L., Ravine, D., Kerr, A., de Klerk, N., Christodoulou, J., Bailey, M. E. S., et al. (2005). p.R270X MECP2 mutation and mortality in Rett syndrome. *European journal of human genetics : EJHG*, *13*(11), 1235–8.

Jones, K. A., Srivastava, D. P., Allen, J. A., Strachan, R. T., Roth, B. L., & Penzes, P. (2009). Rapid modulation of spine morphology by the 5-HT2A serotonin receptor through kalirin-7 signaling. *Proceedings of the National Academy of Sciences of the United States of America*, *106*(46), 19575–80.

Jordan, C., Li, H. H., Kwan, H. C., & Francke, U. (2007). Cerebellar gene expression profiles of mouse models for Rett syndrome reveal novel MeCP2 targets. *BMC medical genetics*, *8*, 36.

Julu, P. O., Kerr, A. M., Hansen, S., Apartopoulos, F., & Jamal, G. A. (1997a). Functional evidence of brain stem immaturity in Rett syndrome. *European child & adolescent psychiatry*, *6 Suppl 1*, 47–54.

Julu, P. O., Kerr, A. M., Hansen, S., Apartopoulos, F., & Jamal, G. A. (1997b). Immaturity of medullary cardiorespiratory neurones leading to inappropriate autonomic reactions as a likely cause of sudden death in Rett's syndrome. *Archives of disease in childhood*, *77*(5), 464–5.

Jung, B. P., Jugloff, D. G. M., Zhang, G., Logan, R., Brown, S., & Eubanks, J. H. (2003). The expression of methyl CpG binding factor MeCP2 correlates with cellular differentiation in the developing rat brain and in cultured cells. *Journal of neurobiology*, *55*(1), 86–96.

Kammermeier, P. J., & Worley, P. F. (2007). Homer 1a uncouples metabotropic glutamate receptor 5 from postsynaptic effectors. *Proceedings of the National Academy of Sciences of the United States of America*, *104*(14), 6055–60.

Karpa, K. D., Lin, R., Kabbani, N., & Levenson, R. (2000). The dopamine D3 receptor interacts with itself and the truncated D3 splice variant d3nf: D3-D3nf interaction causes mislocalization of D3 receptors. *Molecular pharmacology*, *58*(4), 677–83.

Kass, S. U., Landsberger, N., & Wolffe, a P. (1997). DNA methylation directs a time-dependent repression of transcription initiation. *Current biology : CB*, *7*(3), 157–65.

Kaupmann, K., Malitschek, B., Schuler, V., Heid, J., Froestl, W., Beck, P., Mosbacher, J., et al. (1998). GABA(B)-receptor subtypes assemble into functional heteromeric complexes. *Nature*, *396*(6712), 683–7.

Kerr, a M., & Julu, P. O. (1999). Recent insights into hyperventilation from the study of Rett syndrome. *Archives of disease in childhood*, *80*(4), 384–7.

Kerr, A M, Armstrong, D. D., Prescott, R. J., Doyle, D., & Kearney, D. L. (1997). Rett syndrome: analysis of deaths in the British survey. *European child & adolescent psychiatry*, *6 Suppl 1*, 71–4.

Kerr, A., Southall, D., Amos, P., Cooper, R., Samuels, M., Mitchell, J., & Stephenson, J. (1990). Correlation of electroencephalogram, respiration and movement in the Rett syndrome. *Brain & development*, *12*(1), 61–8.

Kerr, Alison M, & Engerström, I. W. (Eds.). (2001). *Rett Disorder and the Developing Brain* (1st ed., p. 398). Oxford: Oxford University Press.

Kinney, H. C., Broadbelt, K. G., Haynes, R. L., Rognum, I. J., & Paterson, D. S. (2011). The serotonergic anatomy of the developing human medulla oblongata: implications for pediatric disorders of homeostasis. *Journal of chemical neuroanatomy*, *41*(4), 182–99.

REFERENCES

Kishi, N., & Macklis, J. D. (2004). MECP2 is progressively expressed in post-migratory neurons and is involved in neuronal maturation rather than cell fate decisions. *Molecular and cellular neurosciences*, *27*(3), 306–21.

Klose, R. J., Sarraf, S. a, Schmiedeberg, L., McDermott, S. M., Stancheva, I., & Bird, A. P. (2005). DNA binding selectivity of MeCP2 due to a requirement for A/T sequences adjacent to methyl-CpG. *Molecular cell*, *19*(5), 667–78.

Kokura, K., Kaul, S. C., Wadhwa, R., Nomura, T., Khan, M. M., Shinagawa, T., Yasukawa, T., et al. (2001). The Ski protein family is required for MeCP2-mediated transcriptional repression. *The Journal of biological chemistry*, *276*(36), 34115–21.

Kriaucionis, S., & Bird, A. (2004). The major form of MeCP2 has a novel N-terminus generated by alternative splicing. *Nucleic acids research*, *32*(5), 1818–23.

Kuhse, J., Betz, H., & Kirsch, J. (1995). The inhibitory glycine receptor: architecture, synaptic localization and molecular pathology of a postsynaptic ion-channel complex. *Current Opinion in Neurobiology*, *5*(3), 318–323.

Kvachnina, E., Dumuis, A., Wlodarczyk, J., Renner, U., Cochet, M., Richter, D. W., & Ponimaskin, E. (2009). Constitutive Gs-mediated, but not G12-mediated, activity of the 5-hydroxytryptamine 5-HT7(a) receptor is modulated by the palmitoylation of its C-terminal domain. *Biochimica et biophysica acta*, *1793*(11), 1646–55.

LOWRY, O. H., ROSEBROUGH, N. J., FARR, A. L., & RANDALL, R. J. (1951). Protein measurement with the Folin phenol reagent. *The Journal of biological chemistry*, *193*(1), 265–75.

Laccone, F., Jünemann, I., Whatley, S., Morgan, R., Butler, R., Huppke, P., & Ravine, D. (2004). Large deletions of the MECP2 gene detected by gene dosage analysis in patients with Rett syndrome. *Human mutation*, *23*(3), 234–44.

Ladd-Acosta, C., Pevsner, J., Sabunciyan, S., Yolken, R. H., Webster, M. J., Dinkins, T., Callinan, P. A., et al. (2007). DNA methylation signatures within the human brain. *American journal of human genetics*, *81*(6), 1304–15.

Ladewig, T., Lalley, P. M., & Keller, B. U. (2004). Serotonergic modulation of intracellular calcium dynamics in neonatal hypoglossal motoneurons from mouse. *Brain research*, *1001*(1-2), 1–12.

Laemmli, U. K. (1970). Cleavage of structural proteins during the assembly of the head of bacteriophage T4. *Nature*, *227*(5259), 680–5.

Laemmli, U. K., & Favre, M. (1973). Maturation of the head of bacteriophage T4. I. DNA packaging events. *Journal of molecular biology*, *80*(4), 575–99.

Laherty, C. D., Yang, W. M., Sun, J. M., Davie, J. R., Seto, E., & Eisenman, R. N. (1997). Histone deacetylases associated with the mSin3 corepressor mediate mad transcriptional repression. *Cell*, *89*(3), 349–56.

Lalley, P. M. (1986). Serotoninergic and non-serotoninergic responses of phrenic motoneurones to raphe stimulation in the cat. *The Journal of physiology*, *380*, 373–85.

Lalley, P. M., Bischoff, A. M., & Richter, D. W. (1994). 5-HT-1A receptor-mediated modulation of medullary expiratory neurones in the cat. *The Journal of physiology*, *476*(1), 117–30.

Lalley, P. M., Bischoff, A. M., Schwarzacher, S. W., & Richter, D. W. (1995). 5-HT2 receptor-controlled modulation of medullary respiratory neurones in the cat. *J. Physiol.*, *487*(Pt_3), 653–661.

REFERENCES

Lauder, J. M. (1993). Neurotransmitters as growth regulatory signals: role of receptors and second messengers. *Trends in neurosciences*, *16*(6), 233–40.

Leung, P.-K., Chow, K. B. S., Lau, P.-N., Chu, K.-M., Chan, C.-B., Cheng, C. H. K., & Wise, H. (2007). The truncated ghrelin receptor polypeptide (GHS-R1b) acts as a dominant-negative mutant of the ghrelin receptor. *Cellular signalling*, *19*(5), 1011–22.

Lewis, J. D., Meehan, R. R., Henzel, W. J., Maurer-Fogy, I., Jeppesen, P., Klein, F., & Bird, a. (1992). Purification, sequence, and cellular localization of a novel chromosomal protein that binds to methylated DNA. *Cell*, *69*(6), 905–14.

Lindsay, A. D., & Feldman, J. L. (1993). Modulation of respiratory activity of neonatal rat phrenic motoneurones by serotonin. *The Journal of physiology*, *461*, 213–33. Retrieved from

Lugaresi, E., Cirignotta, F., & Montagna, P. (1985). Abnormal breathing in the Rett syndrome. *Brain & development*, *7*(3), 329–33.

Lynch, J. W. (2004). Molecular structure and function of the glycine receptor chloride channel. *Physiological reviews*, *84*(4), 1051–95.

Maekawa, T., Kim, S., Nakai, D., Makino, C., Takagi, T., Ogura, H., Yamada, K., et al. (2010). Social isolation stress induces ATF-7 phosphorylation and impairs silencing of the 5-HT 5B receptor gene. *The EMBO journal*, *29*(1), 196–208.

Magalhaes, A. C., Dunn, H., & Ferguson, S. S. G. (2012). Regulation of GPCR activity, trafficking and localization by GPCR-interacting proteins. *British journal of pharmacology*, *165*(6), 1717–36.

Magalhães, C. P., de Freitas, M. F. L., Nogueira, M. I., Campina, R. C. de F., Takase, L. F., de Souza, S. L., & de Castro, R. M. (2010). Modulatory role of serotonin on feeding behavior. *Nutritional neuroscience*, *13*(6), 246–55.

Manzke, T., Dutschmann, M., Schlaf, G., Mörschel, M., Koch, U. R., Ponimaskin, E., Bidon, O., et al. (2009). Serotonin targets inhibitory synapses to induce modulation of network functions. *Philosophical transactions of the Royal Society of London. Series B, Biological sciences*, *364*(1529), 2589–602.

Manzke, T., Guenther, U., Ponimaskin, E. G., Haller, M., Dutschmann, M., Schwarzacher, S., & Richter, D. W. (2003). 5-HT4(a) receptors avert opioid-induced breathing depression without loss of analgesia. *Science (New York, N.Y.)*, *301*(5630), 226–9.

Manzke, T., Niebert, M., Koch, U. R., Caley, A., Vogelgesang, S., Hülsmann, S., Ponimaskin, E., et al. (2010). Serotonin receptor 1A–modulated phosphorylation of glycine receptor α3 controls breathing in mice. *Journal of Clinical Investigation*, *120*(11), 4118–4128.

Marcus, C. L., Carroll, J. L., McColley, S. A., Loughlin, G. M., Curtis, S., Pyzik, P., & Naidu, S. (1994). Polysomnographic characteristics of patients with Rett syndrome. *The Journal of pediatrics*, *125*(2), 218–24.

Markstahler, U., Kremer, E., Kimmina, S., Becker, K., & Richter, D. W. (2002). Effects of functional knock-out of alpha 1 glycine-receptors on breathing movements in oscillator mice. *Respiratory physiology & neurobiology*, *130*(1), 33–42.

Martinowich, K., Hattori, D., Wu, H., Fouse, S., He, F., Hu, Y., Fan, G., et al. (2003). DNA methylation-related chromatin remodeling in activity-dependent BDNF gene regulation. *Science (New York, N.Y.)*, *302*(5646), 890–3.

Matthes, H., Boschert, U., Amlaiky, N., Grailhe, R., Plassat, J. L., Muscatelli, F., Mattei, M. G., et al. (1993). Mouse 5-hydroxytryptamine5A and 5-hydroxytryptamine5B receptors define a new family

of serotonin receptors: cloning, functional expression, and chromosomal localization. *Molecular pharmacology*, *43*(3), 313–9.

McGraw, C. M., Samaco, R. C., & Zoghbi, H. Y. (2011). Adult neural function requires MeCP2. *Science (New York, N.Y.)*, *333*(6039), 186.

Medrihan, L., Tantalaki, E., Aramuni, G., Sargsyan, V., Dudanova, I., Missler, M., & Zhang, W. (2008). Early defects of GABAergic synapses in the brain stem of a MeCP2 mouse model of Rett syndrome. *Journal of neurophysiology*, *99*(1), 112–21.

Meehan, R. R., Lewis, J. D., & Bird, a P. (1992). Characterization of MeCP2, a vertebrate DNA binding protein with affinity for methylated DNA. *Nucleic acids research*, *20*(19), 5085–92.

Meloni, I., Bruttini, M., Longo, I., Mari, F., Rizzolio, F., D'Adamo, P., Denvriendt, K., et al. (2000). A mutation in the rett syndrome gene, MECP2, causes X-linked mental retardation and progressive spasticity in males. *American journal of human genetics*, *67*(4), 982–5.

Merrill, E. G., Lipski, J., Kubin, L., & Fedorko, L. (1983). Origin of the expiratory inhibition of nucleus tractus solitarius inspiratory neurones. *Brain research*, *263*(1), 43–50.

Migeon, B. R., Dunn, M. A., Thomas, G., Schmeckpeper, B. J., & Naidu, S. (1995). Studies of X inactivation and isodisomy in twins provide further evidence that the X chromosome is not involved in Rett syndrome. *American journal of human genetics*, *56*(3), 647–53.

Milligan, G. (2010). The role of dimerisation in the cellular trafficking of G-protein-coupled receptors. *Current opinion in pharmacology*, *10*(1), 23–9.

Mironov, S. L., Skorova, E. Y., & Kügler, S. (2011). Epac-mediated cAMP-signalling in the mouse model of Rett Syndrome. *Neuropharmacology*, *60*(6), 869–77.

Mittal, K., Gupta, N., Kabra, M., Juyal, R., & Thelma, B. K. (2011). Distinct de novo deletions in a brother-sister pair with RTT: a case report. *American journal of medical genetics. Part B, Neuropsychiatric genetics : the official publication of the International Society of Psychiatric Genetics*, *156B*(7), 859–63.

Mnatzakanian, G. N., Lohi, H., Munteanu, I., Alfred, S. E., Yamada, T., MacLeod, P. J. M., Jones, J. R., et al. (2004). A previously unidentified MECP2 open reading frame defines a new protein isoform relevant to Rett syndrome. *Nature genetics*, *36*(4), 339–41.

Monteau, R., & Hilaire, G. (1991). Spinal respiratory motoneurons. *Progress in neurobiology*, *37*(2), 83–144.

Morin, D., Monteau, R., & Hilaire, G. (1991). 5-Hydroxytryptamine modulates central respiratory activity in the newborn rat: an in vitro study. *European journal of pharmacology*, *192*(1), 89–95.

Mount, R. H., Hastings, R. P., Reilly, S., Cass, H., & Charman, T. (2001). Behavioural and emotional features in Rett syndrome. *Disability and rehabilitation*, *23*(3-4), 129–38.

Mullis, K., Faloona, F., Scharf, S., Saiki, R., Horn, G., & Erlich, H. (1986). Specific enzymatic amplification of DNA in vitro: the polymerase chain reaction. *Cold Spring Harbor symposia on quantitative biology*, *51 Pt 1*, 263–73.

Muotri, A. R., Marchetto, M. C. N., Coufal, N. G., Oefner, R., Yeo, G., Nakashima, K., & Gage, F. H. (2010). L1 retrotransposition in neurons is modulated by MeCP2. *Nature*, *468*(7322), 443–6.

Nan, X, Campoy, F. J., & Bird, a. (1997a). MeCP2 is a transcriptional repressor with abundant binding sites in genomic chromatin. *Cell*, *88*(4), 471–81.

REFERENCES

Nan, X, Campoy, F. J., & Bird, a. (1997b). MeCP2 is a transcriptional repressor with abundant binding sites in genomic chromatin. *Cell*, *88*(4), 471–81.

Nan, X, Meehan, R. R., & Bird, A. (1993). Dissection of the methyl-CpG binding domain from the chromosomal protein MeCP2. *Nucleic acids research*, *21*(21), 4886–92.

Nan, X, Ng, H. H., Johnson, C. a, Laherty, C. D., Turner, B. M., Eisenman, R. N., & Bird, a. (1998). Transcriptional repression by the methyl-CpG-binding protein MeCP2 involves a histone deacetylase complex. *Nature*, *393*(6683), 386–9.

Nan, X, Tate, P., Li, E., & Bird, A. (1996). DNA methylation specifies chromosomal localization of MeCP2. *Molecular and cellular biology*, *16*(1), 414–21.

Nan, Xinsheng, Hou, J., Maclean, A., Nasir, J., Lafuente, M. J., Shu, X., Kriaucionis, S., et al. (2007). Interaction between chromatin proteins MECP2 and ATRX is disrupted by mutations that cause inherited mental retardation. *Proceedings of the National Academy of Sciences of the United States of America*, *104*(8), 2709–14.

Niebert, M., Vogelgesang, S., Koch, U. R., Bischoff, A.-M., Kron, M., Bock, N., & Manzke, T. (2011). Expression and Function of Serotonin 2A and 2B Receptors in the Mammalian Respiratory Network. (S. E. Dryer, Ed.)*PLoS ONE*, *6*(7), e21395.

Noda, M., Higashida, H., Aoki, S., & Wada, K. (2004). Multiple signal transduction pathways mediated by 5-HT receptors. *Molecular neurobiology*, *29*(1), 31–9.

Nolte, C., Matyash, M., Pivneva, T., Schipke, C. G., Ohlemeyer, C., Hanisch, U. K., Kirchhoff, F., and Kettenmann, H. (2001). GFAP promoter-controlled EGFP-expressing transgenic mice: a tool to visualize astrocytes and astrogliosis in living brain tissue. *Glia 33*, 72–86.

Nomura, Y, Honda, K., & Segawa, M. (1987). Pathophysiology of Rett syndrome. *Brain & development*, *9*(5), 506–13.

Nomura, Yoshiko. (2005). Early behavior characteristics and sleep disturbance in Rett syndrome. *Brain & development*, *27 Suppl 1*, S35–S42.

Nuber, U. A., Kriaucionis, S., Roloff, T. C., Guy, J., Selfridge, J., Steinhoff, C., Schulz, R., et al. (2005). Up-regulation of glucocorticoid-regulated genes in a mouse model of Rett syndrome. *Human molecular genetics*, *14*(15), 2247–56.

Ogier, M., & Katz, D. M. (2008). Breathing dysfunction in Rett syndrome: understanding epigenetic regulation of the respiratory network. *Respiratory physiology & neurobiology*, *164*(1-2), 55–63.

Ogier, M., Wang, H., Hong, E., Wang, Q., Greenberg, M. E., & Katz, D. M. (2007). Brain-derived neurotrophic factor expression and respiratory function improve after ampakine treatment in a mouse model of Rett syndrome. *The Journal of neuroscience : the official journal of the Society for Neuroscience*, *27*(40), 10912–7.

O'Callaghan, K., Kuliopulos, A., & Covic, L. (2012). Turning Receptors On and Off with Intracellular Pepducins: New Insights into G-protein-coupled Receptor Drug Development. *The Journal of biological chemistry*, *287*(16), 12787–96.

Pagliardini, S., Ren, J., Wevrick, R., & Greer, J. J. (2005). Developmental abnormalities of neuronal structure and function in prenatal mice lacking the prader-willi syndrome gene necdin. *The American journal of pathology*, *167*(1), 175–91.

Paterson, D. S., Hilaire, G., & Weese-Mayer, D. E. (2009). Medullary serotonin defects and respiratory dysfunction in sudden infant death syndrome. *Respiratory physiology & neurobiology*, *168*(1-2), 133–43.

REFERENCES

Paterson, D. S., Thompson, E. G., Belliveau, R. A., Antalffy, B. A., Trachtenberg, F. L., Armstrong, D. D., & Kinney, H. C. (2005). Serotonin transporter abnormality in the dorsal motor nucleus of the vagus in Rett syndrome: potential implications for clinical autonomic dysfunction. *Journal of neuropathology and experimental neurology*, *64*(11), 1018–27.

Paton, J. F. (1996). The ventral medullary respiratory network of the mature mouse studied in a working heart-brainstem preparation. *The Journal of physiology*, *493 (Pt 3*, 819–31.

Paton, J. F., & Richter, D. W. (1995). Role of fast inhibitory synaptic mechanisms in respiratory rhythm generation in the maturing mouse. *The Journal of physiology*, *484 (Pt 2*, 505–21.

Pelka, G. J., Watson, C. M., Christodoulou, J., & Tam, P. P. L. (2005). Distinct expression profiles of Mecp2 transcripts with different lengths of 3′UTR in the brain and visceral organs during mouse development. *Genomics*, *85*(4), 441–452.

Pena, F., & Ramirez, J.-M. (2002). Endogenous Activation of Serotonin-2A Receptors Is Required for Respiratory Rhythm Generation In Vitro. *J. Neurosci.*, *22*(24), 11055–11064.

Percy, A. K., & Lane, J. B. (2004). Rett syndrome: clinical and molecular update. *Current opinion in pediatrics*, *16*(6), 670–7.

Pfaffl, M. W. (2001). A new mathematical model for relative quantification in real-time RT-PCR. *Nucleic acids research*, *29*(9), e45.

Philippe, C., Villard, L., De Roux, N., Raynaud, M., Bonnefond, J. P., Pasquier, L., Lesca, G., et al. (2006). Spectrum and distribution of MECP2 mutations in 424 Rett syndrome patients: a molecular update. *European journal of medical genetics*, *49*(1), 9–18.

Pierrefiche, O., Schwarzacher, S. W., Bischoff, A. M., & Richter, D. W. (1998). Blockade of synaptic inhibition within the pre-Bötzinger complex in the cat suppresses respiratory rhythm generation in vivo. *The Journal of physiology*, *509 (Pt 1*, 245–54

Plassat, J. L., Boschert, U., Amlaiky, N., & Hen, R. (1992). The mouse 5HT5 receptor reveals a remarkable heterogeneity within the 5HT1D receptor family. *The EMBO journal*, *11*(13), 4779–86

Ptak, K., Yamanishi, T., Aungst, J., Milescu, L. S., Zhang, R., Richerson, G. B., & Smith, J. C. (2009). Raphé neurons stimulate respiratory circuit activity by multiple mechanisms via endogenously released serotonin and substance P. *The Journal of neuroscience : the official journal of the Society for Neuroscience*, *29*(12), 3720–37

Quaderi, N. A., Meehan, R. R., Tate, P. H., Cross, S. H., Bird, A. P., Chatterjee, A., Herman, G. E., et al. (1994). Genetic and physical mapping of a gene encoding a methyl CpG binding protein, Mecp2, to the mouse X chromosome. *Genomics*, *22*(3), 648–51.

Rapport, M. M., Green, A. A., & Page, I. H. (1948). Serum vasoconstrictor, serotonin; isolation and characterization. *The Journal of biological chemistry*, *176*(3), 1243–51.

Ramirez, J. M., & Richter, D. W. (1996). The neuronal mechanisms of respiratory rhythm generation. *Current opinion in neurobiology*, *6*(6), 817–25.

Ramirez, J. M., Schwarzacher, S. W., Pierrefiche, O., Olivera, B. M., & Richter, D. W. (1998). Selective lesioning of the cat pre-Bötzinger complex in vivo eliminates breathing but not gasping. *The Journal of physiology*, *507 (Pt 3*, 895–907.

Raymond, J. R., Mukhin, Y. V., Gelasco, a, Turner, J., Collinsworth, G., Gettys, T. W., Grewal, J. S., et al. (2001). Multiplicity of mechanisms of serotonin receptor signal transduction. *Pharmacology & therapeutics*, *92*(2-3), 179–212.

REFERENCES

Reichwald, K., Thiesen, J., Wiehe, T., Weitzel, J., Poustka, W. a, Rosenthal, a, Platzer, M., et al. (2000). Comparative sequence analysis of the MECP2-locus in human and mouse reveals new transcribed regions. *Mammalian genome : official journal of the International Mammalian Genome Society*, *11*(3), 182–90.

Ren, J., Lee, S., Pagliardini, S., Gerard, M., Stewart, C. L., Greer, J. J., & Wevrick, R. (2003). Absence of Ndn, Encoding the Prader-Willi Syndrome-Deleted Gene necdin, Results in Congenital Deficiency of Central Respiratory Drive in Neonatal Mice. *J. Neurosci.*, *23*(5), 1569–1573.

Renner, U., Zeug, A., Woehler, A., Niebert, M., Dityatev, A., Dityateva, G., Gorinski, N., et al. (2012). Heterodimerization of serotonin receptors 5-HT1A and 5-HT7 differentially regulates receptor signalling and trafficking. *Journal of cell science*, *125*(Pt 10), 2486–99.

Rett, A. (1966). [On a unusual brain atrophy syndrome in hyperammonemia in childhood]. *Wiener medizinische Wochenschrift (1946)*, *116*(37), 723–6.

Richter, D W. (1982). Generation and maintenance of the respiratory rhythm. *The Journal of experimental biology*, *100*, 93–107.

Richter, D W, Pierrefiche, O., Lalley, P. M., & Polder, H. R. (1996). Voltage-clamp analysis of neurons within deep layers of the brain. *Journal of neuroscience methods*, *67*(2), 121–3.

Richter, D W, Schmidt-Garcon, P., Pierrefiche, O., Bischoff, a M., & Lalley, P. M. (1999). Neurotransmitters and neuromodulators controlling the hypoxic respiratory response in anaesthetized cats. *The Journal of physiology*, *514 (Pt 2*, 567–78.

Richter, D W, & Spyer, K. M. (2001). Studying rhythmogenesis of breathing: comparison of in vivo and in vitro models. *Trends in neurosciences*, *24*(8), 464–72

Richter, Diethelm W., Manzke, T., Wilken, B., & Ponimaskin, E. (2003). Serotonin receptors: guardians of stable breathing. *Trends in Molecular Medicine*, *9*(12), 542–548.

Rizzuto, R., Nakase, H., Darras, B., Francke, U., Fabrizi, G. M., Mengel, T., Walsh, F., et al. (1989). A gene specifying subunit VIII of human cytochrome c oxidase is localized to chromosome 11 and is expressed in both muscle and non-muscle tissues. *The Journal of biological chemistry*, *264*(18), 10595–600.

Rohdin, M., Fernell, E., Eriksson, M., Albåge, M., Lagercrantz, H., & Katz-Salamon, M. (2007). Disturbances in cardiorespiratory function during day and night in Rett syndrome. *Pediatric neurology*, *37*(5), 338–44.

Romero, G., von Zastrow, M., & Friedman, P. A. (2011). Role of PDZ proteins in regulating trafficking, signaling, and function of GPCRs: means, motif, and opportunity. *Advances in pharmacology (San Diego, Calif.)*, *62*(null), 279–314.

Roux, J.-C., Dura, E., Moncla, A., Mancini, J., & Villard, L. (2007). Treatment with desipramine improves breathing and survival in a mouse model for Rett syndrome. *The European journal of neuroscience*, *25*(7), 1915–22.

Roux, J.-C., Dura, E., & Villard, L. (2008). Tyrosine hydroxylase deficit in the chemoafferent and the sympathoadrenergic pathways of the Mecp2 deficient mouse. *Neuroscience letters*, *447*(1), 82–6.

Roze, E., Cochen, V., Sangla, S., Bienvenu, T., Roubergue, A., Leu-Semenescu, S., & Vidaihet, M. (2007). Rett syndrome: an overlooked diagnosis in women with stereotypic hand movements, psychomotor retardation, Parkinsonism, and dystonia? *Movement disorders : official journal of the Movement Disorder Society*, *22*(3), 387–9.

Rybak, I. A., Shevtsova, N. A., Paton, J. F. R., Dick, T. E., St-John, W. M., Mörschel, M., & Dutschmann, M. (2004). Modeling the ponto-medullary respiratory network. *Respiratory physiology & neurobiology*, *143*(2-3), 307–19.

Sahibzada, N., Ferreira, M., Wasserman, A. M., Taveira-DaSilva, A. M., & Gillis, R. A. (2000). Reversal of morphine-induced apnea in the anesthetized rat by drugs that activate 5-hydroxytryptamine(1A) receptors. *The Journal of pharmacology and experimental therapeutics*, *292*(2), 704–13.

Saito, Y., Ito, M., Ozawa, Y., Obonai, T., Kobayashi, Y., Washizawa, K., Ohsone, Y., et al. (1999). Changes of neurotransmitters in the brainstem of patients with respiratory-pattern disorders during childhood. *Neuropediatrics*, *30*(3), 133–40.

Samaco, R. C., Mandel-Brehm, C., Chao, H.-T., Ward, C. S., Fyffe-Maricich, S. L., Ren, J., Hyland, K., et al. (2009). Loss of MeCP2 in aminergic neurons causes cell-autonomous defects in neurotransmitter synthesis and specific behavioral abnormalities. *Proceedings of the National Academy of Sciences of the United States of America*, *106*(51), 21966–71.

Santos, M., Summavielle, T., Teixeira-Castro, a., Silva-Fernandes, a., Duarte-Silva, S., Marques, F., Martins, L., et al. (2010). Monoamine deficits in the brain of methyl-CpG binding protein 2 null mice suggest the involvement of the cerebral cortex in early stages of Rett syndrome. *Neuroscience*, *170*(2), 453–467.

Schlüter, B., Aguigah, G., Buschatz, D., Trowitzsch, E., & Aksu, F. (1995). Polysomnographic recordings of respiratory disturbances in Rett syndrome. *Journal of sleep research*, *4*(S1), 203–207.

Schmid, D. A., Yang, T., Ogier, M., Adams, I., Mirakhur, Y., Wang, Q., Massa, S. M., et al. (2012). A TrkB small molecule partial agonist rescues TrkB phosphorylation deficits and improves respiratory function in a mouse model of Rett syndrome. *The Journal of neuroscience : the official journal of the Society for Neuroscience*, *32*(5), 1803–10.

Schmid, K., Foutz, A. S., & Denavit-Saubié, M. (1996). Inhibitions mediated by glycine and GABAA receptors shape the discharge pattern of bulbar respiratory neurons. *Brain Research*, *710*(1-2), 150–160.

Schwartzman, J. S., Bernardino, a, Nishimura, a, Gomes, R. R., & Zatz, M. (2001). Rett syndrome in a boy with a 47,XXY karyotype confirmed by a rare mutation in the MECP2 gene. *Neuropediatrics*, *32*(3), 162–4.

Schüle, B., Armstrong, D. D., Vogel, H., Oviedo, a, & Francke, U. (2008). Severe congenital encephalopathy caused by MECP2 null mutations in males: central hypoxia and reduced neuronal dendritic structure. *Clinical genetics*, *74*(2), 116–26.

Seck, T., Pellegrini, M., Florea, A. M., Grignoux, V., Baron, R., Mierke, D. F., & Horne, W. C. (2005). The delta e13 isoform of the calcitonin receptor forms a six-transmembrane domain receptor with dominant-negative effects on receptor surface expression and signaling. *Molecular endocrinology (Baltimore, Md.)*, *19*(8), 2132–44.

Segawa, M. (2001). Discussant--pathophysiologies of Rett syndrome. *Brain & development*, *23 Suppl 1*, S218–23.

Serrats, J., Raurich, A., Vilaró, M. T., Mengod, G., & Cortés, R. (2004). 5-ht5B receptor mRNA in the raphe nuclei: coexpression with serotonin transporter. *Synapse (New York, N.Y.)*, *51*(2), 102–11.

Sethakorn, N., Yau, D. M., & Dulin, N. O. (2010). Non-canonical functions of RGS proteins. *Cellular signalling*, *22*(9), 1274–81.

REFERENCES

Shahbazian, M. D., Antalffy, B., Armstrong, D. L., & Zoghbi, H. Y. (2002). Insight into Rett syndrome: MeCP2 levels display tissue- and cell-specific differences and correlate with neuronal maturation. *Human molecular genetics*, *11*(2), 115–24.

Shahbazian, M., Young, J., Yuva-Paylor, L., Spencer, C., Antalffy, B., Noebels, J., Armstrong, D., et al. (2002). Mice with truncated MeCP2 recapitulate many Rett syndrome features and display hyperacetylation of histone H3. *Neuron*, *35*(2), 243–54.

Sherer, N. M., Lehmann, M. J., Jimenez-Soto, L. F., Ingmundson, A., Horner, S. M., Cicchetti, G., Allen, P. G., et al. (2003). Visualization of retroviral replication in living cells reveals budding into multivesicular bodies. *Traffic (Copenhagen, Denmark)*, *4*(11), 785–801.

Shevtsova, N. a, Manzke, T., Molkov, Y. I., Bischoff, A., Smith, J. C., Rybak, I. a, & Richter, D. W. (2011). Computational modelling of 5-HT receptor-mediated reorganization of the brainstem respiratory network. *The European journal of neuroscience*, *34*(8), 1276–91.

Sinclair, M. L., Wang, X. Y., Mattia, M., Conti, M., Buck, J., Wolgemuth, D. J., & Levin, L. R. (2000). Specific expression of soluble adenylyl cyclase in male germ cells. *Molecular reproduction and development*, *56*(1), 6–11.

Skene, J. H., & Virág, I. (1989). Posttranslational membrane attachment and dynamic fatty acylation of a neuronal growth cone protein, GAP-43. *The Journal of cell biology*, *108*(2), 613–24.

Smeets, E E J, Pelc, K., & Dan, B. (2012). Rett Syndrome. *Molecular syndromology*, *2*(3-5), 113–127.

Smeets, Eric E J, Julu, P. O. O., van Waardenburg, D., Engerström, I. W., Hansen, S., Apartopoulos, F., Curfs, L. M. G., et al. (2006). Management of a severe forceful breather with Rett syndrome using carbogen. *Brain & development*, *28*(10), 625–32.

Smith, J. C., Ellenberger, H. H., Ballanyi, K., Richter, D. W., & Feldman, J. L. (1991). Pre-Bötzinger complex: a brainstem region that may generate respiratory rhythm in mammals. *Science (New York, N.Y.)*, *254*(5032), 726–9.

Sodhi, M. S. K., & Sanders-Bush, E. (2004). Serotonin and brain development. *International review of neurobiology*, *59*, 111–74.

Southall, D. P., Kerr, a M., Tirosh, E., Amos, P., Lang, M. H., & Stephenson, J. B. (1988). Hyperventilation in the awake state: potentially treatable component of Rett syndrome. *Archives of disease in childhood*, *63*(9), 1039–48.

Steffenburg, U., Hagberg, G., & Hagberg, B. (2001). Epilepsy in a representative series of Rett syndrome. *Acta paediatrica (Oslo, Norway : 1992)*, *90*(1), 34–9.

Steinbusch, H. W. (1981). Distribution of serotonin-immunoreactivity in the central nervous system of the rat-cell bodies and terminals. *Neuroscience*, *6*(4), 557–618.

Stettner, G. M., Huppke, P., Brendel, C., Richter, D. W., Gärtner, J., & Dutschmann, M. (2007). Breathing dysfunctions associated with impaired control of postinspiratory activity in Mecp2-/y knockout mice. *The Journal of physiology*, *579*(Pt 3), 863–76.

Twarog, B. M., & Page, I. H. (1953). Serotonin content of some mammalian tissues and urine and a method for its determination. *The American journal of physiology*, *175*(1), 157–61.

Tao, J., Hu, K., Chang, Q., Wu, H., Sherman, N. E., Martinowich, K., Klose, R. J., et al. (2009). Phosphorylation of MeCP2 at Serine 80 regulates its chromatin association and neurological function. *Proceedings of the National Academy of Sciences of the United States of America*, *106*(12), 4882–7.

REFERENCES

Tate, P., Skarnes, W., & Bird, A. (1996). The methyl-CpG binding protein MeCP2 is essential for embryonic development in the mouse. *Nature genetics*, *12*(2), 205–8.

Tecott, L. H. (2007). Serotonin and the orchestration of energy balance. *Cell metabolism*, *6*(5), 352–61.

Teng, Y. D., Bingaman, M., Taveira-DaSilva, A. M., Pace, P. P., Gillis, R. A., & Wrathall, J. R. (2003). Serotonin 1A Receptor Agonists Reverse Respiratory Abnormalities in Spinal Cord-Injured Rats. *J. Neurosci.*, *23*(10), 4182–4189.

Toppin, V. A. L., Harris, M. B., Kober, A. M., Leiter, J. C., & St-John, W. M. (2007). Persistence of eupnea and gasping following blockade of both serotonin type 1 and 2 receptors in the in situ juvenile rat preparation. *Journal of applied physiology (Bethesda, Md. : 1985)*, *103*(1), 220–7.

Trappe, R., Laccone, F., Cobilanschi, J., Meins, M., Huppke, P., Hanefeld, F., & Engel, W. (2001). MECP2 mutations in sporadic cases of Rett syndrome are almost exclusively of paternal origin. *American journal of human genetics*, *68*(5), 1093–101.

Tresguerres, M., Levin, L. R., & Buck, J. (2011). Intracellular cAMP signaling by soluble adenylyl cyclase. *Kidney international*, *79*(12), 1277–88.

Tropea, D., Giacometti, E., Wilson, N. R., Beard, C., McCurry, C., Fu, D. D., Flannery, R., et al. (2009). Partial reversal of Rett Syndrome-like symptoms in MeCP2 mutant mice. *Proceedings of the National Academy of Sciences of the United States of America*, *106*(6), 2029–34.

Tryba, A. K., Peña, F., & Ramirez, J.-M. (2006). Gasping activity in vitro: a rhythm dependent on 5-HT2A receptors. *The Journal of neuroscience : the official journal of the Society for Neuroscience*, *26*(10), 2623–34.

Törk, I. (1990). Anatomy of the serotonergic system. *Annals of the New York Academy of Sciences*, *600*, 9–34; discussion 34–5.

Urdinguio, R. G., Lopez-Serra, L., Lopez-Nieva, P., Alaminos, M., Diaz-Uriarte, R., Fernandez, A. F., & Esteller, M. (2008). Mecp2-null mice provide new neuronal targets for Rett syndrome. *PloS one*, *3*(11), e3669.

Viemari, J.-C., Roux, J.-C., Tryba, A. K., Saywell, V., Burnet, H., Peña, F., Zanella, S., et al. (2005). Mecp2 deficiency disrupts norepinephrine and respiratory systems in mice. *The Journal of neuroscience : the official journal of the Society for Neuroscience*, *25*(50), 11521–30.

Vitalis, T., & Parnavelas, J. G. (2003). The role of serotonin in early cortical development. *Developmental neuroscience*, *25*(2-4), 245–56.

Vogelstein, B., & Gillespie, D. (1979). Preparative and analytical purification of DNA from agarose. *Proceedings of the National Academy of Sciences of the United States of America*, *76*(2), 615–9.

Wallin, E., & von Heijne, G. (1995). Properties of N-terminal tails in G-protein coupled receptors: a statistical study. *Protein engineering*, *8*(7), 693–8.

Wan, M., Lee, S. S., Zhang, X., Houwink-Manville, I., Song, H. R., Amir, R. E., Budden, S., et al. (1999). Rett syndrome and beyond: recurrent spontaneous and familial MECP2 mutations at CpG hotspots. *American journal of human genetics*, *65*(6), 1520–9.

Waters, K. (2010). Serotonin in the sudden infant death syndrome. *Drug news & perspectives*, *23*(9), 537–48.

Weber, K., & Osborn, M. (1969). The reliability of molecular weight determinations by dodecyl sulfate-polyacrylamide gel electrophoresis. *The Journal of biological chemistry*, *244*(16), 4406–12.

REFERENCES

Weese-Mayer, D. E., Berry-Kravis, E. M., Ceccherini, I., & Rand, C. M. C. (2008). Congenital central hypoventilation syndrome (CCHS) and sudden infant death syndrome (SIDS): kindred disorders of autonomic regulation. *Respiratory physiology & neurobiology*, *164*(1-2), 38–48.

Weese-Mayer, D. E., Lieske, S. P., Boothby, C. M., Kenny, A. S., Bennett, H. L., & Ramirez, J.-M. (2008). Autonomic dysregulation in young girls with Rett Syndrome during nighttime in-home recordings. *Pediatric pulmonology*, *43*(11), 1045–60.

White, J. H., Wise, A., Main, M. J., Green, A., Fraser, N. J., Disney, G. H., Barnes, A. A., et al. (1998). Heterodimerization is required for the formation of a functional GABA(B) receptor. *Nature*, *396*(6712), 679–82. doi:10.1038/25354

Wilken, B., Lalley, P., Bischoff, A. M., Christen, H. J., Behnke, J., Hanefeld, F., & Richter, D. W. (1997). Treatment of apneustic respiratory disturbance with a serotonin-receptor agonist. *The Journal of pediatrics*, *130*(1), 89–94.

Woolley, D. W., & Shaw, E. (1954). A BIOCHEMICAL AND PHARMACOLOGICAL SUGGESTION ABOUT CERTAIN MENTAL DISORDERS. *Proceedings of the National Academy of Sciences of the United States of America*, *40*(4), 228–31.

Xia, Z., Hufeisen, S. J., Gray, J. A., & Roth, B. L. (2003). The PDZ-binding domain is essential for the dendritic targeting of 5-HT2A serotonin receptors in cortical pyramidal neurons in vitro. *Neuroscience*, *122*(4), 907–20.

Xiang, F., Buervenich, S., Nicolao, P., Bailey, M. E., Zhang, Z., & Anvret, M. (2000). Mutation screening in Rett syndrome patients. *Journal of medical genetics*, *37*(4), 250–5.

Xie, G., Ito, E., Maruyama, K., Pietruck, C., Sharma, M., Yu, L.-C., & Pierce Palmer, P. (2000). An alternatively spliced transcript of the rat nociceptin receptor ORL1 gene encodes a truncated receptor. *Molecular Brain Research*, *77*(1), 1–9.

Yasui, D. H., Peddada, S., Bieda, M. C., Vallero, R. O., Hogart, A., Nagarajan, R. P., Thatcher, K. N., et al. (2007). Integrated epigenomic analyses of neuronal MeCP2 reveal a role for long-range interaction with active genes. *Proceedings of the National Academy of Sciences of the United States of America*, *104*(49), 19416–21.

Young, J. I., Hong, E. P., Castle, J. C., Crespo-Barreto, J., Bowman, A. B., Rose, M. F., Kang, D., et al. (2005). Regulation of RNA splicing by the methylation-dependent transcriptional repressor methyl-CpG binding protein 2. *Proceedings of the National Academy of Sciences of the United States of America*, *102*(49), 17551–8.

Zanella, S., Mebarek, S., Lajard, A.-M., Picard, N., Dutschmann, M., & Hilaire, G. (2008). Oral treatment with desipramine improves breathing and life span in Rett syndrome mouse model. *Respiratory physiology & neurobiology*, *160*(1), 116–21.

Zappella, M. (1997). The preserved speech variant of the Rett complex: a report of 8 cases. *European child & adolescent psychiatry*, *6 Suppl 1*, 23–5.

Zappella, M., Meloni, I., Longo, I., Hayek, G., & Renieri, A. (2001). Preserved speech variants of the Rett syndrome: molecular and clinical analysis. *American journal of medical genetics*, *104*(1), 14–22.

Zhou, Z., Hong, E. J., Cohen, S., Zhao, W.-N., Ho, H.-Y. H., Schmidt, L., Chen, W. G., et al. (2006). Brain-specific phosphorylation of MeCP2 regulates activity-dependent Bdnf transcription, dendritic growth, and spine maturation. *Neuron*, *52*(2), 255–69.

Zocchi, L., & Sassone-Corsi, P. (2012). SIRT1-mediated deacetylation of MeCP2 contributes to BDNF expression. *Epigenetics : official journal of the DNA Methylation Society*, *7*(7), 695–700.

ACKNOWLEDGMENTS

First and foremost I would like to thank my supervisor **Dr. Dr. Till Manzke** for excellent guidance throughout this project and the pleasant atmosphere in our laboratory, not least through the wonderful piano music.

No less, I am very thankful to **Prof. Diethelm W. Richter**, for the chance to work in his department, for critical discussions, his comments, and his support.

I would like to thank my thesis committee: **Prof. Gabriele Flügge** and **Prof. Andreas Wodarz** for critical comments and suggestions on this work and additionally Prof. Flügge and **Simone** & **Simone** for the support on IHC.

Furthermore, I would like to thank **Prof. Swen Hülsmann** for being the second reviewer and for the support with Plethysmography.

This thesis had never been come to success without my cooperation partners. I would like to thank **Dr. Wiebke Möbius** for the Electron Microscopy, and of course **Anna-Maria Bischoff** for her calm hand during the WHBP. I would like to thank **Dr. Marcus Niebert** for his extensive know-how on great support on many experiments. Furthermore, I am thankful to **Christian Bertram** and **Prof. Peter Lalley** for the nice images and helpful comments.

There are so many friends around me, who helped me and improved my mood: **Christiane M.**, **Oliwia**, **Susann** and **Christian** and especially **Elli** and **Christiane F.** It was often so funny.

Last but not least I am deeply grateful to my family: **my parents**, **my brother** and **my grandmother** and my girlfriend **Jessica** simply for being there and for patient waiting for my calls.

Many thanks to all of you

Publications

Manzke, T.[#], Niebert, M.[#], **Vogelgesang, S.[#]**, Bischoff, A. M., Bidon, O., Renner, U., Opitz, L., Hülsmann, S., Möbius, W., Laccone, F., Flügge, G., Richter, D. W. The truncated serotonin receptor 5B is causal for dangerous breathing disorders in RETT Syndrome. Submitted to Science (in review).

Niebert, M.[#], **Vogelgesang, S.[#]**, Koch, U. R., Bischoff, A. M., Kron, M., Bock, N., Manzke, T. (2011). Expression and Function of Serotonin 2A and 2B Receptors in the Mammalian Respiratory Network. *PLoS One 6*(7), e21395.

Manzke, T., Niebert, M., Koch, U. R., Caley, A., **Vogelgesang, S.**, Hülsmann, S., Ponimaskin, E., Müller, U., Smart, T. G., Harvey, R. J., Richter, D. W. (2010). Serotonin receptor 1A-modulated phosphorylation of glycine receptor α3 controls breathing in mice. *J Clin Invest. 120*(11), 4118-28.

Manzke, T., Niebert, M., Koch, U. R., Caley, A., **Vogelgesang, S.**, Bischoff, A. M., Hülsmann, S., Ponimaskin, E., Müller, U., Smart, T. G., Harvey, R. J., Richter, D. W. (2011). Serotonin receptor 1A-modulated dephosphorylation of glycine receptor α3: A new molecular mechanism of breathing control for compensation of opioid-induced respiratory depression without loss of analgesia. *Schmerz 25*(3), 272-281.

Großer, E., Hirt, U., Janc, O. A., Menzfeld, C., Fischer, M., Kempkes, B., **Vogelgesang, S.**, Manzke, T. U., Opitz, L., Salinas-Riester, G., Müller, M. (2012). Oxidative burden and mitochondrial dysfunction in a mouse model of Rett syndrome. *Neurobiol. Dis. 48*(1), 102-14.

# Equally contributed first authors

Lecture

2011   "Serotonin receptor 5B gene is a regulatory target of MeCP2 in a mouse model of Rett syndrome" (SfN – Washington)

Awards

2011   GGNB Travel Grant

2009   Sertürner Award

Personal Information

Address	Sankt-Martini-Straße 7
	37079 Göttingen
Mobile	0172 / 3765106
Email	svogelg@gwdg.de
Date of birth	27. June 1978
Nationality	German
Sex	male

Education

Since 2009	Ph.D. Student of the **DFG Research Center for Molecular Physiology of the Brain (CMPB**), Göttingen
	Thesis: „Identifying Target Genes related to Respiratory Network Dysfunction in a Mouse Model for the Rett Syndrome"
10/2003 - 09/2008	**Martin Luther University Halle-Wittenberg**, Halle / Saale
	Biology; Diploma in **Biology**
	Thesis:" Danger Signals and its Relevance for the NK cell Answer in Tumors "
11/2000 – 04/2003	**Chemnitz University of Technology**, Chemnitz
	Bachelor in **Multi-media communication**
07/1998	**Werner-Heisenberg-Gymnasium Chemnitz** (grammar school)
	General qualification for university entrance

Internship

2005	**Max Planck Research Unit for Enzymology of Protein Folding**, Halle / Saale